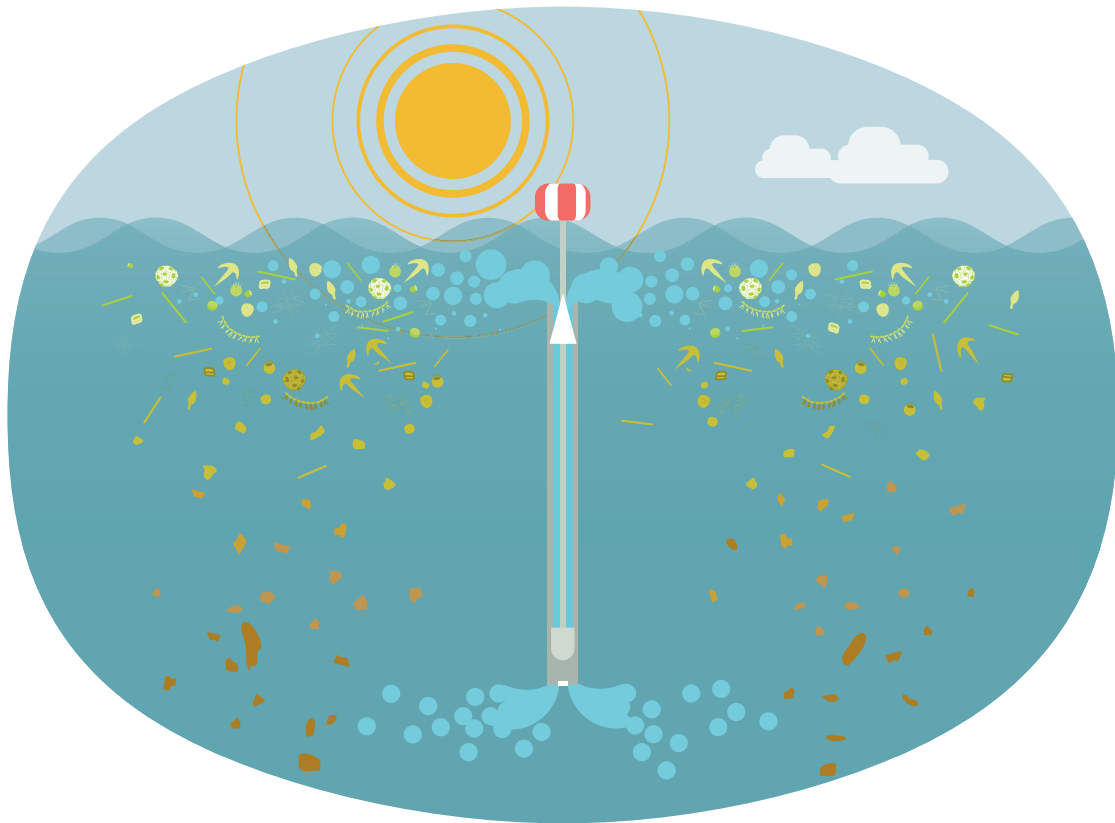# The influence of artificial upwelling on the efficiency of the biological carbon pump

Dissertation

zur Erlangung des Doktorgrades

– Dr. rer. nat. –

der Mathematisch-Naturwissenschaftlichen Fakultät

der Christian-Albrechts-Universität zu Kiel

vorgelegt von

Moritz Baumann

Kiel, 2022

Title page illustration:
Rita Erven, OceanNETs / GEOMAR (modified)

Contents

Zusammenfassung

Um die globale Erwärmung auf 1,5-2° C zu begrenzen, wie im Pariser Klimaabkommen zugesagt, wird die Reduzierung der Kohlendioxidemissionen (CO_2) allein nicht ausreichen. Um einen Netto-Null-Ausstoß an CO_2 zu erreichen, werden Technologien benötigt werden, die aktiv CO_2 aus der Atmosphäre entfernen. Einige solcher Technologien zielen darauf ab, die Kohlenstoff-Speicherkapazität des Ozeans zu erhöhen, indem man die biologische Kohlenstoffpumpe verstärkt. Diese bewirkt den Transport des in der euphotischen Zone produzierten organischen Kohlenstoffs in die Tiefsee. Eine Idee, die Effizienz der biologischen Pumpe zu erhöhen, ist es, mithilfe von künstlichem Auftrieb nährstoffreiches Tiefenwasser an die Oberfläche zu pumpen, um die Primärproduktion und damit den Kohlenstoffexport zu steigern.

Das Hauptziel dieser Doktorarbeit ist es, zu verstehen, wie künstlicher Auftrieb die Parameter beeinflusst, die die Effizienz der biologischen Kohlenstoffpumpe steuern. Dafür wurde künstlicher Auftrieb in schwimmenden experimentellen Testanlagen, so genannten Mesokosmen, simuliert und die ökologischen und biogeochemischen Reaktionen natürlicher Plankton-gemeinschaften über mehrere Wochen beobachtet. Diese Arbeit umfasst drei experimentelle Mesokosmenstudien. Zwei davon untersuchten die Auswirkungen von künstlichem Auftrieb auf eine oligotrophe Planktongemeinschaft vor Gran Canaria im subtropischen Nordatlantik. Die dritte Studie simulierte natürlichen Auftrieb vor Peru, wo die dort lebenden Organismen an regelmäßige Impulse von kaltem, nährstoffreichem Tiefenwasser gewöhnt sind.

Unsere Experimente zeigten, dass der künstliche Auftrieb zu erheblichen Veränderungen in der Zusammensetzung der Phytoplanktongemeinschaft führt, die Primärproduktivität anregt und folglich den Partikelexport erhöht. Darüber hinaus wurde das Kohlenstoff-Stickstoff-Verhältnis (C:N) des absinkenden organischen Materials erhöht, was eine Voraussetzung für die Versenkung von atmosphärischem Kohlendioxid durch künstlichen Auftrieb ist. Allerdings wurden die exportierten Partikel im Allgemeinen schneller abgebaut und sanken langsamer als ohne Auftrieb. Künstlicher Auftrieb erhöht also den Umfang des Kohlenstoffflusses, scheint aber gleichzeitig die Effizienz zu verringern, mit der organisches Material von der Oberfläche ins Innere des Ozeans transportiert wird. Wir fanden heraus, dass die Stärke dieser gegenläufigen Effekte von der Gesamtmenge der zugeführten Nährstoffe, ihrer elementaren Stöchiometrie und davon abhängt, ob der Auftrieb kontinuierlich oder als einmaliger Puls erfolgt ist. Die Auswirkungen des Auftriebs auf die peruanische Planktongemeinschaft waren im Vergleich zu denen auf die oligotrophe kanarische Gemeinschaft weniger stark. Dies lag wahrscheinlich daran, dass die Organismen bereits an den Auftrieb angepasst waren und zudem die Menge der zugeführten Nährstoffe geringer war als bei den vor Gran Canaria durchgeführten Experimenten.

Im letzten Teil dieser Arbeit gehe ich der Frage nach, ob der erhöhte Kohlenstofffluss an der Oberfläche oder die verringerte Transfereffizienz im Hinblick die Kohlenstoffflüsse in der Tiefsee von größerer Bedeutung ist. Durch Extrapolation der experimentell gemessenen Kohlenstoff-flüsse in die Tiefe zeige ich, dass Änderungen der Transfereffizienz mit zunehmender Tiefe wichtiger werden könnten als Änderungen des Kohlenstoffexports an der

Oberfläche. Da Kohlenstoff relativ tief sinken muss, um langfristig sequestriert zu werden, deuten meine Ergebnisse darauf hin, dass relativ hohe Transfereffizienzen erforderlich sind, um eine CO_2-Bindung über längere Zeiträume zu erreichen.

Die Ergebnisse dieser Arbeit könnten in künftige Modellierungsstudien einfließen, indem der künstliche Auftrieb so parametrisiert wird, dass er sowohl das Verhältnis von sinkendem Kohlenstoff zu Nährstoffen, als auch die Abbauraten des sinkenden Materials erhöht. Zudem müssen die Kohlenstoffflüsse in die Tiefsee als Reaktion auf künstlichen Auftrieb in Versuchen im offenen Ozean getestet werden, um eine realistische Einschätzung des CO_2-Bindungspotenzials zu ermöglichen.

Summary

To limit global warming to between 1.5-2° C as committed in the Paris Climate Agreement, reducing carbon dioxide (CO_2) emissions alone will not suffice. Negative emission technologies, which actively remove CO_2 from the atmosphere, will be needed to achieve net zero CO_2 emissions. Some of these approaches aim at increasing the ocean's storage capacity by strengthening the carbon flux from the air-sea-interface to the deep ocean. One component of this flux is the biological carbon pump, which constitutes the transport of organic carbon produced in the euphotic zone to the deep ocean. Artificial upwelling seeks to enhance the efficiency of the biological carbon pump by pumping up nutrient-rich deep ocean water to the surface layer with the goal of enhancing primary production and hence, carbon export.

The major aim of this doctoral thesis is to get an understanding of how artificial upwelling affects parameters that control the efficiency of the biological carbon pump. Therefore, upwelling was simulated inside large pelagic enclosures, so called mesocosms, and the resulting ecological and biogeochemical responses of the plankton community were monitored over multiple weeks. This work comprises three experimental mesocosm studies. Two of them examined the effects of artificial upwelling on an oligotrophic plankton community off of Gran Canaria in the subtropical North Atlantic. The third simulated natural upwelling in the Peruvian Upwelling System, where organisms are used to regular pulses of cold, nutrient-rich deep waters.

Our experiments showed that artificial upwelling causes substantial shifts in the phytoplankton community composition, stimulates primary productivity and consequently enhances particulate matter export. In addition, it elevated the carbon to nitrogen (C:N) ratios of sinking organic matter, which is a prerequisite for carbon dioxide removal through artificial upwelling. On the other hand, exported particles were generally degraded more quickly and sank slower than without upwelling. Artificial upwelling hence increases the carbon flux magnitude but simultaneously seems to decrease the efficiency, with which organic matter is transferred from the surface to the ocean interior. We found that the strength of these counteracting effects was dependent on the total amount of supplied nutrients, their elemental stoichiometry and on whether upwelling was applied continuously or as a one-time fertilization. The impacts of upwelling on the Peruvian plankton community were less intense compared to the ones on the oligotrophic Canarian community. This was probably because the organisms were already adapted to upwelling and the amount of supplied nutrients was lower than in the experiments conducted off of Gran Canaria.

In the final part of this thesis, I address the question whether the increased surface carbon flux or the decreased transfer efficiency is more important with respect to deep ocean carbon fluxes. By extrapolating the experimentally measured carbon fluxes to depth, I show that changes in transfer efficiency might become more important with depth than changes in surface carbon export. Since carbon needs to sink relatively deep in order to be sequestered long-term, my results imply that relatively high transfer efficiencies are needed to achieve CO_2 removal over longer time scales.

The findings of this thesis could inform future modelling studies by parameterizing artificial upwelling to enhance sinking matter carbon to nutrient ratios while at the same time enhancing

degradation rates. Finally, carbon fluxes to the deep ocean as a response to artificial upwelling need to be assessed in open ocean trials in order to enable a realistic assessment of its CO_2 removal potential.

1 Introduction

1.1   The need for carbon dioxide removal

The need for action to fight the ongoing climate change is nowadays more apparent than ever. Although decarbonization efforts during the last decade have somewhat slowed down the increase of yearly greenhouse gas emissions, emissions are still growing and carbon dioxide concentrations in the atmosphere keep on rising (Friedlingstein et al., 2022). The growing global energy demand requires further massive reductions of CO_2 emissions in order to meet the agreed upon temperature goals of the Paris agreement. However, decarbonization alone will not suffice to reach net zero emissions. There are future emissions that will be difficult or impossible to avoid, and that will need to be actively removed from the atmosphere. Such carbon dioxide removal (CDR) will be required at a scale of hundreds of gigatons during the 21st century in order to limit global warming to 1.5 °C (IPCC, 2018).

Currently, the severity of anthropogenic perturbations of the global carbon cycle is buffered by the increased carbon uptake of other planetary reservoirs. Of the 9.5 Gt C of yearly fossil fuel emissions that were released into the atmosphere during the last decade, roughly 3 Gt C were taken up by both the land and the ocean sink (**Fig. 1.1**). The ocean is by far the largest non-geological carbon reservoir, and stores the additional anthropogenic carbon via two different pathways. Firstly, carbon is taken up physically via the influx of atmospheric CO_2 at the ocean-atmosphere interface and its subsequent vertical transport via sinking water masses ("solubility pump", Volk and Hoffert, 2013). Secondly, unicellular primary producers take up dissolved CO_2, which is subsequently transported to the ocean's interior via different biologically-mediated pathways (Boyd et al., 2019). Strengthening this "biological carbon pump" is one way to potentially remove additional large amounts of carbon from the atmosphere and store it in the ocean.
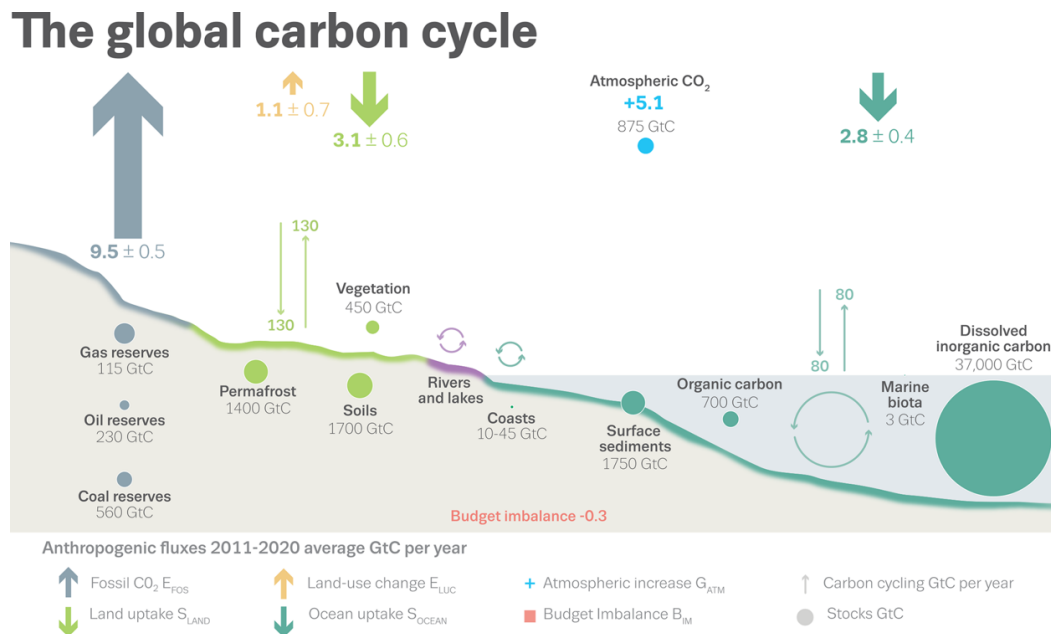
Figure 1.1. The global carbon cycle for the decade 2011–2020 with emphasis on anthropogenic perturbations. Fluxes of the active natural carbon cycle are depicted by narrow arrows in the background, whereas perturbations stemming from globally averaged anthropogenic activities are displayed by bold arrows. Figure taken from Friedlingstein et al. (2022).
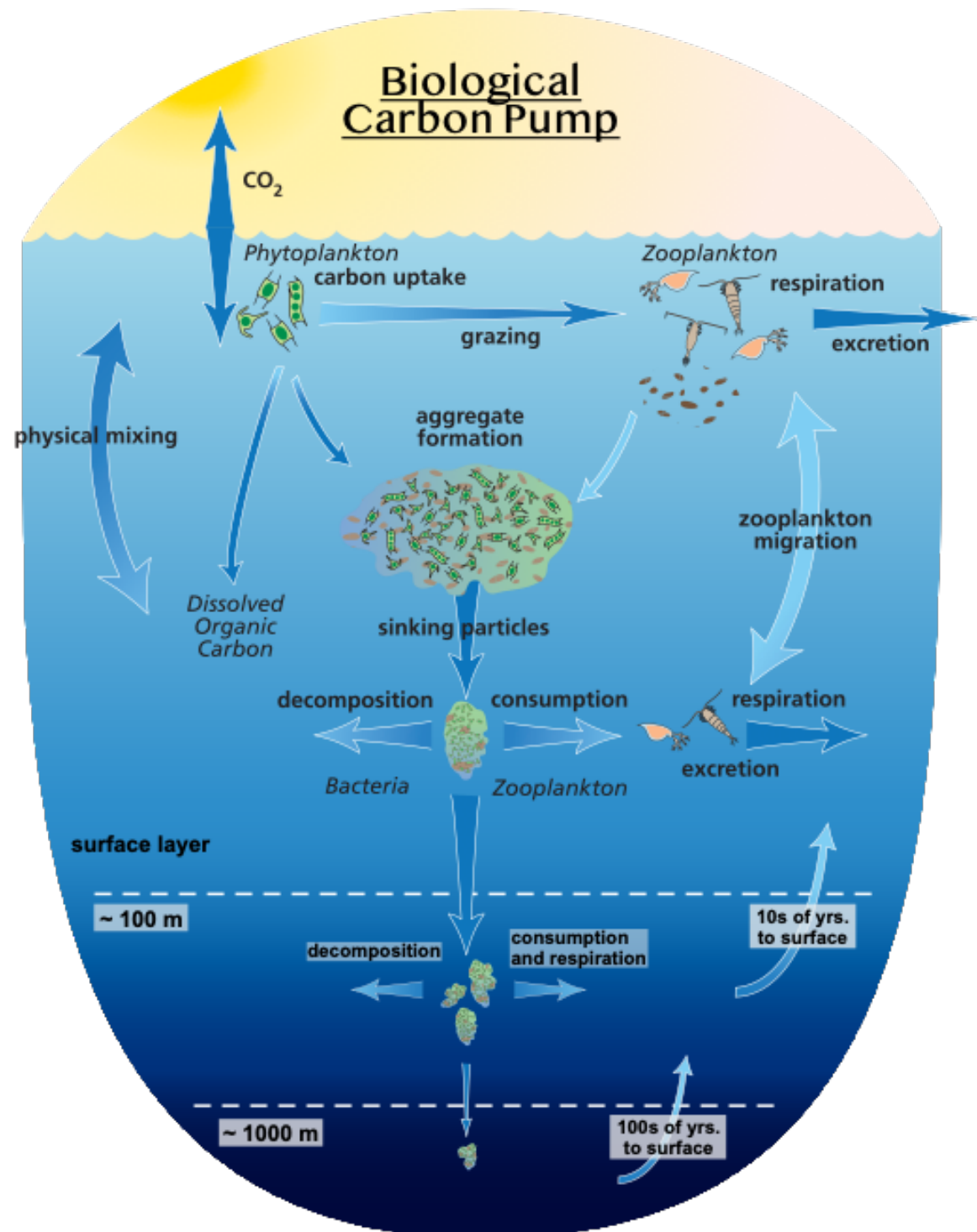
1.2   The biological carbon pump

The basis of the biological carbon pump is photosynthetic primary production. Phytoplankton in the sunlit surface layer of the pelagic ocean (i.e. euphotic zone) take up CO_2 and use it to build their cell structures. By assimilating CO_2 from the surrounding seawater, they promote the influx of additional atmospheric CO_2 at the ocean-atmosphere interface. The carbon incorporated into the organic matter of the microalgae and photosynthesizing bacteria (particulate organic carbon, POC) is now part of the pelagic food web. In there, it can turn to detritus when the phytoplankton cells die from nutrient deprivation or viral lysis. Phytoplankton cells and small particles collide and form aggregates by means of physical coagulation (Jackson, 1990), especially when the density of suspended detritus is high (Logan et al., 1995). As soon as these aggregates become negatively buoyant, either by sheer size or because their incorporated materials increase their density over that of the surrounding seawater (i.e. excess density), they start to sink.

The fixed carbon inside the phytoplankton cells can, however, also be channeled to higher trophic levels, either via direct consumption by zooplankton or via a detour through the "microbial loop". In the latter case, dissolved organic matter (DOM) originating from phytoplankton acts as fuel for microbial growth. The microbes are consumed by predatory protists, which are in turn preyed upon by larger zooplankton (Azam et al., 1983). Whichever way the carbon takes, finally it will partly be respired in the consuming organisms, while another part will be sent on its way to depth in the form of particulate excrements, crustacean molts (exoskeletons) or zooplankton carcasses (Steinberg and Landry, 2017; Turner, 2002). Zooplankton fecal pellets are an important, albeit variable component of the biological carbon pump. They are diverse in size, shape and composition, and most often contribute no more than ~40 % to the total flux (Turner, 2015). Additionally, zooplankton actively transport significant amounts of carbon to depth in their diel vertical migrations (Boyd et al., 2019): they ingest POC in the surface during the night and emit it as respired CO_2, excreted dissolved organic carbon (DOC) or egested fecal pellets in the mesopelagic zone, where they reside during day-time (Turner, 2015).

Marine particles can thus be composed of a variety of different materials, such as organic cell debris, intact phytoplankton cells, zooplankton excrements and carcasses, microbes, transparent exopolymer particles (TEP), as well as litho- and biogenic minerals, either produced by marine organisms or provided via winds from terrestrial sources (see Durkin et al., 2021 for a selection of different particle types). All of this is incorporated in the term "particulate matter". On their way to depth, marine particles become the subject of different forms of consumption (**Fig. 1.2**). Possibly, zooplankton will intercept them in the mesopelagic ocean to feed on them (Steinberg and Landry, 2017). They fragment aggregates to smaller particles, repackage material into fecal pellets and respire carbon, generally attenuating the POC flux. Quite certainly, the particles will have passengers travelling with them. Heterotrophic microbes populate sinking particles and remineralize the organically bound carbon, thereby respiring CO_2. These biological flux attenuation processes are the main reason for why only a small fraction of sinking particles reaches the deep ocean. There, the sinking POC is either buried in the sediments of the ocean floor or it is consumed by the local living fauna. The respired carbon along the way is 'locked' inside the water parcel it resides in. It

becomes a subject of ocean currents, of up- and downwelling, and remains out of touch with the atmosphere until the respective water parcel is transported back up to the surface. Depending on where and how deep the carbon was respired, it might remain sequestered (i.e. stored) in the ocean interior for decades to centuries (DeVries et al., 2012).

Figure 1.2. Overview of the biological carbon pump. Figure modified from the U.S. Joint Global Ocean Flux Study (JGOFS).

This biological uptake of carbon and its transport to depth causes a vertical gradient of dissolved inorganic carbon (DIC, i.e. CO_2, carbonate and bicarbonate) in our oceans. DIC is less abundant at the surface, where it is taken up, and more abundant in the deep ocean, where it is regenerated (Sarmiento, 1993). Because the ocean biology causes the transport of DIC against this gradient, it is considered a "pump". Without it, atmospheric CO_2 concentrations would be considerably higher than what they are.

1.2.1   Efficiency of the biological carbon pump

How much carbon the biological carbon pump transports to the deep ocean each year depends on the strength of the export flux and the efficiency with which carbon is transferred to depth (DeVries et al., 2012). Global estimates are variable and range from 5 to >12 Gt C per year (Boyd and Trull, 2007; Falkowski, 1998; Henson et al., 2011). One important metric for its strength is the export production (EP), which is the POC flux at the base of the euphotic zone. The ratio of export production over primary production (PP) thus describes the export efficiency of primary produced matter from the sunlit surface ocean, and is termed e- or Ez-ratio (e.g. Buesseler et al., 2020).

$$Ez - ratio = \frac{F_{z_0}}{PP} \tag{1.1}$$

where F is the POC flux at the base of the euphotic zone (z_0). This ratio indicates how much of the produced organic matter exits the surface ocean and starts its journey to depth. In order to estimate the POC flux attenuation between the base of the euphotic zone to the deep sea, Martin et al. (1987) used sediment traps deployed at different depths in the North-East Pacific Ocean to estimate flux attenuation profiles. They found that their collected data were best described using a power law function.

$$F_z = F_{z_0} * \left(\frac{z}{z_0}\right)^{-b} \tag{1.2}$$

where z is the respective depth z and the exponent b defines the strength of the flux attenuation, which they calculated to be ~0.86 for their data set. Since then, it has become clear that the factor b strongly varies throughout time and space (e.g. between 0.6 and 2.0, Berelson, 2001; Francois et al., 2002), and no single universal number can be assumed for realistic POC flux estimates on larger spatial or temporal scales (Henson et al., 2012; Marsay et al., 2015). This "Martin Curve" has since likely become the most common approach to estimate POC fluxes to the deep ocean, and it has been continuously improved over the years (e.g. Buesseler et al., 2020).

There are a variety of drivers that determine the magnitude of export production and the shape of the flux attenuation curve (i.e. Martin's b), and thus the strength and efficiency of the biological carbon pump. Firstly, export production is controlled by the amount of organic matter produced by phytoplankton in the euphotic zone, which is in turn bottom-up controlled by abiotic factors (light, nutrients) and top-down controlled by primary consumers. How much of the primary produced POC starts to sink depends on aggregation and disaggregation processes occurring in the euphotic zone. These processes are controlled by physical (e.g. coagulation or turbulence), biochemical (particle composition, TEP abundance) and biological (modulation by heterotrophs) factors (Burd and Jackson, 2009; KiØrboe, 2000; Taucher et al.,

2018). The plankton community composition has been found to play a particularly important role in defining the properties of sinking particles, which in turn affect how deep they will sink before their organically bound carbon is released back to the inorganic carbon pool (Bach et al., 2019; Henson et al., 2012; Iversen and Ploug, 2010; Legendre and Rivkin, 2002; Turner, 2015).

The efficiency with which POC is exported and transferred to depth depends on how fast it sinks and the rate at which it is degraded (Marsay et al., 2015). The variability in remineralization rate and sinking velocity is in turn controlled by a variety of factors. Microbial remineralization is mainly controlled by temperature, with degradation rates decreasing ~1.5–3-fold per 10 °C temperature decrease (Laufkötter et al., 2017; Marsay et al., 2015; Matsumoto, 2007). Since temperatures in the open ocean decrease with depth, this is one mechanism that likely leads to the decrease of flux attenuation with depth (Boyd and Trull, 2007). The oxygen concentration also seems to play a role, although seemingly a minor one (Boyd and Trull, 2007; Devol and Hartnett, 2001; Laufkötter et al., 2017). Sinking velocity, on the other hand, is mainly determined by the properties of the sinking particle. Particle size plays a major role (Alldredge and Gotschalk, 1988; Ploug and Grossart, 2000), as well as porosity, i.e. the fraction of particle volume occupied by seawater (Laurenceau-Cornec et al., 2020). Particle density is influenced by a particle's composition, for which mineral ballasting is key (Armstrong et al., 2002; Francois et al., 2002; Klaas and Archer, 2002; Laurenceau-Cornec et al., 2020), as well as the contribution of TEP (De La Rocha and Passow, 2007; Mari et al., 2017; Passow, 2002). Community structure (Boyd and Newton, 1999), fragmentation (Briggs et al., 2020) and zooplankton-mediated processes (Steinberg and Landry, 2017) can affect both sinking velocity and degradation rates. The POC transfer efficiency is generally higher in tropical than in high latitude ecosystems (Francois et al., 2002; Henson et al., 2012). This is presumably due to differences in ecosystem structure, with high episodic fluxes in high latitudes consisting of more labile material than the low amount of recycled material sinking out of regenerative systems in for instance the subtropical gyres.

It should be noted here that the gravitational sinking of particles is but one of multiple transportation pathways for organic carbon to the deep ocean. There are other modes of transport from the epi- to the mesopelagic zone and below, e.g. physical subduction mechanisms or biologically mediated transport like diurnal or seasonal vertical migration of zooplankton and fish (Boyd et al., 2019). Nonetheless, the sequestration pathway of sinking particles is the largest component of the biological gravitational carbon pump (Boyd et al., 2019; Buesseler et al., 2020). Strengthening this carbon transportation pathway, e.g. via fertilization with growth-limiting nutrients, is the idea of multiple ocean-based CDR technologies.

1.3   Artificial upwelling as CO_2 removal technique

One such technology to remove anthropogenic CO_2 from the atmosphere is artificial upwelling (Lovelock and Rapley, 2007). By transporting cold, nutrient- and DIC-rich deep water to the warm, nutrient-scarce and sunlit surface ocean, phytoplankton growth is stimulated, which enhances export production and strengthens the biological carbon pump

(**Fig. 1.3**). The fertilization of open ocean nutrient-limited regimes should theoretically result in a community shift from small to large, fast-sinking phytoplankton and hence increase export efficiency (Karl and Letelier, 2008). By sequestering additional carbon in the deep sea, the oceanic uptake of atmospheric CO_2 would be enhanced, leading to net carbon dioxide removal. Ideally, the sequestered carbon would remain in the deep ocean for centuries before ocean currents carry it up to the surface, where it is released back to the atmosphere.
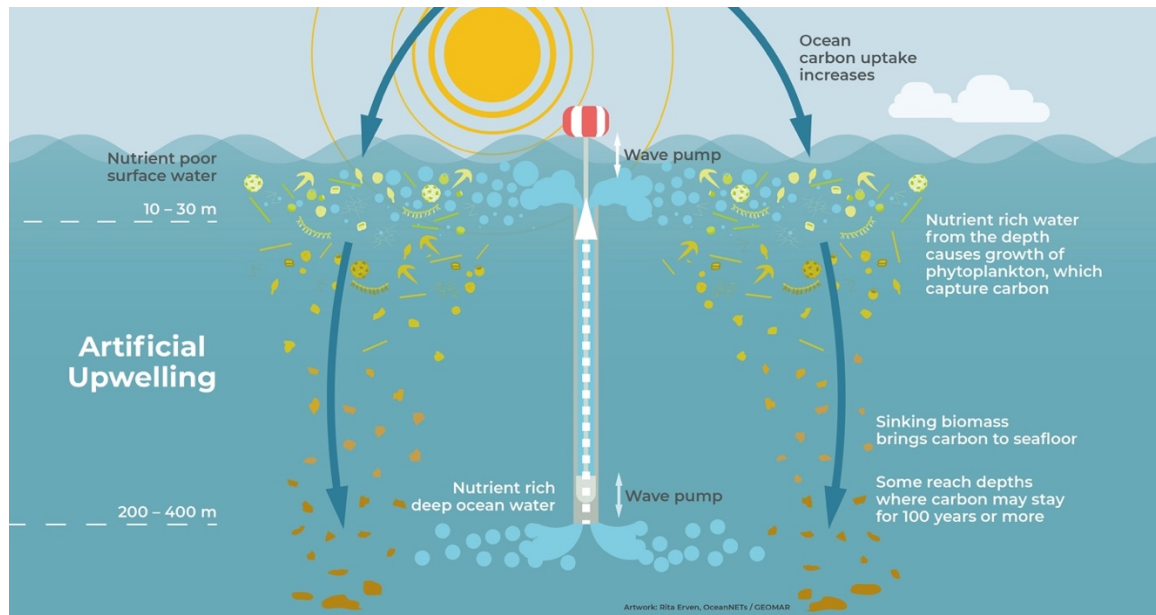
Figure 1.3. The concept of artificial upwelling as a carbon removal technique with a wave pump as upwelling device. Artwork: Rita Erven, OceanNETs, GEOMAR Helmholtz-Centre for Ocean Research Kiel.

Although the idea of fertilizing the surface ocean with artificial upwelling has been around for half a century (Roels et al., 1970), our knowledge about its efficiency and applicability is limited. We know that there are multiple technologies that can lift up water masses in order to achieve artificial upwelling. Thus far, wave pumps (e.g. White et al., 2010) and electrical pumps (Ouchi et al., 2005) have been tested, as well as air-lift and air-bubble pumps (Handå et al., 2013; Liang and Peng, 2005; McClimans et al., 2010) and the perpetual salt fountain (Maruyama et al., 2011). Wave pumps have the advantage that they operate without external energy sources (Isaacs et al., 1976). It has also been shown that surface primary production can be stimulated using artificial upwelling devices (Aure et al., 2007; Casareto et al., 2017; Giraud et al., 2016; Masuda et al., 2010; McClimans et al., 2010; Strohmeier et al., 2015). However, to our knowledge no experimental study has thus far assessed the resulting vertical carbon fluxes. Studies monitoring the fate of the upwelled nutrients and the associated assimilated carbon are hence an important next step in artificial upwelling research.

Multiple modeling studies have simulated artificial upwelling in the last two decades. They generally agree that the technique is no efficient tool for large-scale carbon sequestration (Dutreuil et al., 2009; Keller et al., 2014; Oschlies et al., 2010; Yool et al., 2009), partly because it would require a massive deployment of pumps in order to sequester carbon on climate-relevant (Gt) scales (Yool et al., 2009). However, such models are often not able to accurately capture the complex ecological and biogeochemical responses to oceanic water movements.

They allow for a relatively low level of ecological and biogeochemical complexity. For example, variable nutrient stoichiometries and properties of sinking particles can often not be resolved to a sufficient degree.

What is thus needed for a thorough examination of artificial upwelling as CDR technique are experimental studies assessing the downward flux of POC and associated nutrients and the flux attenuation with depth (National Academies of Sciences, Engineering, and Medicine, 2021). These empirical results then need to be incorporated into existing artificial upwelling models in order to reevaluate previous modeling efforts using a more evidence-based approach. Also the environmental risks and potential co-benefits need to be studied experimentally before companies or other stakeholders start to commercially apply this technique on a grand scale.

1.3.1   CDR efficiency of artificial upwelling

The biogeochemical properties of the upwelled source water have a high impact on the CDR efficiency of artificial upwelling (see e.g. Karl and Letelier, 2008). Artificially upwelled deep water contains more DIC than the surface water, which can potentially outgas to the atmosphere and needs to be compensated for. The difference between the DIC concentration in the upwelled compared to the surface water (excess DIC) directly affects the CDR efficiency of artificial upwelling. Hence, to create a net carbon sink, the amount of carbon sequestered via the biological carbon pump needs to surpass the amount of excess DIC (Pan et al., 2016). Naturally, also technical emissions occurring during manufacturing, transportation or operation of the upwelling device would need to be compensated for. Here however, I focus on emissions resulting from natural mechanisms. In the following, we want to describe some of the physical, biogeochemical and ecological factors that control both the upwelled excess DIC and the carbon sequestration.

The amount of DIC in the upwelled water has a direct negative effect on the net CO_2 removal. DIC concentrations increase with the "age" of the water, i.e. the time since it has last been in contact with the atmosphere, and thus vary across ocean regions (Gao et al., 2022; e.g. Thomas and Ittekkot, 2001). Moreover, the nutrient quantity and composition in the upwelled source water governs the response of the surface community. The quantities of nitrate and phosphate determine the upper limit of primary production and affect the phytoplankton community structure (Villamaña et al., 2019). Additionally, primary producers can assimilate carbon at higher than Redfield stoichiometries (C:N ratio >6.6, Redfield et al., 1963), which further promotes the carbon sequestration potential. The relative contribution of nitrate, phosphate and silicic acid in the upwelled water controls the phytoplankton community composition (Makareviciute-Fichtner et al., 2020; Sommer, 1994; Vrede et al., 2009). In a eutrophic system, silicic acid (Si) replete conditions will allow diatoms to thrive and become the dominant group, whereas flagellates are likely to occupy this role under Si scarcity (Sommer, 1994). As stated earlier, the plankton community composition in turn shapes the properties of sinking particles and thereby their sequestration depth, as well as the export magnitude and C:N stoichiometry (Taucher et al., 2021). Consequently, the location at which artificial upwelling is carried out and the depth from which the upwelled water originates need to be considered, as both nutrient stoichiometry and DIC content vary with region and depth (Karl and Letelier, 2008).

The net CO_2 removal potential also depends on how artificial upwelling is carried out. The frequency and intensity at which the nutrients are provided affect the responses of the plankton community composition and succession (Jakobsen et al., 2015; Leibold et al., 1997). The amount of upwelled water does not only stimulate primary productivity, it also dilutes the plankton community, thereby thinning out the seed population and prolonging its response time. Also the mode with which surface communities are fertilized plays a role. Continuous deep water fertilization results in sustained increased primary productivity (Aure et al., 2007; Strohmeier et al., 2015) and likely in increased POC flux over long timescales. This promotes a match-scenario between phyto- and zooplankton, in which surface remineralization is increased and zooplankton contributes significantly to the export flux. Sporadic upwelling pulses, on the other hand, resemble spring-bloom like conditions with sudden and rapid phytoplankton blooms followed by episodic export events (Sanders et al., 2014). Such POC fluxes are usually not modified by zooplankton and consist mainly of detritus and phytoplankton cells (Martin et al., 2011).

The effect of different deep water sources and the associated nutrient stoichiometries as well as different modes and intensities of artificial upwelling need to be tested in order to investigate under which circumstances this technique could be deployed effectively as negative emission technology. Thereby, studies need to carefully assess the vertical particle flux in order to estimate the potential for carbon dioxide removal via the biological pump.

1.4   Linking particle fluxes to plankton communities

To study the effects of artificial upwelling on the efficiency of the biological pump, an enclosed or semi-enclosed system is advantageous. In the open ocean, sinking matter does not only move vertically, but also horizontally. This lateral advection makes it difficult to monitor organic matter fluxes originating from a specific surface community. Additionally, most of the exported particles are degraded before they reach the sequestration depth, and the respired nutrients and DIC are recycled in the surface. Hence, the time scales between the upwelling of new nutrients and their sequestration in the form of sinking matter can be highly variable. Consequently, screening the fate of upwelled DIC and nutrients in an open ocean with one temporal plus three spatial dimensions is extremely challenging. This can be facilitated by working in systems with smaller and fewer dimensions. Semi-enclosed water bodies such as fjords can facilitate experimental research that involves the movement of water masses and fluxes of dissolved and particulate matter. For example, studies focusing on the potential of artificial upwelling for aquacultural applications have been carried out in Norwegian fjords (Aure et al., 2007; Handå et al., 2013; Strohmeier et al., 2015). Even more experimental control can be exerted using fully enclosed water bodies inside mesocosm systems (**Fig. 1.4**).

Pelagic mesocosms are experimental enclosures designed for working with natural plankton communities. They include all trophic levels up to secondary consumers (small pelagic fish larvae and jellyfish) and integrate their interactions and ecological responses. They offer the possibility to characterize and quantify biogeochemical pools, e.g. dissolved and particulate matter, and allow for the differentiation of suspended and sinking matter (Boxhammer et al., 2018). Cone-shaped sediment traps at the bottom of some mesocosm designs (e.g. KOSMOS

mesocosms, Riebesell et al., 2013) collect sinking particles and allow for accurate quantitative analysis of vertical element fluxes (Boxhammer et al., 2016). Furthermore, regular sampling of settling particles allows for sinking velocity and degradation rate measurements (Bach et al., 2019), and sinking particle properties such as size or porosity can be measured *in* and *ex situ* using optical measurement devices (Bach et al., 2012; Taucher et al., 2018).

Research in the recent years has shown that the plankton community composition is a key driver of vertical organic matter fluxes (see Section 1.2.1). Mesocosms have the advantage of enclosing a community in a defined space and prohibit lateral advection, meaning that the resulting sinking matter fluxes can directly be linked to the overlaying plankton community. Both the community and the export relevant parameters can be sampled repeatedly over long time scales (i.e. multiple months, see Bach et al., 2016), making mesocosms an ideal tool for monitoring temporal developments. They combine the advantages of sediment traps and controlled experimental setups, making them a useful tool to study the biogeochemical and ecological responses of a pelagic system to natural or artificial upwelling.
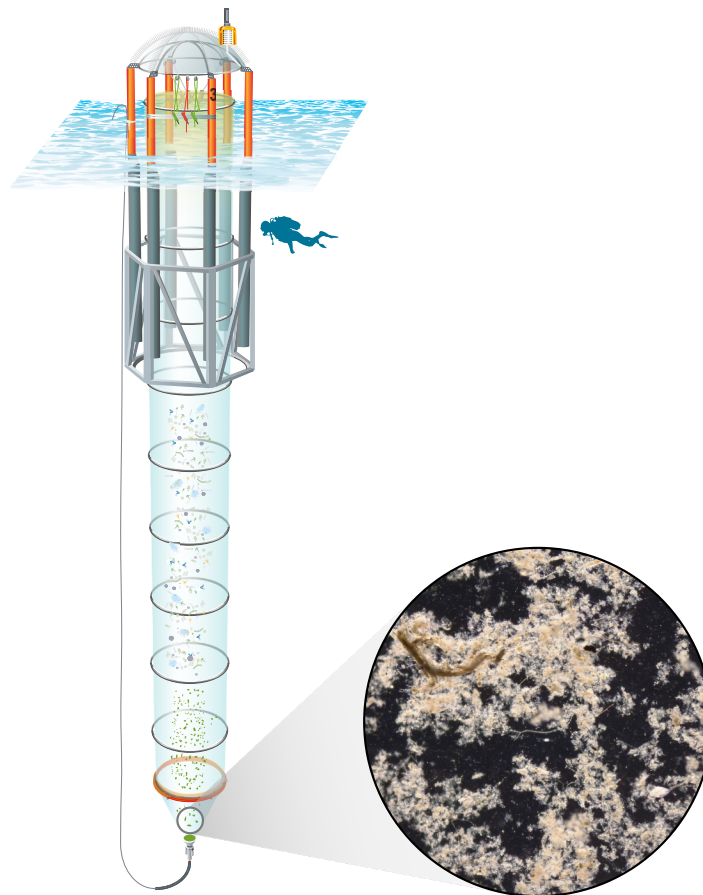
Figure 1.4. Kiel Off-Shore Mesocosm for Ocean Simulation (KOSMOS) and sedimented matter from a mesocosm sediment trap. Technical artwork modified from Rita Erven, OceanNETs, GEOMAR.

1.5   Thesis aims and outline

The following chapters of this dissertation include three first-author publications. This section states the overall aims of this doctoral thesis. It furthermore gives an overview of the research focus of each publication and provides information on the co-author contributions to the experimental design, data acquisition and manuscript writing.

1.5.1   Aims of this doctoral thesis

The overall aim of this doctoral thesis was to get an understanding of how artificial upwelling affects export related parameters and hence the efficiency of the biological carbon pump. Key variables include the magnitude of the export flux, its elemental composition and the characteristics of sinking particles, such as their settling velocity and the rate at which they are degraded. Moreover, some of the mechanisms driving the effects of artificial upwelling are identified. Particular emphasis thereby laid on the overlaying plankton community. By using an experimental setup consisting of pelagic mesocosms, links between export responses and changes in the plankton community composition were examined. As an analogue to artificial upwelling, natural upwelling was investigated using the same experimental approach. In the final part of this thesis, the effects of natural and artificial upwelling on the efficiency of the biological carbon pump are compared. Furthermore, the sequestration potential of artificial upwelling is discussed in the light of our experimental findings, as well as the most feasible artificial upwelling conditions for carbon dioxide removal.

1.5.2   Research focus of first-author publications

Publication I:

1) Investigating how the intensity of artificial upwelling (i.e. the mixing ratio of upwelled and surface water) scales with the buildup and export of particulate organic matter.
2) Comparing the effects of a singular upwelling pulse to a recurring form of upwelling on the community responses and resulting sinking particle characteristics.
3) Assessing how long an oligotrophic community needs to efficiently channel artificially upwelled new nutrients into export production.

Publication II:

1) Reporting particle sinking velocities measured in the Peruvian Upwelling System.
2) Identifying the drivers of sinking velocity in a pelagic community experiencing natural upwelling.
3) Determining the relative importance of the physical particle properties size, compactness and shape as drivers of sinking velocity.

Publication III:

1) Testing the effect of the nutrient composition in artificially upwelled water (Si relative to N) on export production and sinking particle properties.
2) Identifying the key processes controlling the efficiency with which artificially upwelled nutrients get channeled into export production in differently functioning diatom communities.
3) Re-evaluating the importance of biogenic silica as ballast or shielding material for sinking velocities and degradation rates, respectively.

1.5.3   Declaration of contribution

Publication I:

Idea and experimental design: Ulf Riebesell, Jan Taucher, Allanah J. Paul, Lennart T. Bach

Experimental work: Moritz Baumann, Jan Taucher, Allanah J. Paul, Malte Heinemann, Mari Vanharanta, Lennart T. Bach, Kristian Spilling, Joaquin Ortiz, Javier Arístegui, Nauzet Hernández-Hernández, Isabel Baños, Ulf Riebesell

Analysis of data: Moritz Baumann

Preparation of manuscript: Moritz Baumann with comments from co-authors

Publication II:

Idea and experimental design: Ulf Riebesell, Lennart T. Bach, Allanah J. Paul

Experimental work: Paul Stange, Lennart T. Bach, Minutolo Fabrizio, Ulf Riebesell, Allanah J. Paul

Analysis of data: Moritz Baumann and Silvan Goldenberg

Preparation of manuscript: Moritz Baumann with comments from co-authors

Publication III:

Idea and experimental design: Ulf Riebesell, Jan Taucher, Silvan Goldenberg

Experimental work: Moritz Baumann, Silvan Goldenberg, Jan Taucher, Mar Fernández-Méndez, Joaquin Ortiz, Ulf Riebesell

Analysis of data: Moritz Baumann

Preparation of manuscript: Moritz Baumann with comments from co-authors

List of first-author publications

Publication I:

Baumann, M., Taucher, J., Paul, A. J., Heinemann, M., Vanharanta, M., Bach, L. T., Spilling, K., Ortiz, J., Arístegui, J., Hernández-Hernández, N., Baños, I., and Riebesell, U.: Effect of Intensity and Mode of Artificial Upwelling on Particle Flux and Carbon Export, *Frontiers in Marine Science*, 8, 742142, 2021.

Publication II:

Baumann, M., Paul, A. J., Taucher, J., Bach, L. T., Goldenberg, S., Stange, P., Minutolo, F., Riebesell, U.: Drivers of Particle Sinking Velocities in the Peruvian Upwelling System, *Biogeosciences*, submitted.

Publication III:

Baumann, M., Goldenberg, S., Taucher, J., Fernández-Méndez, M., Ortiz, J., Haussmann, J., Riebesell, U.: Counteracting effects of nutrient composition (Si:N) on export flux under artificial upwelling. In preparation.

References

Alldredge, A.L., Gotschalk, C., 1988. In situ settling behavior of marine snow. Limnol. Oceanogr. 33, 339–351. https://doi.org/10.4319/lo.1988.33.3.0339

Armstrong, R.A., Lee, C., Hedges, J.I., Honjo, S., Wakeham, S.G., 2002. A new, mechanistic model for organic carbon fluxes in the ocean based on the quantitative association of POC with ballast minerals. Deep-sea Research Part II: Topical Studies in Oceanography. https://doi.org/10.1016/s0967-0645(01)00101-1

Aure, J., Strand, Ø., Erga, S., Strohmeier, T., 2007. Primary production enhancement by artificial upwelling in a western Norwegian fjord. Mar. Ecol. Prog. Ser. 352, 39–52. https://doi.org/10.3354/meps07139

Azam, F., Fenchel, T., Field, J.G., Gray, J.S., Meyer-Reil, L., Thingstad, F., 1983. The Ecological Role of Water-Column Microbes in the Sea. Mar. Ecol. Prog. Ser. 10, 257–263. https://doi.org/10.3354/meps010257

Bach, L.T., Riebesell, U., Sett, S., Febiri, S., Rzepka, P., Schulz, K.G., 2012. An approach for particle sinking velocity measurements in the 3–400 µm size range and considerations on the effect of temperature on sinking rates. Mar Biol 159, 1853–1864. https://doi.org/10.1007/s00227-012-1945-2

Bach, L.T., Stange, P., Taucher, J., Achterberg, E.P., Algueró-Muñiz, M., Horn, H., Esposito, M., Riebesell, U., 2019. The Influence of Plankton Community Structure on Sinking Velocity and Remineralization Rate of Marine Aggregates. Global Biogeochem. Cycles 33, 971–994. https://doi.org/10.1029/2019GB006256

Bach, L.T., Taucher, J., Boxhammer, T., Ludwig, A., The Kristineberg KOSMOS Consortium, Achterberg, E.P., Algueró-Muñiz, M., Anderson, L.G., Bellworthy, J., Büdenbender, J., Czerny, J., Ericson, Y., Esposito, M., Fischer, M., Haunost, M., Hellemann, D., Horn, H.G., Hornick, T., Meyer, J., Sswat, M., Zark, M., Riebesell, U., 2016. Influence of Ocean Acidification on a Natural Winter-to-Summer Plankton Succession: First Insights from a Long-Term Mesocosm Study Draw Attention to Periods of Low Nutrient Concentrations. PLoS ONE 11, e0159068. https://doi.org/10.1371/journal.pone.0159068

Berelson, W.M., 2001. The flux of particulate organic carbon into the ocean interior: A comparison of four US JGOFS regional studies. Oceanography 14, 59–67.

Boxhammer, T., Bach, L.T., Czerny, J., Riebesell, U., 2016. Technical note: Sampling and processing of mesocosm sediment trap material for quantitative biogeochemical analysis. Biogeosciences 13, 2849–2858. https://doi.org/10.5194/bg-13-2849-2016

Boxhammer, T., Taucher, J., Bach, L.T., Achterberg, E.P., Algueró-Muñiz, M., Bellworthy, J., Czerny, J., Esposito, M., Haunost, M., Hellemann, D., Ludwig, A., Yong, J.C., Zark, M., Riebesell, U., Anderson, L.G., 2018. Enhanced transfer of organic matter to higher

trophic levels caused by ocean acidification and its implications for export production: A mass balance approach. PLoS ONE 13, e0197502. https://doi.org/10.1371/journal.pone.0197502

Boyd, P.W., Claustre, H., Levy, M., Siegel, D.A., Weber, T., 2019. Multi-faceted particle pumps drive carbon sequestration in the ocean. Nature 568, 327–335. https://doi.org/10.1038/s41586-019-1098-2

Boyd, P.W., Newton, P.P., 1999. Does planktonic community structure determine downward particulate organic carbon flux in different oceanic provinces? Deep Sea Research Part I: Oceanographic Research Papers 46, 63–91. https://doi.org/10.1016/S0967-0637(98)00066-1

Boyd, P.W., Trull, T.W., 2007. Understanding the export of biogenic particles in oceanic waters: Is there consensus? Progress in Oceanography 72, 276–312. https://doi.org/10.1016/j.pocean.2006.10.007

Briggs, N., Dall'Olmo, G., Claustre, H., 2020. Major role of particle fragmentation in regulating biological sequestration of CO_2 by the oceans. Science 367, 791–793. https://doi.org/10.1126/science.aay1790

Buesseler, K.O., Boyd, P.W., Black, E.E., Siegel, D.A., 2020. Metrics that matter for assessing the ocean biological carbon pump. Proceedings of the National Academy of Sciences of the United States of America. https://doi.org/10.1073/pnas.1918114117

Burd, A.B., Jackson, G.A., 2009. Particle Aggregation. Annu. Rev. Mar. Sci. 1, 65–90. https://doi.org/10.1146/annurev.marine.010908.163904

Casareto, B.E., Niraula, M.P., Suzuki, Y., 2017. Marine planktonic ecosystem dynamics in an artificial upwelling area of Japan: Phytoplankton production and biomass fate. Journal of Experimental Marine Biology and Ecology 487, 1–10. https://doi.org/10.1016/j.jembe.2016.11.002

De La Rocha, C.L., Passow, U., 2007. Factors influencing the sinking of POC and the efficiency of the biological carbon pump. Deep Sea Research Part II: Topical Studies in Oceanography 54, 639–658. https://doi.org/10.1016/j.dsr2.2007.01.004

Devol, A.H., Hartnett, H.E., 2001. Role of the oxygen-deficient zone in transfer of organic carbon to the deep ocean. Limnol. Oceanogr. 46, 1684–1690. https://doi.org/10.4319/lo.2001.46.7.1684

DeVries, T., Primeau, F., Deutsch, C., 2012. The sequestration efficiency of the biological pump. Geophys. Res. Lett. 39. https://doi.org/10.1029/2012GL051963

Durkin, C.A., Buesseler, K.O., Cetinić, I., Estapa, M.L., Kelly, R.P., Omand, M.M., 2021. A Visual Tour of Carbon Export by Sinking Particles. Global Biogeochemical Cycles. https://doi.org/10.1029/2021gb006985

Dutreuil, S., Bopp, L., Tagliabue, A., 2009. Impact of enhanced vertical mixing on marine biogeochemistry: lessons for geo-engineering and natural variability. Biogeosciences 6, 901–912. https://doi.org/10.5194/bg-6-901-2009

Falkowski, P.G., 1998. Biogeochemical Controls and Feedbacks on Ocean Primary Production. Science 281, 200–206. https://doi.org/10.1126/science.281.5374.200

Francois, R., Honjo, S., Krishfield, R., Manganini, S., 2002. Factors controlling the flux of organic carbon to the bathypelagic zone of the ocean: Factors controlling organic carbon flux. Global Biogeochem. Cycles 16, 34-1-34–20. https://doi.org/10.1029/2001GB001722

Friedlingstein, P., Jones, M.W., O'Sullivan, M., Andrew, R.M., Bakker, D.C.E., Hauck, J., Le Quéré, C., Peters, G.P., Peters, W., Pongratz, J., Sitch, S., Canadell, J.G., Ciais, P., Jackson, R.B., Alin, S.R., Anthoni, P., Bates, N.R., Becker, M., Bellouin, N., Bopp, L., Chau, T.T.T., Chevallier, F., Chini, L.P., Cronin, M., Currie, K.I., Decharme, B., Djeutchouang, L.M., Dou, X., Evans, W., Feely, R.A., Feng, L., Gasser, T., Gilfillan, D., Gkritzalis, T., Grassi, G., Gregor, L., Gruber, N., Gürses, Ö., Harris, I., Houghton, R.A., Hurtt, G.C., Iida, Y., Ilyina, T., Luijkx, I.T., Jain, A., Jones, S.D., Kato, E., Kennedy, D., Klein Goldewijk, K., Knauer, J., Korsbakken, J.I., Körtzinger, A., Landschützer, P., Lauvset, S.K., Lefèvre, N., Lienert, S., Liu, J., Marland, G., McGuire, P.C., Melton, J.R., Munro, D.R., Nabel, J.E.M.S., Nakaoka, S.-I., Niwa, Y., Ono, T., Pierrot, D., Poulter, B., Rehder, G., Resplandy, L., Robertson, E., Rödenbeck, C., Rosan, T.M., Schwinger, J., Schwingshackl, C., Séférian, R., Sutton, A.J., Sweeney, C., Tanhua, T., Tans, P.P., Tian, H., Tilbrook, B., Tubiello, F., van der Werf, G.R., Vuichard, N., Wada, C., Wanninkhof, R., Watson, A.J., Willis, D., Wiltshire, A.J., Yuan, W., Yue, C., Yue, X., Zaehle, S., Zeng, J., 2022. Global Carbon Budget 2021. Earth Syst. Sci. Data 14, 1917–2005. https://doi.org/10.5194/essd-14-1917-2022

Gao, H., Cai, W.-J., Jin, M., Dong, C., Timmerman, A.H.V., 2022. Ocean Ventilation Controls the Contrasting Anthropogenic CO_2 Uptake Rates Between the Western and Eastern South Atlantic Ocean Basins. Global Biogeochemical Cycles 36. https://doi.org/10.1029/2021GB007265

Giraud, M., Boye, M., Garçon, V., Donval, A., de la Broise, D., 2016. Simulation of an artificial upwelling using immersed in situ phytoplankton microcosms. Journal of Experimental Marine Biology and Ecology 475, 80–88. https://doi.org/10.1016/j.jembe.2015.11.006

Handå, A., McClimans, T.A., Reitan, K.I., Knutsen, Ø., Tangen, K., Olsen, Y., 2013. Artificial upwelling to stimulate growth of non-toxic algae in a habitat for mussel farming. Aquac Res. https://doi.org/10.1111/are.12127

Henson, S.A., Sanders, R., Madsen, E., 2012. Global patterns in efficiency of particulate organic carbon export and transfer to the deep ocean: Export and Transfer Efficiency. Global Biogeochem. Cycles 26. https://doi.org/10.1029/2011GB004099

Henson, S.A., Sanders, R., Madsen, E., Morris, P.J., Le Moigne, F.A.C., Quartly, G.D., 2011. A reduced estimate of the strength of the ocean's biological carbon pump. Geophysical Research Letters. https://doi.org/10.1029/2011gl046735

Isaacs, J.D., Castel, D., Wick, G.L., 1976. Utilization of the energy in ocean waves. Ocean Engineering 3, 175–187. https://doi.org/10.1016/0029-8018(76)90022-6

Iversen, M.H., Ploug, H., 2010. Ballast minerals and the sinking carbon flux in the ocean: carbon-specific respiration rates and sinking velocity of marine snow aggregates. Biogeosciences 7, 2613–2624. https://doi.org/10.5194/bg-7-2613-2010

Jackson, G.A., 1990. A model of the formation of marine algal flocs by physical coagulation processes. Deep Sea Research Part A. Oceanographic Research Papers 37, 1197–1211. https://doi.org/10.1016/0198-0149(90)90038-W

Jakobsen, H.H., Blanda, E., Staehr, P.A., Højgård, J.K., Rayner, T.A., Pedersen, M.F., Jepsen, P.M., Hansen, B.W., 2015. Development of phytoplankton communities: Implications of nutrient injections on phytoplankton composition, pH and ecosystem production. Journal of Experimental Marine Biology and Ecology 473, 81–89. https://doi.org/10.1016/j.jembe.2015.08.011

Karl, D.M., Letelier, R.M., 2008. Nitrogen fixation-enhanced carbon sequestration in low nitrate, low chlorophyll seascapes. Mar. Ecol. Prog. Ser. 364, 257–268. https://doi.org/10.3354/meps07547

Keller, D.P., Feng, E.Y., Oschlies, A., 2014. Potential climate engineering effectiveness and side effects during a high carbon dioxide-emission scenario. Nat Commun 5, 3304. https://doi.org/10.1038/ncomms4304

KiØrboe, T., 2000. Colonization of marine snow aggregates by invertebrate zooplankton: Abundance, scaling, and possible role. Limnol. Oceanogr. 45, 479–484. https://doi.org/10.4319/lo.2000.45.2.0479

Klaas, C., Archer, D., 2002. Association of sinking organic matter with various types of mineral ballast in the deep sea: Implications for the rain ratio. Global Biogeochemical Cycles. https://doi.org/10.1029/2001gb001765

Laufkötter, C., John, J.G., Stock, C.A., Dunne, J.P., 2017. Temperature and oxygen dependence of the remineralization of organic matter. Global Biogeochem. Cycles 31, 1038–1050. https://doi.org/10.1002/2017GB005643

Laurenceau-Cornec, E.C., Le Moigne, F.A.C., Gallinari, M., Moriceau, B., Toullec, J., Iversen, M.H., Engel, A., De La Rocha, C.L., 2020. New guidelines for the application of Stokes' models to the sinking velocity of marine aggregates. Limnology and Oceanography 65, 1264–1285. https://doi.org/10.1002/lno.11388

Legendre, L., Rivkin, R.B., 2002. Fluxes of carbon in the upper ocean: regulation by food-web control nodes. Mar. Ecol. Prog. Ser. 242, 95–109. https://doi.org/10.3354/meps242095

Leibold, M.A., Chase, J.M., Shurin, J.B., Downing, A.L., 1997. Species Turnover and the Regulation of Trophic Structure. Annu. Rev. Ecol. Syst. 28, 467–494. https://doi.org/10.1146/annurev.ecolsys.28.1.467

Liang, N.-K., Peng, H.-K., 2005. A study of air-lift artificial upwelling. Ocean Engineering 32, 731–745. https://doi.org/10.1016/j.oceaneng.2004.10.011

Logan, B.E., Passow, U., Alldredge, A.L., Grossartt, H.-P., Simont, M., 1995. Rapid formation and sedimentation of large aggregates is predictable from coagulation rates (half-lives) of transparent exopolymer particles (TEP). Deep Sea Research Part II: Topical Studies in Oceanography 42, 203–214. https://doi.org/10.1016/0967-0645(95)00012-F

Lovelock, J.E., Rapley, C.G., 2007. Ocean pipes could help the Earth to cure itself. Nature 449, 403–403. https://doi.org/10.1038/449403a

Makareviciute-Fichtner, K., Matthiessen, B., Lotze, H.K., Sommer, U., 2020. Decrease in diatom dominance at lower Si:N ratios alters plankton food webs. Journal of Plankton Research 42, 411–424. https://doi.org/10.1093/plankt/fbaa032

Mari, X., Passow, U., Migon, C., Burd, A.B., Legendre, L., 2017. Transparent exopolymer particles: Effects on carbon cycling in the ocean. Progress in Oceanography 151, 13–37. https://doi.org/10.1016/j.pocean.2016.11.002

Marsay, C.M., Sanders, R.J., Henson, S.A., Pabortsava, K., Achterberg, E.P., Lampitt, R.S., 2015. Attenuation of sinking particulate organic carbon flux through the mesopelagic ocean. Proc. Natl. Acad. Sci. U.S.A. 112, 1089–1094. https://doi.org/10.1073/pnas.1415311112

Martin, J.H., Knauer, G.A., Karl, D.M., Broenkow, W.W., 1987. VERTEX: carbon cycling in the northeast Pacific. https://doi.org/10.1016/0198-0149(87)90086-0

Martin, P., Lampitt, R.S., Jane Perry, M., Sanders, R., Lee, C., D'Asaro, E., 2011. Export and mesopelagic particle flux during a North Atlantic spring diatom bloom. Deep Sea Research Part I: Oceanographic Research Papers 58, 338–349. https://doi.org/10.1016/j.dsr.2011.01.006

Maruyama, S., Yabuki, T., Sato, T., Tsubaki, K., Komiya, A., Watanabe, M., Kawamura, H., Tsukamoto, K., 2011. Evidences of increasing primary production in the ocean by Stommel's perpetual salt fountain. Deep Sea Research Part I: Oceanographic Research Papers 58, 567–574. https://doi.org/10.1016/j.dsr.2011.02.012

Masson-Delmotte, V., Zhai, P., Pörtner, H.-O., Roberts, D., Skea, J., Shukla, P.R., Pirani, A., Moufouma-Okia, W., Péan, C., Pidcock, R., Connors, S., Matthews, J.B.R., Chen, Y., Zhou, X., Gomis, M.I., Lonnoy, E., Maycock, T., Tignor, M., Waterfield, T., 2018. IPCC, 2018: Summary for Policymakers. Global Warming of 1.5°C. An IPCC Special Report on the impacts of global warming of 1.5°C above pre-industrial levels and related global greenhouse gas emission pathways, in the context of strengthening the global response to the threat of climate change, sustainable development, and efforts to eradicate poverty.

Masuda, T., Furuya, K., Kohashi, N., Sato, M., Takeda, S., Uchiyama, M., Horimoto, N., Ishimaru, T., 2010. Lagrangian observation of phytoplankton dynamics at an artificially enriched subsurface water in Sagami Bay, Japan. J Oceanogr 66, 801–813. https://doi.org/10.1007/s10872-010-0065-1

Matsumoto, K., 2007. Biology-mediated temperature control on atmospheric pCO$_2$ and ocean biogeochemistry. Geophys. Res. Lett. 34, L20605. https://doi.org/10.1029/2007GL031301

McClimans, T.A., Handå, A., Fredheim, A., Lien, E., Reitan, K.I., 2010. Controlled artificial upwelling in a fjord to stimulate non-toxic algae. Aquacultural Engineering. https://doi.org/10.1016/j.aquaeng.2010.02.002

National Academies of Sciences, Engineering, and Medicine, 2021. A Research Strategy for Ocean-based Carbon Dioxide Removal and Sequestration. National Academies Press, Washington, D.C. https://doi.org/10.17226/26278

Oschlies, A., Pahlow, M., Yool, A., Matear, R.J., 2010. Climate engineering by artificial ocean upwelling: Channelling the sorcerer's apprentice. Geophys. Res. Lett. 37. https://doi.org/10.1029/2009GL041961

Ouchi, K., Otsuka, K., Omura, H., 2005. Recent Advances of Ocean Nutrient Enhancer "TAKUMI" Project. Presented at the Sixth ISOPE Ocean Mining Symposium, Changsha, Hunan, China.

Pan, Y., Fan, W., Zhang, D., Chen, J.W., Huang, H., Liu, S., Jiang, Z., Di, Y., Tong, M., Chen, Y., 2016. Research progress in artificial upwelling and its potential environmental effects. Sci. China Earth Sci. 59, 236–248. https://doi.org/10.1007/s11430-015-5195-2

Passow, U., 2002. Transparent exopolymer particles (TEP) in aquatic environments. Progress in Oceanography 55, 287–333. https://doi.org/10.1016/S0079-6611(02)00138-6

Ploug, H., Grossart, H.-P., 2000. Bacterial growth and grazing on diatom aggregates: Respiratory carbon turnover as a function of aggregate size and sinking velocity. Limnol. Oceanogr 45, 1467–1475. https://doi.org/10.4319/lo.2000.45.7.1467

Redfield, A.C., Ketchum, B.H., Richards, F.A., 1963. The influence of organisms on the composition of seawater, in: The Composition of Seawater: Comparative and

Descriptive Oceanography. The Sea: Ideas and Observations on Progress in the Study of the Seas. Interscience Publishers: New York, pp. 26–77.

Riebesell, U., Czerny, J., von Bröckel, K., Boxhammer, T., Büdenbender, J., Deckelnick, M., Fischer, M., Hoffmann, D., Krug, S.A., Lentz, U., Ludwig, A., Muche, R., Schulz, K.G., 2013. Technical Note: A mobile sea-going mesocosm system – new opportunities for ocean change research. Biogeosciences 10, 1835–1847. https://doi.org/10.5194/bg-10-1835-2013

Roels, O.A., Gerard, R.D., Haines, K.C., Centeno, P.A., 1970. Artificial Upwelling, in: All Days. Presented at the Offshore Technology Conference, OTC, Houston, Texas, p. OTC-1179-MS. https://doi.org/10.4043/1179-MS

Sanders, R., Henson, S.A., Koski, M., De La Rocha, C.L., Painter, S.C., Poulton, A.J., Riley, J., Salihoglu, B., Visser, A., Yool, A., Bellerby, R., Martin, A.P., 2014. The Biological Carbon Pump in the North Atlantic. Progress in Oceanography 129, 200–218. https://doi.org/10.1016/j.pocean.2014.05.005

Sarmiento, J.L., 1993. Ocean Carbon Cycle. Chem. Eng. News 71, 30–43. https://doi.org/10.1021/cen-v071n022.p030

Sommer, U., 1994. Are marine diatoms favoured by high Si:N ratios? Marine Ecology Progress Series 115, 309–315. https://doi.org/10.3354/meps115309

Steinberg, D.K., Landry, M.R., 2017. Zooplankton and the Ocean Carbon Cycle. Annu. Rev. Mar. Sci. 9, 413–444. https://doi.org/10.1146/annurev-marine-010814-015924

Strohmeier, T., Strand, Ø., Alunno-Bruscia, M., Duinker, A., Rosland, R., Aure, J., Erga, S.R., Naustvoll, L.J., Jansen, H.M., Cranford, P.J., 2015. Response of Mytilus edulis to enhanced phytoplankton availability by controlled upwelling in an oligotrophic fjord. Mar. Ecol. Prog. Ser. 518, 139–152. https://doi.org/10.3354/meps11036

Taucher, J., Boxhammer, T., Bach, L.T., Paul, A.J., Schartau, M., Stange, P., Riebesell, U., 2021. Changing carbon-to-nitrogen ratios of organic-matter export under ocean acidification. Nat. Clim. Chang. 11, 52–57. https://doi.org/10.1038/s41558-020-00915-5

Taucher, J., Stange, P., Algueró-Muñiz, M., Bach, L.T., Nauendorf, A., Kolzenburg, R., Büdenbender, J., Riebesell, U., 2018. In situ camera observations reveal major role of zooplankton in modulating marine snow formation during an upwelling-induced plankton bloom. Progress in Oceanography 164, 75–88. https://doi.org/10.1016/j.pocean.2018.01.004

Thomas, H., Ittekkot, V., 2001. Determination of anthropogenic CO_2 in the North Atlantic Ocean using water mass ages and CO_2 equilibrium chemistry. Journal of Marine Systems 27, 325–336. https://doi.org/10.1016/S0924-7963(00)00077-4

Turner, J.T., 2015. Zooplankton fecal pellets, marine snow, phytodetritus and the ocean's biological pump. Progress in Oceanography 130, 205–248. https://doi.org/10.1016/j.pocean.2014.08.005

Turner, J.T., 2002. Zooplankton fecal pellets, marine snow and sinking phytoplankton blooms. Aquat. Microb. Ecol. 27, 57–102. https://doi.org/10.3354/ame027057

Villamaña, M., Marañón, E., Cermeño, P., Estrada, M., Fernández-Castro, B., Figueiras, F.G., Latasa, M., Otero-Ferrer, J.L., Reguera, B., Mouriño-Carballido, B., 2019. The role of mixing in controlling resource availability and phytoplankton community composition. Progress in Oceanography 178, 102181. https://doi.org/10.1016/j.pocean.2019.102181

Volk, T., Hoffert, M.I., 2013. Ocean Carbon Pumps: Analysis of Relative Strengths and Efficiencies in Ocean-Driven Atmospheric CO_2 Changes, in: Sundquist, E.T., Broecker, W.S. (Eds.), Geophysical Monograph Series. American Geophysical Union, Washington, D. C., pp. 99–110. https://doi.org/10.1029/GM032p0099

Vrede, T., Ballantyne, A., Mille-Lindblom, C., Algesten, G., Gudasz, C., Lindahl, S., Brunberg, A.K., 2009. Effects of N:P loading ratios on phytoplankton community composition, primary production and N fixation in a eutrophic lake. Freshwater Biology 54, 331–344. https://doi.org/10.1111/j.1365-2427.2008.02118.x

White, A., Björkman, K., Grabowski, E., Letelier, R., Poulos, S., Watkins, B., Karl, D., 2010. An Open Ocean Trial of Controlled Upwelling Using Wave Pump Technology. Journal of Atmospheric and Oceanic Technology 27, 385–396. https://doi.org/10.1175/2009JTECHO679.1

Yool, A., Shepherd, J.G., Bryden, H.L., Oschlies, A., 2009. Low efficiency of nutrient translocation for enhancing oceanic uptake of carbon dioxide. J. Geophys. Res. 114, C08009. https://doi.org/10.1029/2008JC004792

2   Manuscript I

Effect of Intensity and Mode of Artificial Upwelling on Particle Flux and Carbon Export

Moritz Baumann[1]*, Jan Taucher[1], Allanah Joy Paul[1], Malte Heinemann[2], Mari Vanharanta[3, 4], Lennart Thomas Bach[5], Kristian Spilling[3, 6], Joaquin Ortiz-Cortes[1], Javier Arístegui[7], Nauzet Hernández-Hernández[7], Ulf Riebesell[1]

[1]Marine Biogeochemistry, Biological Oceanography, GEOMAR Helmholtz Centre for Ocean Research Kiel, Kiel, Germany
[2]Institute of Geosciences, Kiel University, Kiel, Germany
[3]Marine Research Centre, Finnish Environment Institute, Helsinki, Finland
[4]Tvärminne Zoological Station, University of Helsinki, Hanko, Finland
[5]Institute for Marine and Antarctic Studies, University of Tasmania, Hobart, Tasmania, Australia
[6]Centre for Coastal Research, University of Agder, Kristiansand, Norway
[7]Oceanografía Biológica, Instituto de Oceanografía y Cambio Global, Universidad de Las Palmas de Gran Canaria, Las Palmas de Gran Canaria, Spain

Abstract. Reduction of anthropogenic CO_2 emissions alone will not sufficiently restrict global warming and enable the 1.5°C goal of the Paris agreement to be met. To effectively counteract climate change, measures to actively remove carbon dioxide from the atmosphere are required. Artificial upwelling has been proposed as one such carbon dioxide removal technique. By fueling primary productivity in the surface ocean with nutrient-rich deep water, it could potentially enhance downward fluxes of particulate organic carbon (POC) and carbon sequestration. In this study we investigated the effect of different intensities of artificial upwelling combined with two upwelling modes (recurring additions vs. one singular addition) on POC export, sinking matter stoichiometry and remineralization depth. We carried out a 39 day-long mesocosm experiment in the subtropical North Atlantic, where we fertilized oligotrophic surface waters with different amounts of deep water. The total nutrient inputs ranged from 1.6 to 11.0 $\mu mol\ NO_3^-\ L^{-1}$. We found that on the one hand POC export under artificial upwelling more than doubled, and the molar C:N ratios of sinking organic matter increased from values around Redfield (6.6) to ~8–13, which is beneficial for potential carbon dioxide removal. On the other hand, sinking matter was remineralized at faster rates and showed lower sinking velocities, which led to shallower remineralization depths. Particle properties were more favorable for deep carbon export in the recurring upwelling mode, while in the singular mode the C:N increase of sinking matter was more pronounced. In both upwelling modes roughly half of the produced organic carbon was retained in the water column until the end of the experiment. This suggests that the plankton communities were still in the process of adjustment, possibly due to the different response times of producers and consumers. There is thus a need for studies with longer experimental durations to quantify the responses of fully adjusted communities. Finally, our results revealed that artificial upwelling affects a variety of sinking particle properties, and that the intensity and mode with which it is applied control the strength of the effects.

Introduction

To limit global warming to between 1.5-2° C as committed in the Paris Climate Agreement, reducing carbon dioxide (CO_2) emissions alone will most likely not suffice. Negative emission technologies, which actively remove CO_2 from the atmosphere, will be needed to achieve net zero CO_2 emissions (IPCC 2018). Many such technologies focus on the ocean (GESAMP 2019), which has the capacity to potentially store large amounts of extra carbon (Sabine et al. 2004). The world ocean has already absorbed roughly a third of cumulated anthropogenic CO_2 emissions (Khatiwala et al. 2013), thereby mitigating a substantial part of global warming. The ocean's storage capacity might be further enhanced by strengthening the carbon flux from the air-sea-interface to the deep ocean. One component of this flux is the biological carbon pump, which mediates the transport of organic carbon produced in the euphotic zone to the deep ocean. Once the carbon reaches the deep ocean, it remains out of touch with the atmosphere for decades to centuries (i.e. sequestered, Boyd et al. 2019). Some negative emission technologies focus on strengthening the biological carbon pump to enhance this natural carbon sink. In the oligotrophic ocean, increased vertical mixing and resulting nutrient-upwelling can enhance carbon fluxes to the deep ocean (Pedrosa-Pàmies et al. 2019). This principle is utilized by a negative emission technology called 'artificial upwelling', an approach in which nutrient- and CO_2-rich deep ocean water is pumped to the surface layer with the goal of enhancing primary production and hence, carbon export.

The feasibility of artificial upwelling as a CO_2-sequestration technique has been disputed by several modelling studies. Although it has the potential to sequester additional atmospheric carbon (Pan et al. 2015), Yool et al. (2009) found this potential to be rather small and connected to very high efforts; i.e. the upwelling of massive amounts of water (117 Sv) from 1000 m depth would achieve an additional oceanic CO_2 uptake of 1 Gt C yr^{-1}. For comparison, in the year 2008 the oceans took up ~2.5 Gt of anthropogenic carbon (Khatiwala et al. 2009). Furthermore, modeling studies have suggested that geophysical ocean-atmosphere feedbacks might lead to undesirable side-effects, e.g. that stopping artificial upwelling after several decades of large-scale operation would increase global temperatures to levels higher than if it had not been applied at all (Keller, Feng, and Oschlies 2014; Kwiatkowski, Ricke, and Caldeira 2015; Oschlies et al. 2010). Beside such geophysical feedbacks, other major unknowns are the biological and biogeochemical responses of pelagic communities to artificial upwelling. Basically all our knowledge about potential effects of artificial upwelling is based on models with a low degree of ecological complexity and simplified biogeochemistry (e.g. constant stoichiometry and particle properties). So far, there is little empirical research on the effects of artificial upwelling on the ecology and biogeochemistry of pelagic plankton communities.

The limited number of experimental studies so far have shown that artificial upwelling can significantly increase phytoplankton biomass in oligotrophic waters (Casareto, Niraula, and Suzuki 2017; Giraud et al. 2016; 2018; McAndrew et al. 2007; Strohmeier et al. 2015). However, studies considering its effect on the export production and carbon sequestration processes are scarce, mostly due to the methodological difficulties of simulating artificial upwelling under close-to-natural conditions. Svensen et al. (2002) carried out a mesocosm nutrient enrichment experiment, in which they found that nutrient enrichment increases particulate organic carbon (POC) sedimentation and that the effect size is dependent on the frequency of nutrient

additions. However, no study so far has examined in detail the properties of sinking particles, particularly sinking velocity and degradation rates, which together determine the remineralization depth and thus the potential for deep carbon export.

To create a net carbon sink using artificial upwelling, the export flux needs to overcompensate for the CO_2 upwelled with deep water (Pan et al. 2016). The most important export conditions determining carbon sequestration potential are (i) elemental stoichiometry of sinking particles and (ii) the remineralization depth of these particles. While artificially upwelled deep water usually contains more nitrogen and phosphorus than the surface water, it also contains more dissolved inorganic carbon (DIC), which could potentially outgas to the atmosphere. Hence, for artificial upwelling to increase the ocean's function as a net carbon sink, more carbon must be sequestered than is brought up as excess DIC (excess DIC = deep water DIC - surface water DIC). Carbon sequestration is thereby promoted by a high C:N ratio of sequestered particulate material (POC:PON). How much of the exported matter reaches the sequestration depth (i.e. the depth at which sinking material is regarded as sequestered) is determined by the remineralization length scale (RLS). It is a proxy for how deep particles can sink before being remineralized. Both parameters are dependent on the plankton community that develops as a response to artificial upwelling. Plankton community composition shapes not only the magnitude and C:N stoichiometry of the mass flux (Taucher et al. 2021), but also the characteristics of the sinking particles, such as their sinking velocities (SV) and carbon-specific remineralization rates (C_{remin}) (e.g. Bach et al. 2019; Henson, Sanders, and Madsen 2012; Iversen and Ploug 2010; Legendre and Rivkin 2002; Turner 2015). Community composition and succession are in turn controlled by the amount of added nutrients and the frequency with which they are supplied (Leibold et al. 1997; Jakobsen et al. 2015). This is why the intensity of artificial upwelling, as well as the mode of the application (i.e. the frequency of deep water addition) are important parameters that impact the export of organic matter.

Here, we present results from a mesocosm experiment where we studied the impact of different intensities and modes of artificial upwelling on arising food web dynamics and particulate matter export. We addressed the question whether increasing intensity of artificial upwelling leads to a higher mass flux and increased potential for carbon sequestration. Additionally, we compared the particle properties and their implications for deep carbon export of a singular upwelling event with a recurring mode of upwelling. The singular upwelling mode resembled an application of artificial upwelling that fertilizes each patch of water only once, e.g. by means of a moored wave pump (see e.g. Fan et al. 2016; Liu et al. 1999). The recurring mode on the other hand resembled an approach where the upwelling device drifts within a patch of water and fertilizes it over longer periods of time. Mesocosms are useful to study effects on whole pelagic communities, since they incorporate the responses of multiple trophic levels of a food web and allow for the assessment of a variety of ecological and biogeochemical parameters in an enclosed and well-characterized (eco-)system. Our study is the first to analyze the combined effects of upwelling intensity and upwelling mode on pelagic communities.

Materials and Methods

Experimental setup

The mesocosm experiment was conducted from 5th of November 2018 and lasted for 39 days. Nine Kiel Off-Shore Mesocoms for Ocean Simulations (KOSMOS, see Riebesell et al. 2013 for technical information) were deployed in Gando Bay off the east coast of Gran Canaria (27°55.673' N, 15°21.870' W). They enabled us to monitor the temporal development of the enclosed pelagic communities at *in situ* conditions. The mesocosms contained a 15 m long water column with a volume of ~38 m^3. We simulated artificial upwelling by replacing part of the oligotrophic mesocosm water with nutrient rich deep water. Our experimental design comprised one mesocosm as a control (i.e. no deep water addition), while the remaining eight received deep water additions in different modes and intensities. Four of these mesocosms were fertilized once with one big addition at the beginning of our study, i.e. the "singular treatments". The other four were fertilized eight times throughout the experiment with lower amounts of deep water per addition, but comparable total amounts of deep water summed up over the study period, i.e. the "recurring treatments". Both addition modes had four different levels of mixing ratio (low, medium, high and extreme), with two respective mesocosms of different modes receiving similar amounts of deep water in total (**Table 1**).

We collected deep water for fertilization off the coast of Gran Canaria using a deep water collector, an opaque synthetic bag with 100 m^3 carrying capacity (see Taucher et al. 2017 for technical details), and moored it at the mesocosm site after each of two collections. The water was supposed to originate from ~600 m depth, where NO_3^- concentrations are as high as 20-25 µmol L^{-1} (Llinás et al. 1994), in order to enhance primary and export production. However, due to loss of equipment under rough conditions we could not as planned collect water from that depth. Instead, we collected water from 330 m depth on the 26th of October 2018 (experimental day -10 = T-10) and from 280 m depth on the 28th of November (T23). Therefore, to reach the macronutrient concentrations necessary to achieve our planned experimental fertilization, we added nitrate (NO_3^-), phosphate (PO_4^{3-}) and silicate ($Si(OH)_4$) to the deep water prior to the first addition, resulting in concentrations of 25 µmol L^{-1}, 1.38 µmol L^{-1} and 12.1 µmol L^{-1}, respectively. We calculated the amount of new N added to the mesocosms in the course of the whole experiment (**Table 1**) by calculating and adding up the net N inputs of each deep water replacement. For more details on the experimental setup and mesocosm activities see Sswat et al. (in prep.).

Sampling procedure and maintenance

Sampling for various parameters was generally carried out every second day (see **Figure 1**). A higher sampling frequency was pursued at the beginning of the experiment in order to cover the biological responses to the first two deep water additions in higher temporal resolution. The samples were either analyzed at our on-shore lab facilities at the Oceanic Platform of the Canary Islands (PLOCAN), the Marine Science and Technology Park (Parque Científico Tecnológico Marino, PCTM) or the University of Las Palmas (ULPGC), or transported back to Kiel for analysis at the GEOMAR Helmholtz Centre for Ocean Research Kiel.

Table 1: Treatment overview indicating different upwelling modes and intensities, mean net volume exchange of surface water with nutrient-rich deep water per addition and the total amount of new nitrogen that was added via the addition of deep water throughout the experiment.

Upwelling mode	Control	Singular				Recurring			
Upwelling intensity	—	Low •	Medium ●	High ●	Extreme ●	Low •	Medium ●	High ●	Extreme ●
Volume exchange per addition (%)	0	6.4	12.0	22.4	39.2	0.8	1.6	3.2	6.4
Total new N added ($\mu mol\ L^{-1}$)	0	1.6	3.1	5.6	9.8	1.6	3.1	6.2	11.0
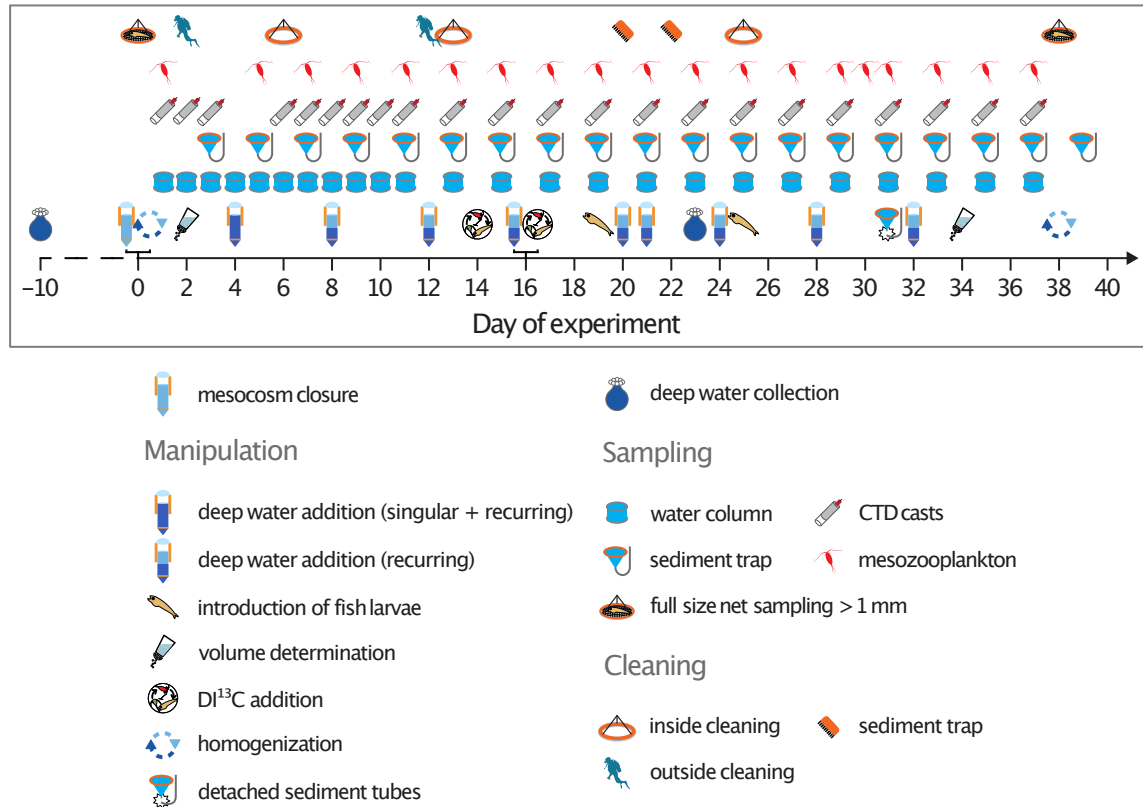
Figure 1: Timeline of the experiment depicting the sampling schedule, cleaning activities and manipulations.

A CTD60M (Sea & Sun Technology GmbH, Trappenkamp, Germany) was cast to get depth profiles for temperature, salinity, density, pH, turbidity, oxygen (O_2) and photosynthetically active radiation. Bulk samples from the upper 13 m of the water column (WC) were taken for the analysis of primary productivity, chlorophyll *a* (Chl *a*), photosynthetic pigments, phyto- and microzooplankton analysis, prokaryotic heterotrophic production, and for the analysis of suspended particulate matter (PM_{wc}). The latter was composed of particulate organic and inorganic carbon (POC_{wc}/PIC_{wc}), particulate organic nitrogen (PON_{wc}) and phosphorus (POP_{wc}), and biogenic silica (BSi_{wc}). Bulk samples were collected with integrated water samplers (HYDRO-BIOS Apparatebau GmbH, Kiel, Germany), which performed depth-integrated sampling from the upper 13 m of the water column. On each sampling day, around 40-60 L of bulk samples (i.e. 8-12 water samplers) were sampled per mesocosm. These were filled into 10 L carboys and stored dark and cool until arrival in the on-shore labs. Dissolved nutrients

and carbonate chemistry (DIC and total alkalinity) were also sampled from the integrated water samplers.

Sedimented particulate matter was pumped out of the sediment trap (depth = 15 m) with a manual vacuum pump, not exceeding 0.3 bar during the process. Sediments were collected in 5 L glass bottles (Schott Scandinavia A/S, Kgs. Lyngby, Denmark) and stored in darkness until arrival in the lab, where they were subsampled for various parameters. The bottles were gently rotated to resuspend the material before homogeneous subsamples were taken. These subsamples were used for particle sinking velocity measurements and measurements of carbon-specific remineralization rates. For the latter, seven glass bottles (Schott, 310 mL volume) were additionally sampled with mesocosm water without headspace. They were used for incubating the sediment subsamples. The remaining sediment sample was weighed and analyzed for particulate carbon, nitrogen, phosphorus and biogenic silica content (see Boxhammer et al. 2016 for details of the method).

To prevent wall growth on the inside walls of the mesocosms, a ring-shaped wiper was pulled through each mesocosm roughly every ten days (see **Figure 1**). This counteracted nutrient consumption by fouling organisms and their alteration of incoming light. For the latter reason, also the outside walls were cleaned twice during the study by divers equipped with brushes.

The sediment tubes of all mesocosms detached from the sediment traps on T30 due to strong winds and currents. They were reinforced and refitted on T31, however no sediment samples could be recovered that day and thus sedimented matter elemental composition, sinking velocity and remineralization rate could not be measured on T31. The tubes of the singular medium and high treatments and of the recurring extreme treatment disconnected again and had to be reattached a second time on T33. We were not able to sample the singular medium treatment that day, and the singular high and recurring extreme treatments had short incubation periods of only 18 h between the T33 and T35 samplings. We discarded all sinking velocity measurements from these days, since they showed systematically higher values than the measurements of the surrounding days. The mean seawater density inside all mesocosms between 0.5 and 15 m was slightly higher than in the surrounding water (1025.69 ± 0.11 and 1025.42 kg m^{-3} on T31, respectively), so that we assume no Atlantic water entered the small opening at the base of the sediment trap (ø ~1 cm). An outflow of mesocosm water into the surrounding seems more likely under these circumstances. Nevertheless, we cannot rule out the possibility that e.g. due to wave and current action some Atlantic water entered the mesocosms. The surrounding water was however oligotrophic, and had substantially lower POC concentrations than any of the mesocosms on T33 according to our measurements (7.9 μmol POC L^{-1} in the Atlantic water compared to 35.7 ± 21.4 μmol POC L^{-1} in the mesocosms). This makes an influential contamination with biogenic material and/or species from the outside less probable, even if Atlantic water had entered the mesocosms. At the end of the experiment the water column in the mesocosms was mixed by pumping compressed air through the sediment hose. This might have altered the sediment flux and quality of the last sampling on T39.

Sample processing and measurement

Sediment trap material

At PLOCAN the sediment trap (ST) material was prepared for elemental analysis of POC_{ST}, PON_{ST}, and BSi_{ST} by first of all separating the particles from the seawater. 3 mol L^{-1} ferric chloride ($FeCl_3$) were added to each 2.5 L bottle of sediment material to enhance flocculation and coagulation, followed by 3 mol L^{-1} NaOH addition to compensate for the decrease in pH (as described in detail in Boxhammer et al. 2016). After letting the material settle for 1 h, the supernatant was gently decanted. The remaining flocculated material was then centrifuged for 10 min at ~5200 g in a 6-16KS centrifuge (Sigma Laborzentrifugen GmbH, Osterode am Harz, Germany). An additional 10 min centrifugation step at ~5000 g in a 3K12 centrifuge (Sigma) resulted in compact sediment pellets, which were frozen at -20 °C and transported to Kiel for further processing. In Kiel, the pellets were freeze-dried to remove any leftover moisture and then ground in a cell mill (Edmund Bühler GmbH, Bodelshausen, Germany) to a fine homogeneous powder that was suitable for subsampling and further elemental analysis (Boxhammer et al. 2016). Subsamples for POC/N were weighed into tin capsules, acidified with 1 mol L^{-1} HCl, dried over night at 50 °C, and then measured in duplicate on a CN analyzer (Euro EA-CN, HEKAtech GmbH, Wegberg, Germany) according to Sharp et al. (1974). To determine BSi concentrations, ~2 mg subsamples of the sediment powder were measured spectrophotometrically following Hansen and Koroleff (1999).

The sediment powder was stored dark and cool in glass vials. As some samples required multiple vials due to their high amounts, subsamples from all bottles were measured for each variable. If they differed among each other in elemental composition, the sample was pooled, homogenized, split up and remeasured until all bottles yielded the same results.

Water column samples

Water column samples were subsampled for elemental (POC_{WC}/PON_{WC}) and pigment analysis (Chlorophyll a/Chl a) by collection on pre-combusted glass fiber filters (0.7 μm, Whatman) in our on-shore labs. POC and PON filters were acidified for ~2 h to remove inorganic carbon, using 1 mol L^{-1} HCl, and dried over night at 60 °C in pre-combusted glass petri dishes. Filters for total particulate carbon (TPC) were dried without prior acidification. All filters were packed in tin cups (8 x 8 x 15 mm, LabNeed GmbH, Nidderau, Germany) and measured back in Kiel on a CN analyzer (Euro EA-CN, HEKAtech) as described for sediment C and N content above. Due to sample handling and/or measurement errors, measured POC_{wc} concentrations were sometimes higher than those of TPC_{wc}. Whenever the difference was greater than 10 %, we report the TPC_{wc} instead of the POC_{wc} concentration (i.e. assuming that no PIC was present). Samples for Chl a were stored at -80 °C in cryovials until analysis in Kiel. They were extracted in acetone (100%) and homogenised with glass beads in a cell mill. After centrifugation (10 min, 5,200 rpm, 4 °C) they were filtered through 0.2 μm PTFE filters (VWR International GmbH, Darmstadt, Germany). Phytoplankton pigments, including Chl a in the supernatant were measured by an HPLC Ultimate 3,000 (Thermo Scientific GmbH, Schwerte, Germany).

Primary productivity was measured in the on-shore labs using a modified Nielsen (1952) ^{14}C uptake method described by Cermeño et al. (2012). Four water column subsamples (70 mL) per mesocosm were prefiltered and peaked with $2.96 \cdot 10^5$ Bq of ^{14}C-labeled sodium bicarbonate solution (NaH^{14}CO$_3$, PerkinElmer Inc., Waltham, USA). They were subsequently incubated *in vitro* for 24 h in a 12 h dark-light cycle. One of the subsamples was thereby covered with an opaque foil in order to measure the dark carbon uptake. Light intensity and temperature were set to *in situ* conditions based on CTD measurements. Thereafter, size fractions were filtered, the PIC and DIC fractions removed through acidification and the filters and filtrates were treated with a scintillation cocktail (Ultima Gold XR). Disintegrations per minute were counted on a scintillation counter (Beckmann LS-6500, Beckman Coulter Inc., Brea, USA). From these, knowing the concentration of added ^{14}C isotope and the measured *in situ* DIC concentration (see paragraph on DIC below), primary productivity rates (μmol C L^{-1} d^{-1}) were calculated. For a more detailed description of the sampling and measurement procedure, see Ortiz-Cortes et al. (submitted).

Prokaryotic heterotrophic production (PHP) was estimated from rates of protein synthesis determined by the incorporation of tritiated leucine ([^{3}H]leucine; Perkin Elmer) using the centrifugation method (Smith and Azam, 1992). Four subsamples (1 mL) and two trichloroacetic acid killed blanks were dispensed into screw-cap Eppendorf tubes. They were spiked with [^{3}H]leucine (final concentration: 20 nmol L^{-1}, specific activity 123 Ci mmol^{-1}) and incubated at in situ temperature (21 °C) in the dark for 2 to 3 h. After the incubation, 100 μL of 50 % trichloroacetic acid were added to the subsamples, which were kept with the blanks at -20 °C until centrifugation at 12 000 rpm for 20 min. The supernatant was carefully removed, and 1 mL of scintillation cocktail (Ultima Gold XR) was added to the Eppendorf tubes. They were stored in darkness for 24 h, after which the incorporated radioactivity was determined on a scintillation counter (Beckmann LS-6500). PHP was calculated using a conservative theoretical conversion factor of 1.55 kg C mol^{-1} Leu assuming no internal isotope dilution (Kirchman and Ducklow 1993).

Samples for dissolved inorganic nutrients were filtered (0.45 μm Sterivex filters, Merck KGaA, Darmstadt, Germany) upon arrival in the on-shore lab. Nitrate (NO$_3^-$), nitrite (NO$_2^-$), ammonium (NH$_4^+$), phosphate (PO$_4^{3-}$) and silicic acid (Si(OH)$_4$) concentrations were subsequently measured spectrophotometrically on a five channel continuous flow analyzer (QuAAtro AutoAnalyzer, SEAL Analytical Inc., Mequon, USA).

Samples for DIC measurements were filtered to remove particulate inorganic carbon (0.7 μm, Whatman) with an overflow of 1.5 times the volume of the filtrate. Inclusion of air in the filtration process was carefully avoided. The filtrate was fixed with mercuric chloride (HgCl$_2$). DIC concentrations were measured in triplicate on an AIRICA system (MARIANDA, Kiel, Germany) in Kiel, using a LI-COR LI-7000 Analyzer (LI-COR Biosciences GmbH, Bad Homburg, Germany). Certified reference materials (CRM batch 142, supplied by A. Dickson, Scripps Institution of Oceanography, USA) were used to determine the accuracy of DIC measurements.

Dissolved organic carbon (DOC) samples were filtered through pre-combusted GF/F filters (450 °C, 6 h) into polypropylene copolymer Nalgene^{TM} bottles (Thermo Scientific), and stored at -20 °C. Prior to analysis, samples were acidified to a pH<2 to remove inorganic carbon.

Subsequently, DOC concentrations were measured by high temperature catalytic oxidation on a total organic carbon analyzer (TOC-V, Shimadzu Europa GmbH, Duisburg, Germany). The instrument was calibrated daily using potassium hydrogen phthalate (99.95–100.05%, p.a., Merck), which yielded an analytical precision of $\pm$ 1 μmol C L^{-1}. The accuracy was determined using certified reference materials (provided by D. A. Hansell, University of Miami, USA). Measured CRM concentrations were 43.39 $\pm$ 0.92 μmol C L^{-1} (n = 33), at a reference value of 42–45 μmol C L^{-1}.

Sinking velocity of sediment trap particles

Sinking velocity and remineralization rates of sedimented particulate matter were measured in a temperature-controlled on-shore lab at PCTM. Sinking velocity was determined by video microscopy using the method described in Bach et al. (2012). Sediment subsamples were diluted with filtered seawater according to their particle density (1:25 - 1:100) and injected to a sinking chamber (a cuvette with the dimensions: 10x10x350 mm), which was mounted vertically on a FlowCam 8000 (Fluid Imaging Technologies Inc., Scarborough, USA). Gravitational settling of particles in the cuvette was subsequently monitored for 20 minutes. Measurements were carried out at in situ temperatures (~21 °C) under ventilation to prevent a temperature gradient around the sinking chamber. Particles between 25 and 1000 μm were identified at a frame rate of 15-20 fps. The FlowCam measures more than 60 visually assessed parameters, which were read into MATLAB (version R2018b) for data analysis. The MATLAB script described by Bach et al. (2012, see: "Evaluation of sinking velocities") was adjusted for the more recent FlowCam version and used for calculation of sinking velocities. By finding multiple captures of the same particle on a y-position-gradient and applying a linear regression model against time, sinking velocities were calculated. They were corrected for wall effects of the sinking chamber according to the equation given by Ristow (1997). Further data analysis was carried out with the programming software R (R Core Team 2017) using RStudio (version 1.3.959) and the package 'tidyverse' (Wickham et al. 2019). An optical proxy for particle porosity (P_{int}) was calculated according to Bach et al. (2019). It is essentially a measure of the brightness of a particle, scaled with its size.

Analysis of the distribution of sinking particle volume showed that most of the volume was contained in a small fraction of particles with high equivalent spherical diameter (ESD) in all measurements (largest 10% accounted for >75% of total particle biovolume). The smaller size fractions however, constituted the majority of particle counts (~90 % in the 25-200 μm fraction). To not give the more numerous small particles undue weight, we calculated a 'weighted SV'. It gives more weight to the high-volume, but underrepresented bigger particles, which consequently contain more biomass (see **Figure S2** for an illustration of weighted SV calculation). In order to do so, we determined the ESD for which at least 25% of the summed-up particle volume was contained in the smaller particles and 75% in the bigger ones. For this 'weighted ESD' we calculated the corresponding 'weighted SV' by fitting a linear model to the mean sinking velocities as a function of their ESD across different size classes (log-spaced). We used size class means to – again – not give the numerous small particles undue weight. This weighted sinking velocity (hereinafter referred to as sinking velocity or SV) is thus the sinking velocity that corresponds to the ESD which segments the measurement into two particle volume fractions containing 25% and 75% of the total particle volume. We calculated

the 'weighted particle porosity' in the same way (hereinafter referred to as porosity or P_{int}). We used the weighted SV for all following sinking velocity dependent calculations such as the remineralization length scale (see below).

Remineralization rates of sinking particles

Remineralization rates were determined every four to six days. We therefore took samples from the sediment trap material, collected in four replicate and three control bottles per mesocosm ((4 + 3) bottles x 9 mesocosms = 63 bottles in total). They were transported back to the temperature-controlled lab (set to *in situ* temperature based on CTD measurements), where they acclimatized in a water bath for 2 h. Then, 0.5-3 mL of sediment subsample of the respective mesocosm were added to the four replicate bottles. The control bottles were left untreated. To examine the rate at which sedimented POC was remineralized back to DIC, all bottles were incubated in the dark on a rotating plankton wheel (~1 rpm) and Oxygen depletion over time was measured. O_2 measurements were carried out using a handheld optical measurement device (Fibox4 Trace, PreSens - Precision Sensing GmbH, Regensburg, Germany), measuring non-invasively on PSt3 optodes (PreSens) mounted inside the bottles. O_2 measurements were automatically corrected for temperature (measured in a dummy bottle) and atmospheric pressure by the Fibox4. We adjusted the optode salinity correction according to the daily observed salinity measurements of the CTD cast. The second O_2 measurement was carried out after the bottles had been mixed properly, about 2 h after the incubation start, and were repeated continuously in 2 to 6 h intervals. The incubations lasted between 19 and 43 hours, during which O_2 measurements were done at least 7 and up to 16 times. Particles in the incubation bottles were then collected on pre-combusted glass fiber filters (0.7 μm, Whatman) and analyzed for their POC content the same way as the water column POC filters.

By dividing the O_2 consumption rate (r in μmol O_2 L^{-1} d^{-1}) of the sedimented matter by its POC content at the end of the incubation (μmol C L^{-1}), the carbon-specific remineralization rate of the sedimented particulate matter (C_{remin} in d^{-1}) was calculated according to:

$$C_{remin} = \frac{(r * RQ)}{(POC + r * RQ * \Delta t)}$$

where RQ is the respiratory quotient (μmol C μmol O_2^{-1}), which is commonly used as 1-mol CO_2 produced:1-mol O_2 consumed (= 1) (Bach et al. 2019; Iversen and Ploug 2013; Ploug and Grossart 2000) and Δt (d) as the time interval from the start of the incubation until the start of the filtration. In order to distinguish the response of the sedimented matter from any background seawater oxygen consumption, the C_{remin} rates of the sediment-containing bottles were corrected for the mean C_{remin} rates in the blank bottles.

Calculation of export flux and remineralization depth

The mass flux to the sediment trap (POC_{ST}, PON_{ST}, BSi_{ST}) was calculated for each element from the amount measured in the sediment powder. The total content per sample was calculated and normalized to the volume of the mesocosm and the time between sample collection (48 h), which yielded the daily mass flux in μmol per liter mesocosm water (μmol L^{-1} d^{-1}). Ten data points were missing due to the detachment of the sediment trap hoses

on and around T30 (all mesocosms on T31 and the singular medium mesocosm on T33, see Section 2.2, "Sampling procedure and maintenance"). To calculate the cumulative POC_{ST} flux (ΣPOC_{ST}), daily POC_{ST} fluxes were summed up, whereby the missing data points were interpolated using the two surrounding data points (T29 and T33, or T29 and T35 for the singular medium treatment). Cumulative mass fluxes are reported in $\mu mol\ L^{-1}$.

To find out how much of the produced organic carbon had been exported from the water column until a specific experimental day (Tx), total organic carbon in the water column (TOC_{WC}) was calculated, subtracted by the initial TOC_{WC} concentration on T01 (= ΔTOC_{WC}), and finally compared to the cumulative POC_{ST} flux (ΣPOC_{ST}).

$$\frac{\Delta TOC_{WC}(Tx)}{\Sigma POC_{ST}(Tx)} = \frac{(POC_{WC}(Tx) + DOC_{WC}(Tx)) - (POC_{WC}(T01) + DOC_{WC}(T01))}{\Sigma POC_{ST}(Tx)}$$

Finally, the remineralization length scale (RLS, i.e. remineralization depth) was calculated, which is the quotient of sinking velocity and carbon specific remineralization rate.

$$RLS = \frac{SV}{C_{remin}}$$

It is the depth (m) by which 63% of the sinking organic particle flux have been remineralized (Cavan et al. 2017) and thus a proxy for the POC transfer efficiency to depth.

Results

Primary production, export flux and stoichiometry

Primary productivity as well as Chl a and POC_{WC} concentrations increased in all treatment mesocosms following the first deep water addition on T4. Phytoplankton blooms dominated by diatoms (Ortiz-Cortes et al., submitted) developed in the singular treatments with intensity and duration depending on their upwelling intensity. The highest phytoplankton biomass (measured as Chl a concentration) was observed in the extreme singular treatment (11.2 $\mu g\ L^{-1}$ on T9). Recurring upwelling sustained more stable phytoplankton biomass and productivity compared to singular upwelling. In the high and extreme recurring treatments primary productivity rates increased until well into the second half of the experiment (**Figures 2A,B**). Note that in most mesocosms a large fraction of produced organic matter was retained in the water column as suspended POC_{wc} at the end of the experiment (**Figure 2C**). This was particularly evident in the recurring treatments, which received nutrients until T32. In the extreme recurring treatment, the amount of POC_{WC} at the end of the experiment was higher than its total cumulative POC mass flux (**Figures 2C,E**: 102 $\mu mol\ L^{-1}$ POC_{WC} vs 82 $\mu mol\ L^{-1}$ of cumulative POC_{ST}, on T39).

The treatment differences observed in Chl a and primary productivity were mirrored in the POC mass flux. A post-bloom export event occurred in the singular treatments four to ten days after their bloom peak in the water column, with the time lag being longer at higher intensities of deep water addition. This is based on visual inspection (comparison of **Figures 2B,D**, e.g. extreme singular treatment bloom peak on T9, highest POC_{ST} flux between

T17-T21), since the temporal variation in the POC_{ST} data did not allow a reliable calculation of time lags as e.g. in Stange et al. (2017). In contrast, the recurring mode led to POC_{ST} maxima 20 to 30 days after initial fertilization (**Figure 2D**). In both modes, the overall cumulated POC_{ST} at the end of the experiment correlated positively with the cumulated primary productivity (**Figure 2F)**. The control mesocosm was excluded from this regression analysis, because it had unexplainably high export rates, although it did not receive any new N via deep water addition. When comparing the total amount of dissolved and particulate N at the beginning and end of the study period in the control, we found that approx. 4.2 μmol L^{-1} N sank out to the sediment trap, which were not accounted for in the initial N pools, according to our measurements. Apparently, there was an N source (or multiple) in the control, which we did not capture, e.g. fouling residues on the inside walls of the sediment trap or large swimmers (zooplankton, small fish), which were initially present but not accounted for. Other causes for the discrepancy might have been methodology-related, e.g. inaccurate sampling of patchily distributed PON_{WC}. Regarding the test statistics, removing the control from the quantitative regression analysis in **Figure 2F** decreased the p-values (from 0.014 to 0.044 in the singular and from 0.015 to 0.060 in the recurring upwelling mode) and did not considerably affect the R-values (from 0.90 to 0.91 in the singular and from 0.89 to 0.88 in the recurring upwelling mode).
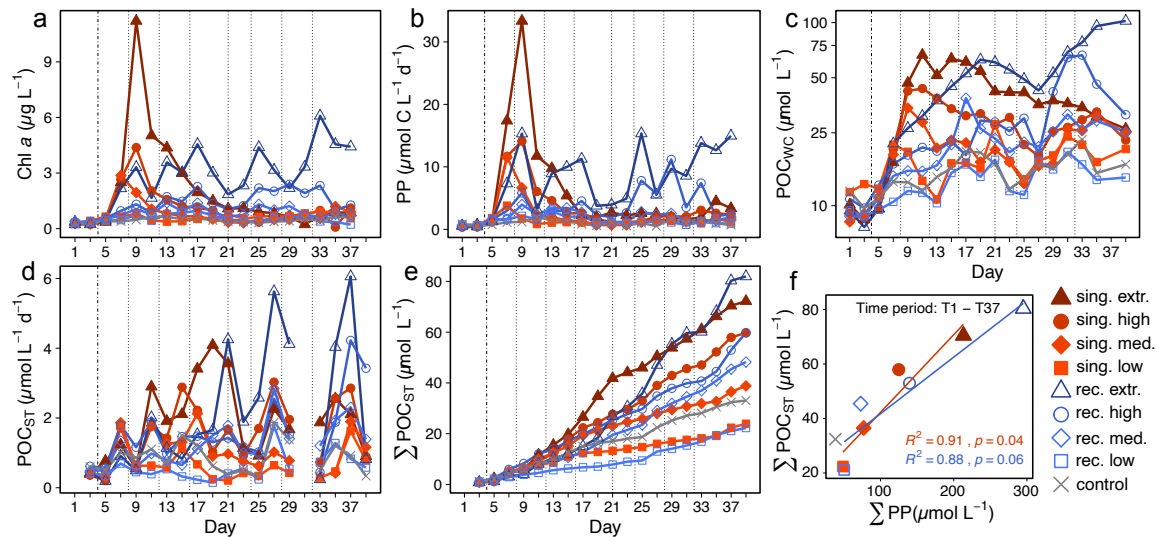
Figure 2: Chl a concentration (**A**), primary productivity (**B**), suspended POC concentration in the water column (**C**), POC mass flux to the sediment trap (**D**) and cumulative mass flux (**E**) during the 39 day experiment. The vertical lines indicate the deep water additions with the dashed one on the left representing the one for the singular and recurring treatment, the dotted ones being the following recurring additions. Panel **(F)** shows the correlation between the cumulative POC flux and the cumulative primary productivity on T37. Regression lines are plotted in the color of the corresponding upwelling mode (singular or recurring) and exclude the control data point. Regression equations are provided in **Supplementary Table 1**.

The peaks in POC_{ST} on T7 and T27 (**Figure 2D**) in all mesocosms likely occurred due to the preceding cleaning of the inside mesocosm walls on T6 and T25, respectively. It appears that a carbon-rich biofilm was growing on the walls, which was removed during cleaning and subsequently sank into the sediment traps. This is also indicated by the high C:N ratios of POC flux on these days (compare **Figures 2D** and **3A**). On T33 and T39, POC_{ST} was lower than

expected for most mesocosms, contrasting the time points before and after these days. For T33, the reason for this was probably a lower than usual accumulation period of material due to the preceding sediment tube detachments (see Section 2.2, "Sampling procedure and maintenance"). Many large and heavy particles might have sunk out before the reattachment of the tubes, leaving a higher proportion of slower sinking particles with lower POC content for the accumulation period. Regarding T39, the final fish net haul and the mixing of the water column through the sediment hose on T38 likely caused lower sedimentation rates of organic matter. The fish net haul by removing large and sticky aggregates, the mixing by resuspending already settled material.

In all treatment mesocosms except for the recurring low treatment more organic carbon was retained in the water column as POC and DOC than exported to the sediment trap as POC (ratio between ΣPOC_{ST} and ΔTOC_{WC} <1). The ratios did not substantially differ among the singular treatments, whereas they decreased with increasing upwelling intensity in the recurring mode (**Table 2**).

Upwelling mode	Control	Singular				Recurring			
Upwelling intensity	—	Low •	Medium ●	High ●	Extreme ●	Low •	Medium ●	High ●	Extreme ●
ΔTOC_{WC} (µmol L^{-1})	20.5	29.1	47.0	58.7	85.6	17.0	50.3	83.1	149.3
ΣPOC_{ST} (µmol L^{-1})	30.6	20.4	34.5	53.0	66.5	19.5	42.0	48.3	70.1
$\Sigma POC_{ST}:\Delta TOC_{WC}$ (mol:mol)	1.49	0.70	0.73	0.90	0.78	1.15	0.84	0.58	0.47

Table 2: Mean ΔTOC_{WC} and ΣPOC_{ST} values, as well as $\Delta TOC_{WC}:\Sigma POC_{ST}$ ratios calculated from T33, T35 and T39. Data for T37 is missing because POC_{WC} was not measured on that day.

In the singular upwelling treatments, the C:N ratios in the suspended particulate matter pool generally increased to higher than Redfield ratios on T11, one week after the deep water addition (**Figure 3B**). This occurred precisely when the blooming phytoplankton communities became nutrient limited (see Sswat et al. in prep. for inorganic nutrient concentrations), and was particularly prominent under high upwelling intensities. In the recurring treatments, the C:N ratios of POM_{WC} showed a high temporal variation, they however tended to increase throughout the study period.

The C:N ratio of the mass flux was higher than the canonical Redfield ratio of 6.6 in all mesocosms throughout the experiment (**Figure 3A**). Increasing amounts of deep water addition, however, enhanced the mass flux C:N ratios further. We found a positive correlation between N addition and the C:N of the mass flux in the singular treatment between T11-T21, when most of the post-bloom flux occurred (**Figure 3C**). Furthermore, the Si:C ratio during this time was higher in the singular treatments compared to the recurring ones and the control (**Figure 3D**).
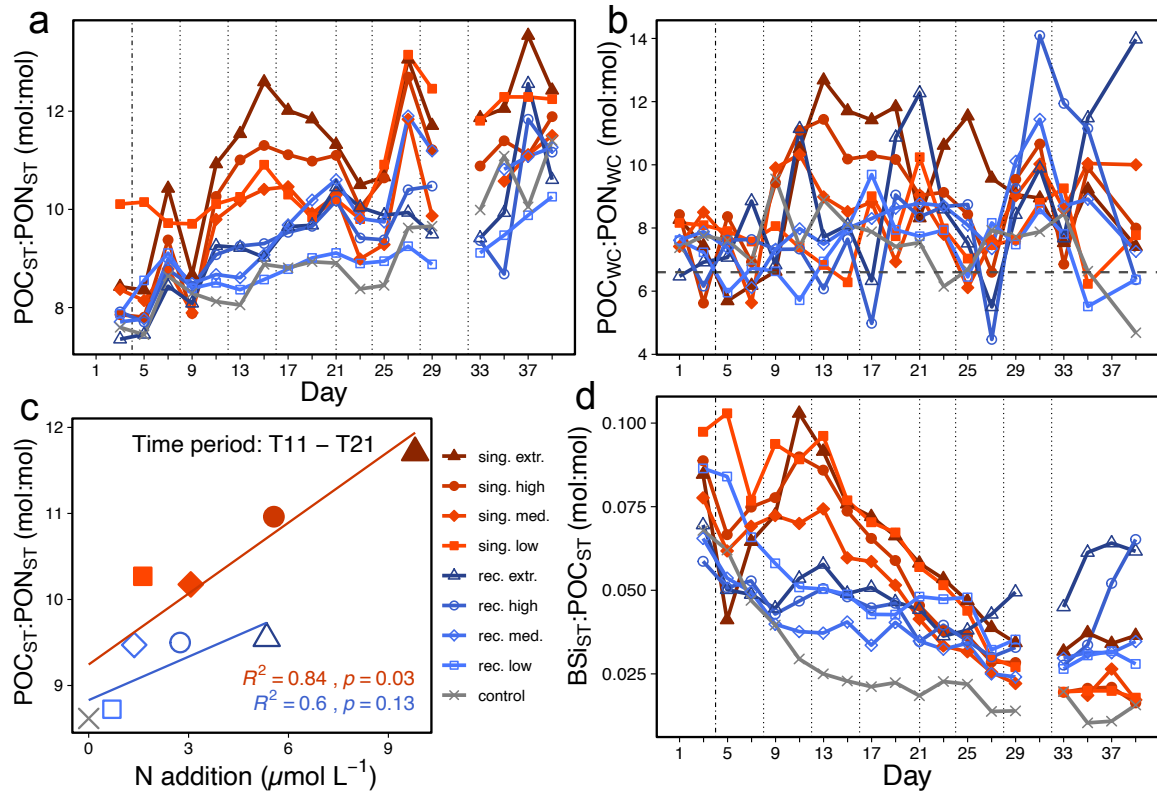
Figure 3: C:N ratios of the mass flux to the sediment trap (**A**) and suspended particulate matter C:N ratios (**B**) over time. The horizontal line in (**B**) indicates the C:N Redfield ratio of 6.6. Panel (**C**) displays the correlation between the mean C:N ratio of the mass flux and the mean cumulative N addition. It considers the time frame of the singular bloom export event (T11-T21), from which means over time were calculated. Regression lines are plotted in the color of the corresponding upwelling mode (singular or recurring). Regression equations are provided in **Supplementary Table 1**. Panel (**D**) shows the mass flux Si:C ratios over time. The vertical lines are used as described in **Figure 2**.

Particle properties and remineralization depth

Remineralization rates of sinking particles ranged from 0.09 to 0.12 d^{-1} initially, and peaked in most mesocosms a week after the first deep water addition (T11). Thereafter, they decreased in all treatments (**Figure 4A**). Sinking velocities were generally lower in the singular treatments than in the recurring ones (**Figure 4B**). This difference between the two modes was confirmed by a t-test for mean sinking velocities calculated for days T7 to T15 (two-sample t(6) = -4.019, p = 0.007). Low sinking velocities in the singular mode were accompanied by high porosities in particles > 90 μm (**Figure 4D**). The difference in porosity between particles sinking under different upwelling modes is highlighted by the visual assessment of FlowCam pictures from T11 (**Figure 4E**).
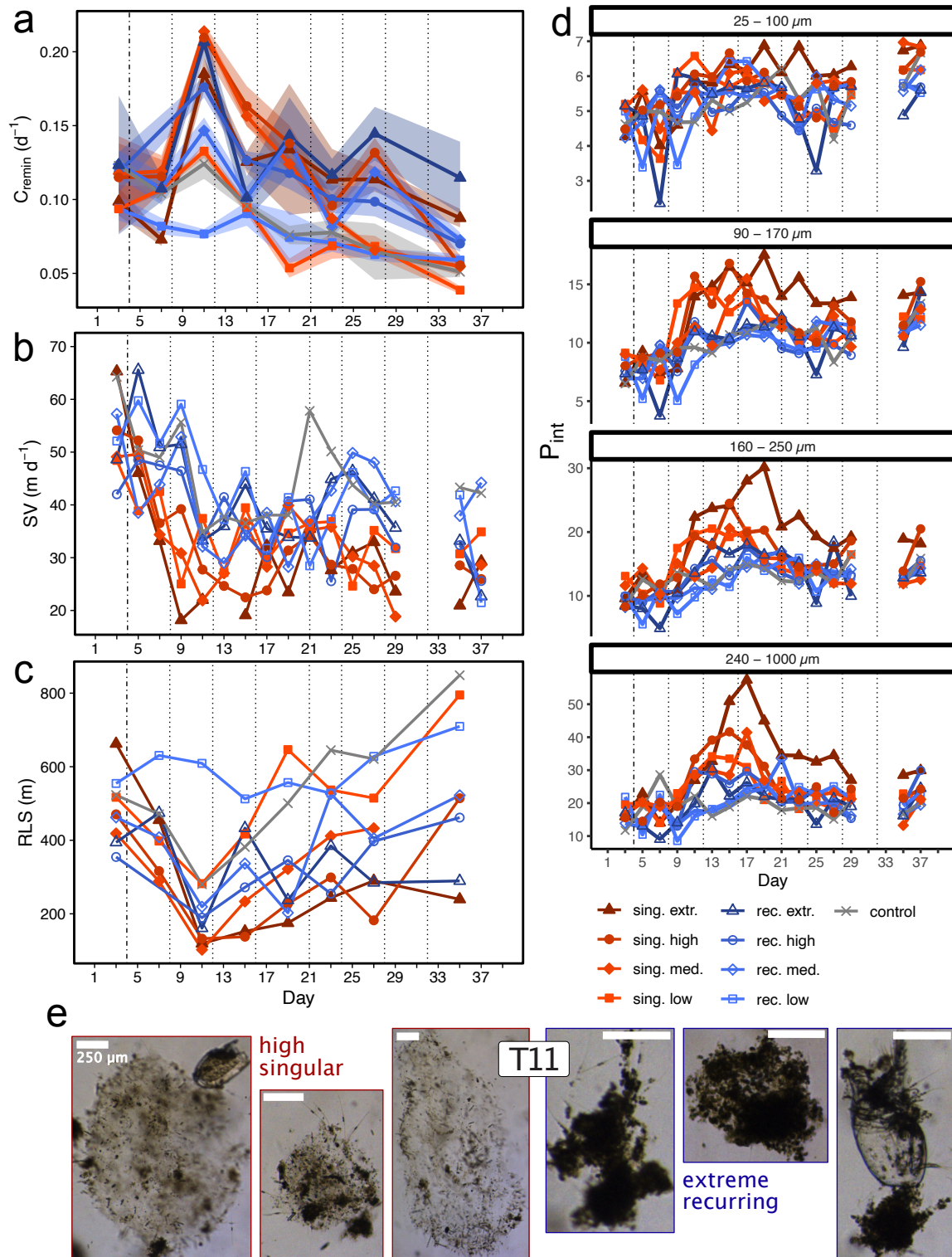
Figure 4: Carbon-specific remineralization rates (**A**), sinking velocities (**B**), remineralization length scale (**C**) and particle porosities in four different size classes (**D**) during the 39 days of experiment. Shaded areas in (**A**) depict the standard deviation of measurements (n=4). Mind the different y-axis scales in (**D**). The vertical lines are used as described in **Figure 2**. Panel (**E**) shows a selection of FlowCam pictures illustrating sinking aggregates from the high singular (three pictures on the left side) and the extreme recurring treatment (three pictures on the right side) on T11. The scale bar depicts 250 µm.

Altogether, the singular treatments exported sedimented particulate matter which was carbon- and biogenic silica-rich and sank slowly during the export event. Particles >100 μm were more porous compared to those in the recurring treatments. In contrast, the recurring treatments generally produced sinking particles which had lower C:N ratios, sank faster and were less porous than the ones in the singular treatments throughout the experiment.

We found that upwelling intensity had significant effects on sinking particle properties and on the remineralization depth during the time we observed increased mass flux (T11-T39, **Figures 5A-C**). Particles sampled from the sediment trap sank slowest and were remineralized most rapidly in mesocosms with high and extreme upwelling intensities. The fast remineralization rates correlated with high prokaryotic heterotrophic production in the water column during the same time period (**Figure 5D**). The RLS, as the quotient of SV and C_{remin}, also decreased with increasing deep water fertilization.
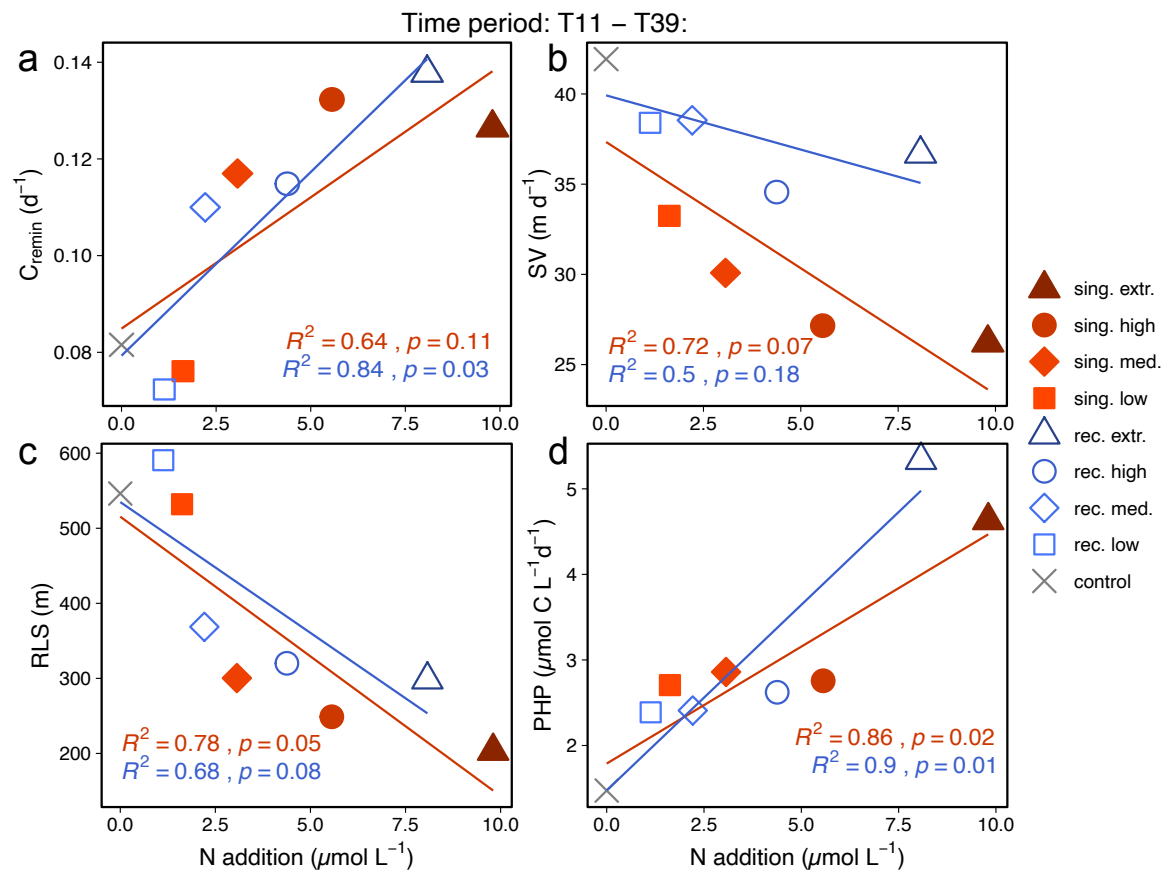
Figure 5: Correlations between mean carbon-specific remineralization rate (**A**), mean sinking velocity (**B**), mean remineralization length scale (**C**) and mean prokaryotic heterotrophic production (**D**) against cumulative N addition. It considers the time frame starting with the singular bloom export event until the end of the experiment (T11-T39), for which means of each of the parameters shown on y-axes were calculated. Since the recurring treatments received multiple deep water additions over time, mean cumulative N additions were calculated for the considered time period. Regression lines are plotted in the color of the corresponding upwelling mode (singular or recurring) and include the control treatment. Regression equations are provided in **Supplementary Table 1**.

Discussion

Temporal decoupling of biomass production and POC export

We found that increased intensities of artificial upwelling resulted in higher primary productivity and POC export from the surface. However, upwelling also resulted in a temporal decoupling between biomass production (ΔTOC_{WC}) and POC export (cumulative POC_{ST}). We found that less than half of the produced organic carbon was exported in most of our upwelling treatments during our experimental duration, while the rest was retained in the water column (see **Table 2**). This is consistent with findings by Taucher et al. (2017), who also fertilized Gran Canarian oligotrophic communities with a single pulse of nutrient-rich deep water, and found that roughly half of the produced particulate carbon was retained in the water column for at least 25 days after the fertilization. Seemingly, artificial upwelling in oligotrophic surface waters does thus not lead to rapid export of most of the produced organic matter in the time scale of weeks.

Such decoupling between production and export occurs in a variety of oceanic re gions (Cavan et al. 2015; Henson, Le Moigne, and Giering 2019; Laws and Maiti 2019), including eastern boundary upwelling systems (e.g. Bach et al. 2020; Kelly et al. 2018). It is thus no peculiarity of artificial upwelling. In natural upwelling systems reasons for a temporal decoupling can be e.g. persistent phytoplankton species in the water column (Bach et al. 2020) or weak trophic links in the planktonic food web (Stukel et al. 2011). A tight coupling of primary production and zooplankton consumers can generally lead to the export of high amounts of fast sinking fecal pellets, which can increase the POC export efficiency (Le Moigne et al. 2016; Stukel et al. 2011) and its transfer efficiency to depth (Steinberg and Landry 2017). In our study, the response of the mesozooplankton community to the deep water fertilization was not very pronounced. Although a treatment effect on mesozooplankton biomass established towards the end of the experiment, values mostly stayed on a similar or lower level compared to before the first fertilization (~20 µg C L^{-1} or lower, C. Spisla, in prep.). We also rarely observed fecal pellets in the FlowCam measurements of the sediment subsamples. The low mesozooplankton biomass and fecal pellet abundances indicate a limited impact of the mesozooplankton community on the POC flux. This hints at a potential caveat of short-term artificial upwelling as a tool for enhancing C sequestration: The fauna adapted to oligotrophic systems may not be able to readily consume great amounts of primary produced biomass and efficiently channel it into the export pathway. The dilution effect of the deep water addition amplifies the zooplankton handicap, making it even more difficult for them to catch up with the rapid phytoplankton reproduction.

Another factor that delayed the sedimentation of primary produced matter was surface microbial recycling. Henson et al. (2019) and Le Moigne et al. (2016) found high bacterial abundances to be associated with high primary production and low export efficiency (i.e. only a small fraction of primary produced biomass is exported). Microbial recycling can channel particulate organic matter into the dissolved organic matter pool, thereby making it unavailable for metazoan consumers. Hence the breakdown of POC into DOC reduces the chances for either direct sinking of particles or incorporation and active transportation by zooplankton

(Legendre and Le Fèvre 1995). We found similar patterns of microbial activity as the above mentioned studies associated to the decoupling of primary production and export. Microbial production increased significantly with upwelling intensity in both upwelling modes (**Figure 5D**), thereby retaining organic matter in the surface microbial loop and making it unavailable for immediate export.

Due to the retention of organic matter in the water column, we were not able to capture the whole export response of our fertilized mesocosms, especially of the recurring highly fertilized ones. We argue that the high amounts of suspended POC (see **Figure 2C**) in the high and extreme recurring treatments at the end of the experiment represented a high potential for POC export, e.g. by particle aggregation and gravitational settling. Nevertheless, the retention of organic matter in the water column makes a quantitative mass flux comparison between the two upwelling modes difficult. Laws and Maiti (2019) found that the decoupling between primary and export production at the ALOHA time-series station disappears when taking into account data of monthly time intervals. We argue that the same is needed in future artificial upwelling studies. The experimental duration must be long enough to allow for the quantitative assessment of export fluxes as well as the long-term response of higher trophic levels to the enhanced surface primary production.

Upwelling mode shapes sinking particle properties

The export events in the singular treatments were strongly linked to the preceding diatom blooms, as indicated by the elevated BSi:POC ratios in the sedimented matter (**Figure 3D**). They featured relatively porous particles, which sank slower than the ones in the recurring treatments (**Figures 4B,D**), and hence resulted in a low RLS (**Figure 4C**). Multiple studies have shown that diatom blooms typically result in inefficient particle transfer to depth (e.g. Guidi et al. 2009; Henson, Lampitt, and Johns 2012; Maiti et al. 2013), potentially due to the associated high particle porosities (Bach et al. 2019; Lam, Doney, and Bishop 2011; Puigcorbé et al. 2015). Our data supports these observations, stressing the importance of a particle's porosity for its sinking velocity and thus for its potential to be transported to depth.

The influence of transparent exopolymer particles (TEP) may explain the low sinking velocities and high porosities in the singular treatments. TEP are exuded by microbial cells and facilitate the formation of aggregates (Passow 2002; Engel et al. 2004). They can lower particle density and increase porosity, which in turn reduces particle sinking velocity (Azetsu-Scott and Passow 2004; Mari et al. 2017). TEP production is favored by high primary productivity and nutrient limitation (Obernosterer and Herndl 1995), both of which occurred in the higher singular treatments on T9 (**Figure 2B**). Additionally, the POC:PON ratio in the water column increased by >60 % from T9 to T11 in the three highest singular treatments (mean values: 7.3 on T9 to 12.2 on T11, see **Figure 4C**), which indicates potentially enhanced TEP exudation. The same scenario has already been observed in a previous mesocosm experiment off Gran Canaria (Taucher et al. 2017), in which TEP concentrations were measured. During that experiment, TEP increased when the blooming phytoplankton community became nutrient limited (compare Taucher et al. 2017 and 2018). We thus argue that also in our experiment increased TEP exudation was likely the cause for the reduction of particle sinking velocity in

the singular upwelling mode, rendering it less efficient regarding the potential for deep POC export than the recurring mode.

Besides sinking velocity, respiration of sinking matter was another equally important factor determining the remineralization depth of sinking particles in our experiment. The temporal changes in C_{remin} were equally high (about fourfold) as the changes in sinking velocity over time. We measured the highest remineralization rates during the initial export event on T11, shortly after phytoplankton communities had shifted to diatom dominance (T7-T9, Ortiz-Cortes et al., submitted). This is in accordance with earlier studies, which speculated that the structure of the phytoplankton community affects remineralization rates (e.g. Guidi et al. 2015), and have shown that diatom-dominated systems can lead to the export of sinking particles which are quickly respired (Bach et al. 2019; Guidi et al. 2015). In our case, the mechanistic reason for this could be that the particles contained a large fraction of easily degradable organic matter. We believe that the increasing porosities from T11 onwards (**Figure 4D**) support this hypothesis. Although there are, to the best of our knowledge, no studies which found a direct positive effect of aggregate porosity on degradability, it stands to reason that higher porosities increase a particle's surface-to-volume-ratio, thus possibly enhancing its susceptibility to microbial attachment and respiration. This is in line with a hypothesis by Francois et al. (2002), who postulate that the settling of loosely packed (i.e. highly porous) aggregates leads to higher respiration rates in the mesopelagic zone. Respiration of sinking particles during this time was higher in the singular compared to the recurring treatments, likely owing to higher porosities and possibly also higher TEP concentrations. Beside the phytoplankton community structure, the zooplankton community is another factor that determines particle properties (Cavan et al. 2019). Through the packaging of phytoplankton cells into dense fecal pellets, zooplankton can make organic matter less susceptible to respiration (Steinberg and Landry 2017). As discussed above, mesozooplankton was not abundant in our experiment, and therefore potentially not capable of repackaging the high amounts of particulate matter in the high upwelling treatments. This left the sinking biomass loosely packed for the bacterial community to feed on. We suggest that the missing repackaging of particles and the resulting high lability of sinking organic matter was the reason for increasing remineralization with increasing upwelling intensity.

The differences in particle properties between our singular and recurring form of artificial upwelling indicate variability in the efficiency of their POC transfer to depth. Diatom spring blooms (Martin et al. 2011) and diatom communities in coastal upwelling systems (Abrantes et al. 2016) have been reported to promote efficient carbon deep export. However, the diatom blooms in our singular upwelling mode led to the export of porous, slow sinking particles, which were quickly remineralized by microbial processes. A single pulse of artificial upwelling thus resulted in a system likely to recycle the vast majority of the freshly produced organic matter in the surface ocean. Although particles in the recurring upwelling mode were respired similarly quickly, they were less porous and sank faster, which led to a slightly higher mean RLS in the recurring upwelling treatment (**Figure 5C**). This suggests a more efficient transfer of produced organic matter to depth under recurring upwelling conditions compared to a singular upwelling pulse.

Potential of artificial upwelling for carbon sequestration

As discussed above, one of the major factors that influence the potential of artificial upwelling for net carbon sequestration is how deep particles sink before they are remineralized (RLS). Another factor is the C:N ratio of the sinking organic matter (POC:PON), or, more generally speaking, the ratio of C to the limiting nutrient. The influence of both of these factors on carbon sequestration efficiency will be discussed in the following. We emphasize that the discussion is based upon a highly simplified 1-dimensional view of the water column, and neglects 3 dimensional movements of water masses, carbon, and nutrients through the ocean.

We start this discussion with the influence of the ratio of carbon to the limiting nutrient. Since the latter was nitrogen in our case, as is typical for large parts of the Atlantic (Moore et al. 2013), we will focus on the C:N ratio in the following. Let us assume that over long enough time scales all upwelled nutrients will be sequestered (i.e. exported to the sequestration depth), and that the upwelled deep water contains excess DIC (excess DIC = deep water DIC - surface water DIC) and excess DIN (excess DIN = deep water DIN - surface water DIN) compared to the surface ocean. In this case, a system will act as a net carbon sink if it sequesters organic matter with a C:N ratio higher than that of the upwelled excess DIC and nitrogen. In the Canary Island region, excess DIC and excess DIN between surface and 1000 m depth (here assumed as sequestration depth) are approximately ~150 and ~20 $\mu mol\ L^{-1}$, respectively (González-Dávila et al. 2010; Llinás et al. 1994). This corresponds to a C:N ratio of 7.5 of upwelled excess DIC and DIN. Accordingly, for the artificial upwelling approach to generate a net carbon sink, the C:N of sequestered organic matter would need to exceed 7.5 on average, until all N added via deep water has been sequestered.

We found that artificial upwelling led to an increase in C:N ratios of sedimented matter to well above 7.5. There was a trend of increasing $POC_{ST}:PON_{ST}$ ratios over time in all mesocosms (**Figure 3A**). The ratios in the singular treatment mesocosms correlated positively with upwelling intensity in the period of highest export (T11-T21, **Figure 3C**). It is likely that these high ratios would have either prevailed with depth or increased even further, owing to preferential N remineralization by heterotrophic microorganisms (Boyd and Trull 2007).

It should be noted that the control mesocosm also displayed increasing C:N ratios during the experiment. This suggests that increasing C:N might have at least partly been an enclosure effect, which also occurred in absence of an artificial upwelling treatment. By enclosing a planktonic community inside a mesocosm, the vertical mixing is reduced from the depth of the mixed layer (20-120 m in the Canary Island region, see Troupin, Sangrà, and Arístegui 2010) to the depth of the mesocosm (15 m in our setup). This leads e.g. to an increase of depth- and time-integrated light intensity experienced by the phytoplankton community, which may affect phytoplankton photophysiology. Moreover, the community gets truncated as large grazers (>3 mm) are excluded from the food web, thus relieving lower trophic levels like microzooplankton of grazing pressure. Both effects could have caused changes in lower trophic level productivity in our mesocosm experiment, which was fueled by leftover nutrients enclosed at experiment start (see **Figure S1**), thereby leading to an increase in POC_{WC} and $POC_{ST}:PON_{ST}$ ratios (**Figures 2C** and **3A**). Nevertheless, the increase in sedimented matter

C:N ratios was larger in those mesocosms that received deep water fertilizations, and scaled almost linearly with high upwelling rates.

Artificial upwelling can consequently enhance C:N ratios of sinking organic matter in the surface, which would favor potential carbon sequestration. This is especially the case when fertilization is carried out in single pulses. We cannot assess, however, if these ratios would have prevailed over longer time scales, i.e. until all added N had been exported with the remaining suspended particulate organic matter.

A mechanism that might counteract the positive effect of elevated C:N ratios is the observed decrease in RLS with increasing upwelling intensity in both upwelling modes. Particle sinking velocities decreased while at the same time respiration of sinking organic material accelerated with increasing nutrient input via deep water addition. Both effects resulted in a lower RLS and thus higher flux attenuation with increasing fertilization (**Figures 5A-C**). Earlier studies have shown that a higher fraction of export production makes it through the mesopelagic zone in less productive ecosystems and ends up in the deep ocean (e.g. Henson, Sanders, and Madsen 2012). Our results match this finding, with less productive mesocosms showing a higher RLS than the very productive ones. These differences in RLS and thus particle transfer efficiency to depth, as well as the differences in C:N stoichiometries of sinking matter are illustrated in **Figure 6**.
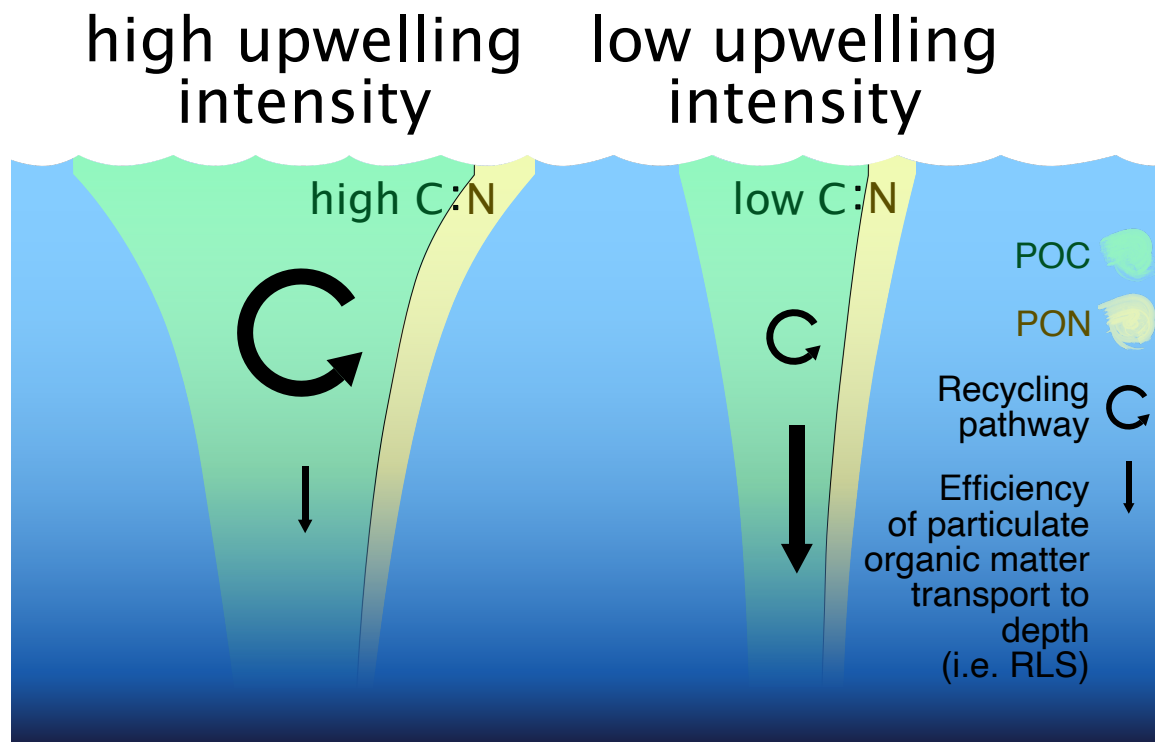
Figure 6: Scheme depicting the effects that upwelling intensity had on carbon sequestration-relevant parameters in our high and low upwelling scenarios. It visualizes the strength and C:N ratio of the export flux (POC_{ST}:PON_{ST}), as well as the arrow size indicating strength of the recycling pathway and the efficiency of particle transport to depth. Note that we put more emphasis on the difference between POC:PON ratios than on the quantitative PON difference between high and low upwelling intensities. It should also be noted, that the effects depicted here only reflect the initial responses to artificial upwelling in oligotrophic waters. They do not cover the ultimate fate of the upwelled inorganic nutrients and hence do not represent the long-term potential for carbon sequestration.

It should be noted that our study could not assess several factors that might play an important role in determining the potential of artificial upwelling for carbon export and sequestration. First of all, our study did not account for any active biological or physical processes occurring further down the water column. Processes such as repackaging and consumption of settling particles by zooplankton (Stukel et al. 2019; Turner 2015) or the active diel migration of mesopelagic biota (Boyd et al. 2019 and references therein) play an important role in regulating particle transfer to depth and thus carbon sequestration (Buesseler et al. 2007; Cavan et al. 2019; Giering et al. 2014; Robinson et al. 2010; Sanders et al. 2016). Due to the limited vertical dimensions of our mesocosms, we were not able to resolve these complex processes occurring throughout the water column, and they are thus not incorporated in **Figure 6**. Secondly, due to the limited experimental duration and the decoupling between production and export of organic matter (especially in the high recurring treatments, see Section 4.1), we could not cover the whole export response period. We were therefore not able to draw quantitative conclusions for the carbon sequestration potential of artificial upwelling. It is likely that this potential would have increased, had the plankton communities had more time to adapt. For example, increased repackaging of suspended biomass into dense, fast-sinking fecal pellets could have favored POC deep export. Hence, we stress the need for monthly to seasonal experimental durations to validate the long-term potential of artificial upwelling for enhanced export production and carbon sequestration.

Conclusion and outlook

Artificial upwelling had opposing effects on carbon export and potential transfer to the deep ocean. On the one hand, it enhanced the mass flux and C:N ratios of sinking matter. The latter is a key prerequisite for enhancing ocean carbon sequestration. Biogeochemical modelling studies examining the feasibility of artificial upwelling in terms of carbon sequestration usually assume a static stoichiometry of C and N according to the Redfield-ratio (= 6.6). An important next step would be to re-evaluate the findings of these studies with a higher than Redfield C:N ratio as we found in our experiment. On the other hand, artificial upwelling resulted in a shallower remineralization depth and a stronger temporal decoupling between POC production and its export. The grazer community was not able to capitalize on the enhanced primary production, and hence could not form the link between biomass production and vertical flux. Thus, artificial upwelling resulted in the export of relatively porous, slowly sinking particles, which were susceptible to remineralization and therefore of low potential for deep export and sequestration. Future work should thus focus on responses of the zooplankton community and allow it more time to react to phytoplankton growth. We furthermore found that the mode, with which upwelling is applied, is an important factor for particle properties and carbon export. We found that the post-bloom export event in the singular mode produced carbon-rich particles, which were however respired faster and sank slower than under recurring upwelling conditions. In contrast, particle properties and the resulting RLS in the recurring mode were more favorable for POC deep export. Additionally, the continuously elevated primary and export production in the recurring mode might be more advantageous for linking the primary and export production of a slow reacting oligotrophic food web. Our assessment thus suggests that a recurring fertilization mode might be more suitable for net CO_2 removal

from the atmosphere than a singular upwelling pulse. However, further research will be needed to verify if either the higher C:N ratios of sinking matter in the singular mode or the more suitable particle properties in the recurring mode are more critical for carbon dioxide removal.

Conflict of Interest

The authors declare that the research was conducted in the absence of any commercial or financial relationships that could be construed as a potential conflict of interest.

Author Contributions

Experimental concept and design: UR, JT, AP, LB. Execution of the experiment: All authors. Data analysis: MB, JO, MV, MH, JT, NH. Manuscript writing: MB with input from all co-authors.

Funding

Acknowledgments

Data availability

The datasets for the water column biogeochemistry and sediment trap parameters are available on PANGAEA under https://doi.pangaea.de/10.1594/PANGAEA.933090 and https://doi.pangaea.de/10.1594/PANGAEA.933089, respectively.

Bibliography

Abrantes, F., Cermeño, P., Lopes, C., Romero, O., Matos, L., Van Iperen, J., Rufino, M., Magalhães, V., 2016. Diatoms Si uptake capacity drives carbon export in coastal upwelling systems. Biogeosciences 13, 4099–4109. https://doi.org/10.5194/bg-13-4099-2016

Azetsu-Scott, K., Passow, U., 2004. Ascending marine particles: Significance of transparent exopolymer particles (TEP) in the upper ocean. Limnol. Oceanogr. 49, 741–748. https://doi.org/10.4319/lo.2004.49.3.0741

Bach, L.T., Paul, A.J., Boxhammer, T., von der Esch, E., Graco, M., Schulz, K.G., Achterberg, E., Aguayo, P., Arístegui, J., Ayón, P., Baños, I., Bernales, A., Boegeholz, A.S., Chavez, F., Chavez, G., Chen, S.-M., Doering, K., Filella, A., Fischer, M., Grasse, P., Haunost, M., Hennke, J., Hernández-Hernández, N., Hopwood, M., Igarza, M., Kalter, V., Kittu, L., Kohnert, P., Ledesma, J., Lieberum, C., Lischka, S., Löscher, C., Ludwig, A., Mendoza, U., Meyer, Jana, Meyer, J., Minutolo, F., Ortiz Cortes, J., Piiparinen, J., Sforna, C., Spilling, K., Sanchez, S., Spisla, C., Sswat, M., Zavala Moreira, M., Riebesell, U., 2020. Factors controlling plankton community production, export flux, and particulate matter stoichiometry in the coastal upwelling system off Peru. Biogeosciences 17, 4831–4852. https://doi.org/10.5194/bg-17-4831-2020

Bach, L.T., Riebesell, U., Sett, S., Febiri, S., Rzepka, P., Schulz, K.G., 2012. An approach for particle sinking velocity measurements in the 3–400 µm size range and considerations on the effect of temperature on sinking rates. Mar Biol 159, 1853–1864. https://doi.org/10.1007/s00227-012-1945-2

Bach, L.T., Stange, P., Taucher, J., Achterberg, E.P., Algueró-Muñiz, M., Horn, H., Esposito, M., Riebesell, U., 2019. The Influence of Plankton Community Structure on Sinking Velocity and Remineralization Rate of Marine Aggregates. Global Biogeochem. Cycles 33, 971–994. https://doi.org/10.1029/2019GB006256

Boxhammer, T., Bach, L.T., Czerny, J., Riebesell, U., 2016. Technical note: Sampling and processing of mesocosm sediment trap material for quantitative biogeochemical analysis. Biogeosciences 13, 2849–2858. https://doi.org/10.5194/bg-13-2849-2016

Boyd, P.W., Claustre, H., Levy, M., Siegel, D.A., Weber, T., 2019. Multi-faceted particle pumps drive carbon sequestration in the ocean. Nature 568, 327–335. https://doi.org/10.1038/s41586-019-1098-2

Boyd, P.W., Trull, T.W., 2007. Understanding the export of biogenic particles in oceanic waters: Is there consensus? Progress in Oceanography 72, 276–312. https://doi.org/10.1016/j.pocean.2006.10.007

Buesseler, K.O., Antia, A.N., Chen, M., Fowler, S.W., Gardner, W.D., Gustafsson, O., Harada, K., Michaels, A.F., Rutgers van der Loeff, M., Sarin, M., Steinberg, D.K., Trull, T., 2007. An assessment of the use of sediment traps for estimating upper ocean particle fluxes. j mar res 65, 345–416. https://doi.org/10.1357/002224007781567621

Casareto, B.E., Niraula, M.P., Suzuki, Y., 2017. Marine planktonic ecosystem dynamics in an artificial upwelling area of Japan: Phytoplankton production and biomass fate. Journal of Experimental Marine Biology and Ecology 487, 1–10. https://doi.org/10.1016/j.jembe.2016.11.002

Cavan, E.L., Laurenceau-Cornec, E.C., Bressac, M., Boyd, P.W., 2019. Exploring the ecology of the mesopelagic biological pump. Progress in Oceanography 176, 102125. https://doi.org/10.1016/j.pocean.2019.102125

Cavan, E.L., Le Moigne, F.A.C., Poulton, A.J., Tarling, G.A., Ward, P., Daniels, C.J., Fragoso, G.M., Sanders, R.J., 2015. Attenuation of particulate organic carbon flux in the Scotia Sea, Southern Ocean, is controlled by zooplankton fecal pellets. Geophys. Res. Lett. 42, 821–830. https://doi.org/10.1002/2014GL062744

Cavan, E.L., Trimmer, M., Shelley, F., Sanders, R., 2017. Remineralization of particulate organic carbon in an ocean oxygen minimum zone. Nat Commun 8, 14847. https://doi.org/10.1038/ncomms14847

Cermeño, P., Fernández, A., Marañón, E., 2012. Deteminación de la producción primaria por tamaños, in: Expedición de Circunnavegación Malaspina 2010: Cambio Global y Exploración de La Biodiversidad Del Océano Global: Libro Blanco de Métodos y Técnicas de Trabajo Oceanográfico. CSIC, pp. 437–442.

Engel, A., Delille, B., Jacquet, S., Riebesell, U., Rochelle-Newall, E., Terbrüggen, A., Zondervan, I., 2004. Transparent exopolymer particles and dissolved organic carbon production by Emiliania huxleyi exposed to different CO_2 concentrations: a mesocosm experiment. Aquat. Microb. Ecol. 34, 93–104. https://doi.org/10.3354/ame034093

Fan, W., Pan, Y., Zhang, D., Xu, C., Qiang, Y., Chen, Y., 2016. Experimental study on the performance of a wave pump for artificial upwelling. Ocean Engineering 113, 191–200.

Francois, R., Honjo, S., Krishfield, R., Manganini, S., 2002. Factors controlling the flux of organic carbon to the bathypelagic zone of the ocean: Factors controlling organic carbon flux. Global Biogeochem. Cycles 16, 34-1-34–20. https://doi.org/10.1029/2001GB001722

GESAMP, 2019. High level review of a wide range of proposed marine geoengineering techniques (No. 98). IMO/FAO/UNESCO-IOC/UNIDO/WMO/IAEA/UN/UN

Environment/ UNDP/ISA Joint Group of Experts on the Scientific Aspects of Marine Environmental Protection.

Giering, S.L.C., Sanders, R., Lampitt, R.S., Anderson, T.R., Tamburini, C., Boutrif, M., Zubkov, M.V., Marsay, C.M., Henson, S.A., Saw, K., Cook, K., Mayor, D.J., 2014. Reconciliation of the carbon budget in the ocean's twilight zone. Nature 507, 480–483. https://doi.org/10.1038/nature13123

Giraud, M., Boye, M., Garçon, V., Donval, A., de la Broise, D., 2016. Simulation of an artificial upwelling using immersed in situ phytoplankton microcosms. Journal of Experimental Marine Biology and Ecology 475, 80–88. https://doi.org/10.1016/j.jembe.2015.11.006

Giraud, M., Garçon, V., De La Broise, D., L'Helguen, S., Sudre, J., Boye, M., 2018. Potential effects of deep seawater discharge by an Ocean Thermal Energy Conversion plant on the marine microorganisms in oligotrophic waters (preprint). Biogeochemistry: Open Ocean. https://doi.org/10.5194/bg-2018-306

González-Dávila, M., Santana-Casiano, J.M., Rueda, M.J., Llinás, O., 2010. The water column distribution of carbonate system variables at the ESTOC site from 1995 to 2004. Biogeosciences 7, 3067–3081. https://doi.org/10.5194/bg-7-3067-2010

Guidi, L., Legendre, L., Reygondeau, G., Uitz, J., Stemmann, L., Henson, S.A., 2015. A new look at ocean carbon remineralization for estimating deepwater sequestration. Global Biogeochem. Cycles 29, 1044–1059. https://doi.org/10.1002/2014GB005063

Guidi, L., Stemmann, L., Jackson, G.A., Ibanez, F., Claustre, H., Legendre, L., Picheral, M., Gorskya, G., 2009. Effects of phytoplankton community on production, size, and export of large aggregates: A world-ocean analysis. Limnol. Oceanogr. 54, 1951–1963. https://doi.org/10.4319/lo.2009.54.6.1951

Hansen, H.P., Koroleff, F., 1999. Determination of nutrients, in: Methods of Seawater Analysis, Third, Completely Revised and Extended Edition. WILEY-VCH, pp. 159–228.

Henson, S.A., Lampitt, R.S., Johns, D., 2012a. Variability in phytoplankton community structure in response to the North Atlantic Oscillation and implications for organic carbon flux. Limnol. Oceanogr. 57, 1591–1601. https://doi.org/10.4319/lo.2012.57.6.1591

Henson, S.A., Le Moigne, F., Giering, S.L.C., 2019. Drivers of Carbon Export Efficiency in the Global Ocean. Global Biogeochem. Cycles 33, 891–903. https://doi.org/10.1029/2018GB006158

Henson, S.A., Sanders, R., Madsen, E., 2012b. Global patterns in efficiency of particulate organic carbon export and transfer to the deep ocean: Export and Transfer Efficiency. Global Biogeochem. Cycles 26. https://doi.org/10.1029/2011GB004099

Iversen, M.H., Ploug, H., 2013. Temperature effects on carbon-specific respiration rate and sinking velocity of diatom aggregates – potential implications for deep ocean export processes. Biogeosciences 10, 4073–4085. https://doi.org/10.5194/bg-10-4073-2013

Iversen, M.H., Ploug, H., 2010. Ballast minerals and the sinking carbon flux in the ocean: carbon-specific respiration rates and sinking velocity of marine snow aggregates. Biogeosciences 7, 2613–2624. https://doi.org/10.5194/bg-7-2613-2010

Jakobsen, H.H., Blanda, E., Staehr, P.A., Højgård, J.K., Rayner, T.A., Pedersen, M.F., Jepsen, P.M., Hansen, B.W., 2015. Development of phytoplankton communities: Implications of nutrient injections on phytoplankton composition, pH and ecosystem production. Journal of Experimental Marine Biology and Ecology 473, 81–89. https://doi.org/10.1016/j.jembe.2015.08.011

Keller, D.P., Feng, E.Y., Oschlies, A., 2014. Potential climate engineering effectiveness and side effects during a high carbon dioxide-emission scenario. Nat Commun 5, 3304. https://doi.org/10.1038/ncomms4304

Kelly, T.B., Goericke, R., Kahru, M., Song, H., Stukel, M.R., 2018. CCE II: Spatial and interannual variability in export efficiency and the biological pump in an eastern boundary current upwelling system with substantial lateral advection. Deep Sea Research Part I: Oceanographic Research Papers 140, 14–25. https://doi.org/10.1016/j.dsr.2018.08.007

Khatiwala, S., Primeau, F., Hall, T., 2009. Reconstruction of the history of anthropogenic CO_2 concentrations in the ocean. Nature 462, 346–349. https://doi.org/10.1038/nature08526

Khatiwala, S., Tanhua, T., Mikaloff Fletcher, S., Gerber, M., Doney, S.C., Graven, H.D., Gruber, N., McKinley, G.A., Murata, A., Ríos, A.F., Sabine, C.L., 2013. Global ocean storage of anthropogenic carbon. Biogeosciences 10, 2169–2191. https://doi.org/10.5194/bg-10-2169-2013

Kirchman, D.L., Ducklow, H.W., 1993. Estimating conversion factors for thymidine and leucine methods for measuring bacterial production, in: Kemp, P.F., Sherr, B.F., Sherr, E.B., Cole, J.J. (Eds.), Handbook of Methods in Aquatic Microbial Ecology. Lewis Publishers, pp. 513–517.

Kwiatkowski, L., Ricke, K.L., Caldeira, K., 2015. Atmospheric consequences of disruption of the ocean thermocline. Environ. Res. Lett. 10, 034016. https://doi.org/10.1088/1748-9326/10/3/034016

Lam, P.J., Doney, S.C., Bishop, J.K.B., 2011. The dynamic ocean biological pump: Insights from a global compilation of particulate organic carbon, $CaCO_3$, and opal concentration profiles from the mesopelagic: The dynamic ocean biological pump. Global Biogeochem. Cycles 25, n/a-n/a. https://doi.org/10.1029/2010GB003868

Laws, E.A., Maiti, K., 2019. The relationship between primary production and export production in the ocean: Effects of time lags and temporal variability. Deep Sea Research Part I: Oceanographic Research Papers 148, 100–107. https://doi.org/10.1016/j.dsr.2019.05.006

Le Moigne, F.A.C., Henson, S.A., Cavan, E., Georges, C., Pabortsava, K., Achterberg, E.P., Ceballos-Romero, E., Zubkov, M., Sanders, R.J., 2016. What causes the inverse relationship between primary production and export efficiency in the Southern Ocean?: PP and *e* Ratio in the Southern Ocean. Geophys. Res. Lett. 43, 4457–4466. https://doi.org/10.1002/2016GL068480

Legendre, L., Le Fèvre, J., 1995. Microbial food webs and the export of biogenic carbon in oceans. Aquat. Microb. Ecol. 9, 69–77. https://doi.org/10.3354/ame009069

Legendre, L., Rivkin, R.B., 2002. Fluxes of carbon in the upper ocean: regulation by food-web control nodes. Mar. Ecol. Prog. Ser. 242, 95–109. https://doi.org/10.3354/meps242095

Leibold, M.A., Chase, J.M., Shurin, J.B., Downing, A.L., 1997. Species Turnover and the Regulation of Trophic Structure 29.

Liu, C.C.K., Dai, J.J., Lin, H., Guo, F., 1999. Hydrodynamic Performance of Wave-Driven Artificial Upwelling Device. J. Eng. Mech. 125, 728–732.

Llinás, O., Rodríguez de León, A., Siedler, G., Wefer, G., 1994. ESTOC Data Report 1994 77.

Maiti, K., Charette, M.A., Buesseler, K.O., Kahru, M., 2013. An inverse relationship between production and export efficiency in the Southern Ocean. Geophys. Res. Lett. 40, 1557–1561. https://doi.org/10.1002/grl.50219

Mari, X., Passow, U., Migon, C., Burd, A.B., Legendre, L., 2017. Transparent exopolymer particles: Effects on carbon cycling in the ocean. Progress in Oceanography 151, 13–37. https://doi.org/10.1016/j.pocean.2016.11.002

Martin, P., Lampitt, R.S., Jane Perry, M., Sanders, R., Lee, C., D'Asaro, E., 2011. Export and mesopelagic particle flux during a North Atlantic spring diatom bloom. Deep Sea Research Part I: Oceanographic Research Papers 58, 338–349. https://doi.org/10.1016/j.dsr.2011.01.006

Masson-Delmotte, V., Zhai, P., Pörtner, H.-O., Roberts, D., Skea, J., Shukla, P.R., Pirani, A., Moufouma-Okia, W., Péan, C., Pidcock, R., Connors, S., Matthews, J.B.R., Chen, Y., Zhou, X., Gomis, M.I., Lonnoy, E., Maycock, T., Tignor, M., Waterfield, T., 2018. IPCC, 2018: Summary for Policymakers. Global Warming of 1.5°C. An IPCC Special Report on the impacts of global warming of 1.5°C above pre-industrial levels and related global greenhouse gas emission pathways, in the context of strengthening the global

response to the threat of climate change, sustainable development, and efforts to eradicate poverty.

McAndrew, P.M., Björkman, K.M., Church, M.J., Morris, P.J., Jachowski, N., Williams, P.J. le B., Karl, D.M., 2007. Metabolic response of oligotrophic plankton communities to deep water nutrient enrichment. Mar. Ecol. Prog. Ser. 332, 63–75. https://doi.org/10.3354/meps332063

Moore, C.M., Mills, M.M., Arrigo, K.R., Berman-Frank, I., Bopp, L., Boyd, P.W., Galbraith, E.D., Geider, R.J., Guieu, C., Jaccard, S.L., Jickells, T.D., La Roche, J., Lenton, T.M., Mahowald, N.M., Marañón, E., Marinov, I., Moore, J.K., Nakatsuka, T., Oschlies, A., Saito, M.A., Thingstad, T.F., Tsuda, A., Ulloa, O., 2013. Processes and patterns of oceanic nutrient limitation. Nature Geosci 6, 701–710. https://doi.org/10.1038/ngeo1765

Nielsen, E.S., 1952. The Use of Radio-active Carbon (C14) for Measuring Organic Production in the Sea. ICES Journal of Marine Science 18, 117–140. https://doi.org/10.1093/icesjms/18.2.117

Obernosterer, I., Herndl, G.J., 1995. Phytoplankton extracellular release and bacterial growth: dependence on the inorganic N: P ratio. Mar. Ecol. Prog. Ser. 116, 247–257. https://doi.org/10.3354/meps116247

Oschlies, A., Pahlow, M., Yool, A., Matear, R.J., 2010. Climate engineering by artificial ocean upwelling: Channelling the sorcerer's apprentice: OCEAN PIPE IMPACTS. Geophys. Res. Lett. 37. https://doi.org/10.1029/2009GL041961

Pan, Y., Fan, W., Huang, T.-H., Wang, S.-L., Chen, C.-T.A., 2015. Evaluation of the sinks and sources of atmospheric CO_2 by artificial upwelling. Science of The Total Environment 511, 692–702. https://doi.org/10.1016/j.scitotenv.2014.11.060

Pan, Y., Fan, W., Zhang, D., Chen, J.W., Huang, H., Liu, S., Jiang, Z., Di, Y., Tong, M., Chen, Y., 2016. Research progress in artificial upwelling and its potential environmental effects. Sci. China Earth Sci. 59, 236–248. https://doi.org/10.1007/s11430-015-5195-2

Passow, U., 2002. Transparent exopolymer particles (TEP) in aquatic environments. Progress in Oceanography 55, 287–333. https://doi.org/10.1016/S0079-6611(02)00138-6

Pedrosa-Pàmies, R., Conte, M.H., Weber, J.C., Johnson, R., 2019. Hurricanes Enhance Labile Carbon Export to the Deep Ocean. Geophysical Research Letters 46, 11. https://doi.org/10.1029/2019GL083719

Ploug, H., Grossart, H.-P., 2000. Bacterial growth and grazing on diatom aggregates: Respiratory carbon turnover as a function of aggregate size and sinking velocity. Limnol. Oceanogr 45, 1467–1475. https://doi.org/10.4319/lo.2000.45.7.1467

Puigcorbé, V., Benitez-Nelson, C.R., Masqué, P., Verdeny, E., White, A.E., Popp, B.N., Prahl, F.G., Lam, P.J., 2015. Small phytoplankton drive high summertime carbon and nutrient export in the Gulf of California and Eastern Tropical North Pacific. Global Biogeochem. Cycles 29, 1309–1332. https://doi.org/10.1002/2015GB005134

R Core Team, 2021. R: A Language and Environment for Statistical Computing.

Riebesell, U., Czerny, J., von Bröckel, K., Boxhammer, T., Büdenbender, J., Deckelnick, M., Fischer, M., Hoffmann, D., Krug, S.A., Lentz, U., Ludwig, A., Muche, R., Schulz, K.G., 2013. Technical Note: A mobile sea-going mesocosm system – new opportunities for ocean change research. Biogeosciences 10, 1835–1847. https://doi.org/10.5194/bg-10-1835-2013

Ristow, G.H., 1997. Wall correction factor for sinking cylinders in fluids. Phys. Rev. E 55, 2808–2813. https://doi.org/10.1103/PhysRevE.55.2808

Robinson, C., Steinberg, D.K., Anderson, T.R., Arístegui, J., Carlson, C.A., Frost, J.R., Ghiglione, J.-F., Hernández-León, S., Jackson, G.A., Koppelmann, R., Quéguiner, B., Ragueneau, O., Rassoulzadegan, F., Robison, B.H., Tamburini, C., Tanaka, T., Wishner, K.F., Zhang, J., 2010. Mesopelagic zone ecology and biogeochemistry – a synthesis. Deep Sea Research Part II: Topical Studies in Oceanography 57, 1504–1518. https://doi.org/10.1016/j.dsr2.2010.02.018

Sabine, C.L., Feely, R.A., Gruber, N., Key, R.M., Lee, K., Bullister, J.L., Wanninkhof, R., Wong, C.S., Wallace, D.W.R., Tilbrook, B., Millero, F.J., Huang, T.-H., Kozyr, A., Ono, T., Rios, A.F., 2004. The Oceanic Sink for Anthropogenic CO_2. Science 305, 367–371.

Sanders, R.J., Henson, S.A., Martin, A.P., Anderson, T.R., Bernardello, R., Enderlein, P., Fielding, S., Giering, S.L.C., Hartmann, M., Iversen, M., Khatiwala, S., Lam, P., Lampitt, R.S., Mayor, D.J., Moore, M.C., Murphy, E., Painter, S.C., Poulton, A.J., Saw, K., Stowasser, G., Tarling, G.A., Torres-Valdes, S., Trimmer, M., Wolff, G.A., Yool, A., Zubkov, M., 2016. Controls over Ocean Mesopelagic Interior Carbon Storage (COMICS): Fieldwork, Synthesis, and Modeling Efforts. Front. Mar. Sci. 3. https://doi.org/10.3389/fmars.2016.00136

Sharp, J.H., 1974. Improved analysis for "particulate" organic carbon and nitrogen from seawater. Limnol. Oceanogr. 19, 984–989. https://doi.org/10.4319/lo.1974.19.6.0984

Stange, P., Bach, L.T., Le Moigne, F.A.C., Taucher, J., Boxhammer, T., Riebesell, U., 2017. Quantifying the time lag between organic matter production and export in the surface ocean: Implications for estimates of export efficiency: Time Lag and Export Efficiency. Geophys. Res. Lett. 44, 268–276. https://doi.org/10.1002/2016GL070875

Steinberg, D.K., Landry, M.R., 2017. Zooplankton and the Ocean Carbon Cycle. Annu. Rev. Mar. Sci. 9, 413–444. https://doi.org/10.1146/annurev-marine-010814-015924

Strohmeier, T., Strand, Ø., Alunno-Bruscia, M., Duinker, A., Rosland, R., Aure, J., Erga, S.R., Naustvoll, L.J., Jansen, H.M., Cranford, P.J., 2015. Response of Mytilus edulis to enhanced phytoplankton availability by controlled upwelling in an oligotrophic fjord. Mar. Ecol. Prog. Ser. 518, 139–152. https://doi.org/10.3354/meps11036

Stukel, M.R., Landry, M.R., Benitez-Nelson, C.R., Goericke, R., 2011. Trophic cycling and carbon export relationships in the California Current Ecosystem. Limnol. Oceanogr. 56, 1866–1878. https://doi.org/10.4319/lo.2011.56.5.1866

Stukel, M.R., Ohman, M.D., Kelly, T.B., Biard, T., 2019. The Roles of Suspension-Feeding and Flux-Feeding Zooplankton as Gatekeepers of Particle Flux Into the Mesopelagic Ocean in the Northeast Pacific. Front. Mar. Sci. 6, 397. https://doi.org/10.3389/fmars.2019.00397

Svensen, C., Nejstgaard, J.C., Egge, J.K., Wassmann, P., 2002. Pulsing versus constant supply of nutrients (N, P and Si): effect on phytoplankton, mesozooplankton and vertical flux of biogenic matter. Sci. Mar. 66, 189–203. https://doi.org/10.3989/scimar.2002.66n3189

Taucher, J., Bach, L.T., Boxhammer, T., Nauendorf, A., Achterberg, E.P., Algueró-Muñiz, M., Arístegui, J., Czerny, J., Esposito, M., Guan, W., Haunost, M., Horn, H.G., Ludwig, A., Meyer, J., Spisla, C., Sswat, M., Stange, P., Riebesell, U., 2017. Influence of Ocean Acidification and Deep Water Upwelling on Oligotrophic Plankton Communities in the Subtropical North Atlantic: Insights from an In situ Mesocosm Study. Front. Mar. Sci. 4. https://doi.org/10.3389/fmars.2017.00085

Taucher, J., Boxhammer, T., Bach, L.T., Paul, A.J., Schartau, M., Stange, P., Riebesell, U., 2021. Changing carbon-to-nitrogen ratios of organic-matter export under ocean acidification. Nat. Clim. Chang. 11, 52–57. https://doi.org/10.1038/s41558-020-00915-5

Taucher, J., Stange, P., Algueró-Muñiz, M., Bach, L.T., Nauendorf, A., Kolzenburg, R., Büdenbender, J., Riebesell, U., 2018. In situ camera observations reveal major role of zooplankton in modulating marine snow formation during an upwelling-induced plankton bloom. Progress in Oceanography 164, 75–88. https://doi.org/10.1016/j.pocean.2018.01.004

Troupin, C., Sangrà, P., Arístegui, J., 2010. Seasonal variability of the oceanic upper layer and its modulation of biological cycles in the Canary Island region. Journal of Marine Systems 80, 172–183. https://doi.org/10.1016/j.jmarsys.2009.10.007

Turner, J.T., 2015. Zooplankton fecal pellets, marine snow, phytodetritus and the ocean's biological pump. Progress in Oceanography 130, 205–248. https://doi.org/10.1016/j.pocean.2014.08.005

Wickham, H., Averick, M., Bryan, J., Chang, W., D'Agostino McGowan, L., François, R., Grolemund, G., Hayes, A., Henry, L., Hester, J., Kuhn, M., Pedersen, T.L., Miller, E.,

Bache, S.M., Müller, K., Ooms, J., Robinson, D., Seidel, D.P., Spinu, V., Takahashi, K., Vaughan, D., Wilke, C., Woo, K., Hiroaki, Y., 2019. Welcome to the tidyverse. Journal of Open Source Software 4, 1686. https://doi.org/10.21105/joss.01686

Yool, A., Shepherd, J.G., Bryden, H.L., Oschlies, A., 2009. Low efficiency of nutrient translocation for enhancing oceanic uptake of carbon dioxide. J. Geophys. Res. 114, C08009. https://doi.org/10.1029/2008JC004792

3 Manuscript II

Drivers of Particle Sinking Velocities in the Peruvian Upwelling System

Moritz Baumann[1], Allanah Joy Paul[1], Jan Taucher[1], Lennart Thomas Bach[2], Silvan Goldenberg[1], Paul Stange[1], Fabrizio Minutolo[3], Ulf Riebesell[1]

[1]Biological Oceanography, GEOMAR Helmholtz Centre for Ocean Research Kiel, Kiel, Germany
[2]Institute for Marine and Antarctic Studies, University of Tasmania, Hobart, Tasmania, Australia
[3]Helmholtz Centre Hereon, Institute of Carbon Cycles, Geesthacht, Germany

Abstract. As one of earth's most productive marine ecosystems, the Peruvian Upwelling System transports large amounts of biogenic matter from the surface to the deep ocean. Whilst particle sinking velocity is a key driver of O_2-depletion processes and carbon sequestration, it has not yet been measured in this system. During a 50-day mesocosm experiment in the surface waters off the coast of Peru, we measured particle sinking velocities and their biogeochemical and physical drivers. Sinking velocities varied between size classes and ranged from 12.8 ± 0.7 m d^{-1} (particles 40–100 μm), to 19.4 ± 0.7 m d^{-1} (particles 100–250 μm), and 34.2 ± 1.5 m d^{-1} (particles 250–1000 μm) ($\pm$ 95% confidence interval). We found connections between the phytoplankton community succession and sinking particle properties that were, however, only weakly reflected by sinking velocities. Surprisingly, we did not find a clear relationship between opal ballast and sinking velocity, despite a pronounced temporal variability in opal. This suggest that opal ballast is not a relevant proxy for sinking velocity. Furthermore, we found faster sinking velocities with increasing particle size, compactness and roundness. Size was by far the strongest driver among these physical particle properties. Our study provides a detailed analysis of drivers influencing particle sinking velocity in the Peruvian Upwelling System, which allows modelers to optimize local particle flux parameterization. This will help to better project oxygen concentrations and carbon sequestration in a region that is subject to substantial climate-driven changes.

Introduction

The Peruvian Upwelling System is one of the most productive marine ecosystems in the world (Pennington et al., 2006). It is situated along the Peruvian and northern Chilean coasts in the boundary current system of the Eastern Tropical South Pacific and is one of four major Eastern Boundary Upwelling Systems (EBUS). It is characterized by strong Ekman-transport-induced upwelling of nutrient-rich subsurface water along the coast, which results in a shallow thermocline that confines an optimal phytoplankton habitat. The high primary productivity of Peru's "brown waters" sustains a rich ecosystem with abundant fish and other larger organisms and leads to the vertical transport of large amounts of biogenic matter (Kämpf and Chapman, 2016). This sinking flux fuels high respiration rates in the subsurface, which in combination with slow ventilation results in permanently oxygen deficient waters (Chavez and Messié, 2009). These can start at 50 m depth and shallower (Kämpf and Chapman, 2016; Karthäuser et al., 2021a), stretch hundreds of meters of depth (Karstensen et al., 2008) and extend up to 1000 km from the coast. The dimensions and biogeochemical properties of this oxygen minimum zone (OMZ) are directly affected by the amount and properties of sinking material (Kalvelage et al., 2013; Karthäuser et al., 2021b).

A key metric of sinking biogenic matter is the velocity with which particles settle (e.g. Marsay et al., 2015). Sinking velocity influences the transfer efficiency of biogenic matter to depth and hence the export of carbon via the biological pump, which sequesters CO_2 in the ocean interior (Khatiwala et al., 2013; McDonnell et al., 2015). In the Peruvian Upwelling System, sinking velocity additionally determines the length of exposure of a particle to deoxygenated OMZ waters. Here, the degradation of small sinking particles (<500 μm) might contribute significantly to the loss of nitrogen via anammox (Karthäuser et al., 2021b) and hence to the sustained presence of the subsurface OMZ.

Sinking velocity is controlled by a variety of physical characteristics. A particle's excess density compared to sea water ultimately determines whether it sinks and how fast. Amongst particles of the same composition and structure, larger particles sink faster (Riley et al., 2012). Yet, a small but dense particle can also sink fast (McDonnell and Buesseler, 2010). Although a size-sinking velocity relationship has not been detected in some observational datasets (Iversen and Lampitt 2020), a recent meta-analysis resolved a relatively weak but clear relationship (Cael et al., 2021). Particle size is hence considered relevant, but not the primary factor determining sinking velocity.

Particle density and size are dependent on biological processes, which influence the structure, shape and composition of a particle. Diatom blooms can produce large cells with appendages, that promote aggregation, and can lead to fast sinking matter (Smetacek et al., 2012). An oligotrophic phytoplankton community, on the other hand, consists of smaller cells, which tend to sink slower (Guidi et al., 2009). Biomineral ballast produced by phyto- and zooplankton is denser than organic matter (calcium carbonate, opal and organic matter densities: 2.71, 2.1 and ~1.06 g cm^{-3}, respectively; Klaas and Archer 2002) and can enhance particle sinking velocities (Armstrong et al., 2009). Furthermore, the porosity of a particle (i.e. the fraction of particle volume occupied by seawater) affects its density (Laurenceau-Cornec et al., 2020). If organic matter is densely packed, e.g. by zooplankton into a fecal pellet, it has a higher excess density and sinks faster compared to one that is packed more loosely (Steinberg and Landry,

2017; Bach et al., 2019). The plankton community structure thus influences physical characteristics of sinking particles (Bach et al., 2019; Turner, 2015; Guidi et al., 2009).

Here, we report sinking velocities and physical particle properties of more than 100.000 individual particles collected during a mesocosm study in the Peruvian Upwelling System (Bach et al., 2020). We determine relationships between velocity and particle size, shape and porosity. We further assessed how sinking velocities change with the quantity and stoichiometry of the overall export flux, as well as with the proportion of biogenic ballast, and try to decipher the influence of the prevailing phytoplankton community. Our study provides insights into the controls of particle sinking velocity, a key aspect of carbon sequestration and OMZ shaping processes.

Materials and Methods

Experimental Setup

Our experimental setup consisted of eight sea-going mesocosms (M1–M8, see Riebesell et al., 2013), which were moored in the coastal upwelling area off Callao, Peru (12.06°S, 77.23°W), on February 23rd, 2017 (late austral summer). The top and bottom openings were equipped with screens of 3 mm mesh size to keep larger organisms such as small pelagic fish out of the mesocosms. The mesocosms were left fully submerged for two days after mooring to ensure a flow-through of surrounding Pacific water. Afterwards, the two screens of each mesocosm were removed, the top was pulled above sea level and a cone-shaped sediment trap was attached to the bottom, thereby enclosing a pelagic community inside the mesocosms. They contained ~ 54 m^3 of sea water and extended 19 m below the water surface. The closing of the mesocosms marked the start of the experiment (t0, February 25th), which lasted for 50 days until April 16th.

To simulate an upwelling event and test the effect of oxygen minimum zone (OMZ)-influenced water masses on the natural plankton community, we collected two different OMZ-influenced water batches and added them to the mesocosms. The batches differed from each other in terms of NO_x^- (nitrate + nitrite) concentrations. One had low and the other very low NO_x^- concentrations of 4 and 0.3 μmol L^{-1}, respectively, compared to the naturally occurring waters of the coastal upwelling area. Our OMZ treatment thus had two levels: low NO_x^- and very low NO_x^-. The upwelling event was simulated on t11 and t12 by replacing 20 m^3 of mesocosm water with OMZ-influenced water in every mesocosm. Mesocosms M1, M4, M5 and M8 received water from station 1 (low NO_x^-), whereas mesocosms M2, M3, M6 and M7 were fertilized with water from station 3 (very low NO_x^-). Figure 2 in Bach et al. (2020) shows the changes in the dissolved nutrient pools following the additions.

An overview of the basic system parameters, as well as detailed information on the experimental setup, mesocosm maintenance, sampling procedure and sample analysis is given in the overview paper by Bach et al. (2020).

Sampling procedure

Long silicon tubes were connected to the bottom of the sediment traps, through which sedimented matter was sampled using a manual vacuum pump (< 0.3 bar, see Boxhammer et al., 2016). The sediments were pumped into 5L glass bottles (Schott, Denmark), which were stored dark and cool until arrival in the lab. There, the sample bottles were gently rotated and the mixed sediment suspension was subsampled for particle sinking velocity measurements using a pipette.

Bulk water column samples were taken at least every second day and were used for a variety of parameters, among which were chlorophyll *a* and phytoplankton community composition (Bach et al., 2020). Depth-integrated water samples were taken using 5 L water samplers equipped with pressure sensors (Hydro-Bios, Germany). The samples were transferred into 10 L carboys and transported to the on-shore laboratories.

Sample analysis

All samples were processed in on-shore laboratories inside the Club Náutico Del Centro Naval and the Instituto del Mar del Perú (IMARPE), both located in La Punta (Callao), and were either measured directly or prepared for transport to the GEOMAR Helmholtz-Centre for Ocean Research Kiel for later analyses.

Sinking velocity and particle properties

Sinking velocity and optical particle properties were measured via video microscopy using the method described in Bach et al. (2012) and further developed in previous studies (Bach et al., 2019; Baumann et al., 2021). The sediment subsamples were transferred to a sinking chamber (edge length: 1 x 1 cm), which was mounted vertically in a FlowCam device (Fluid Imaging Technologies, United States). The trajectories of sinking particles were recorded for 20 min at ~7 frames per second and sinking velocities were calculated by fitting a linear model to the vertical positions and time stamps of multiple captures of the same particle. Besides position and time, the FlowCam measured proxies for several physical particle properties for each individual particle. Particle size was estimated as equivalent spherical diameter (ESD), shape as the aspect ratio (length to width ratio) and porosity as a size-normalized measure for particle intensity (P_{int}). To calculate the porosity-proxy, each particle image was transformed to a greyscale with dark pixels considered optically opaque (low intensity) and bright pixels translucent (high intensity, pixel intensity ranging from 0 to 255). The underlying assumption is that a particle looks brighter when it is more porous, compared to a darker-appearing particle. Since larger particles are generally more porous than smaller ones (Laurenceau-Cornec et al., 2020), we combined the intensity value with particle size (i.e. ESD) and calculated porosity (P_{int}) following Bach et al. (2019).

$$P_{int} = (intensity/255)^2 * ESD \qquad (1)$$

Particles out of focus were excluded from the analysis based on their sharpness. Sinking velocities were corrected for wall effects of the sinking chamber using the equation given in Ristow (1997). Measurements were carried out in a temperature controlled lab, which was set

to daily *in situ* temperatures of between 16 and 21 °C. Calculations were done using the MATLAB script described by Bach et al. (2012), which was adjusted for a broader particle size spectrum (40–1000 μm). Further data analysis was carried out using the R software (R Core Team, 2021; version 4.1.2), and the package "tidyverse" (Wickham et al., 2019).

The size distribution of the measured particles was heavily right-skewed, i.e. there were far more small than large particles. Based on the ESD, the sinking velocity data were thus separated into three size classes, 40–100 μm, 100–250 μm, and 250–1000 μm. The increasing bin widths thereby consider the particle size distribution, resulting in narrower size classes for small particles and broader ones for larger particles. Due to the relatively low contribution of large particles in general, for some measurements there were too few particles in the large size class to be considered for further analysis. We hence removed the 250–1000 μm size class of those measurements that consisted of fewer than 3 particles. This affected the measurements of M5 and M7 on T32, as well as M5 on T40, and M7 on T48. The right-skewed size distribution was also the reason why we plotted the median ESD, porosity and aspect ratio in **Fig. 3a**, since the mean would have given the few large particles undue weight.

Furthermore, our sinking velocity and ESD measurements of all particles measured across mesocosms were collated and used to resolve the relationship between sinking velocity and particle size, following the power function of Cael et al (2021, Eq. 3).

$$SV(ESD) = \alpha * ESD^{\beta} \qquad (2)$$

Here, α and β are scaling factors, whose variability is based on the particle characteristics and environmental conditions (e.g. composition, porosity, temperature). They were estimated for our data set using the linearized logarithmic function.

$$\log SV = \beta * \log ESD + \log \alpha \qquad (3)$$

In order to not give the numerous small particles in our measurements undue weight, the sinking velocity and ESD data were binned into log-spaced size classes (40–63, 63–100, 100–158, 158–251, 251–398, 398–631, 631–1000). Per size class, log(sinking velocity) and log(ESD) means from all eight mesocosms were calculated for each experimental day. Based on these, size-sinking relationships were calculated by fitting linear models, in which the slope represented the scaling factor β and the y-intercept log(α). From these daily α and β coefficients average values (± SD) over time were calculated, and the corresponding relationships were plotted in **Fig. 4** (Sect. 4.2.3). Since the largest size class (631–1000 μm) had too few particle counts (<500 particles), in order to calculate a meaningful and representative size-sinking relationship, we only used the size classes between 40 and ~630 μm.

Elemental analysis of sediment trap samples

The remaining sediment trap samples were prepared for elemental analysis by removing the particulate material from the water. For this, the samples were treated with 3 M FeCl$_3$ to induce particle flocculation, coagulation and subsequent sedimentation inside the 5 L bottle and with 3 M NaOH to adjust the pH to 8.1. Subsequently, they went through multiple centrifugation steps (see Bach et al., 2020 for details), after each of which the supernatant was carefully decanted. The resulting sediment pellets were deep-frozen and transported to Kiel, where they were freeze-dried to remove the remaining moisture. The dry pellets were ground in a ball mill,

which produced a fine homogeneous powder (Boxhammer et al., 2016). Representative subsamples of the sediment powder were analyzed for their contents of particulate organic carbon and nitrogen (POC/PON), particulate inorganic carbon (PIC, i.e. calcium carbonate), biogenic silica (BSi, i.e. opal) and total particulate phosphorus (TPP). In contrast to the sinking velocity measurements, the elemental analysis of sediment samples was not carried out for single particles, but for the bulk particulate matter flux.

TPP and BSi contents were measured spectrophotometrically after Hansen and Koroleff (1999) and C and N contents were measured on an elemental analyzer (EuroEA) following Sharp (1974). While PON samples were measured directly, subsamples for POC were fumed with 1 mol L^{-1} HCl and dried at 50 °C overnight to remove the inorganic carbon fraction prior to its measurement. PIC was calculated as the difference between the carbon contents of HCl-untreated and HCl-treated subsamples, i.e. between subsamples containing inorganic carbon and subsamples not containing any. Total mass fluxes to the sediment trap were obtained by upscaling the measured contents of each compound to the total sample weight. Mass fluxes were then normalized to the mesocosm volume and the time between sampling collection (48 h) to obtain mass flux data in µmol L^{-1} d^{-1}.

We further calculated the relative contribution of opal and calcium carbonate to the total export flux, i.e. their biomineral weight fractions (BSi$_{WF}$ and PIC$_{WF}$), on each sampling day according to Bach et al. (2016) as

$$biomineral_{WF} = \frac{biomineral_{ST}*density_{biomineral}}{1.06*POC_{ST}+2.1*BSi_{ST}+2.7*PIC_{ST}} \quad (4)$$

where 'biomineral' stands for either BSi or PIC, and POC$_{ST}$, BSi$_{ST}$ and PIC$_{ST}$ are the daily mass fluxes to the sediment trap of the respective compound.

Chlorophyll *a* and phytoplankton pigments

Samples for chlorophyll *a* and other phytoplankton pigments were filtered through combusted (450 °C, 6h) GF/F glass fiber filters (0.7 µm pore size, Whatman) in the on-shore laboratories. Directly after filtration the filters were flash-frozen in cryo-vials and stored at -80 °C. Back in Kiel, phytoplankton pigments were extracted from the filters using 100 % acetone as described by Paul et al. (2015) and then analyzed using reverse-phase high-performance liquid chromatography (HPLC, Barlow et al., 1997). The output was analyzed using CHEMTAX, which classifies phytoplankton taxa based on their pigment ratios (Mackey et al., 1996) and allows to estimate the contribution of different phytoplankton taxa to the total amount of chlorophyll *a*. We employed the reference pigment ratios described for the Peruvian Upwelling System by DiTullio et al. (2005).

Data analysis

Linear mixed effects models were used to investigate the relationship between our predictors and particle sinking velocity as central response variable. *Day* (of the experiment) was always employed as categorical fixed effect and *Mesocosm* as random effect (n=8, random intercept) to account for the repeated measures of the mesocosms over time. The models were fitted using

restricted maximum likelihood. Analysis of variance was used to test for significances of the fixed effects (type III test, Satterthwaite's approximation, $\alpha = 0.05$).

Firstly, we tested the effect of the upwelling with different oxygen minimum zone water (*OMZ*, categorical with 2 levels: very low and low NO_x). Average *sinking velocity* of each size fraction (40–100, 100–250 and 250–1000 μm) was modelled as a function of *OMZ*, *Day* and their interaction (*OMZ × Day*). We only included data obtained after the application of the treatment (OMZ water addition on t11/t12). *OMZ × Day* or *OMZ* was clearly insignificant for all size classes (all p-values >0.318, see **Table A1** in the Appendices). For the purpose of parsimony, we therefore removed the factor *OMZ* from all our subsequent investigations. The appropriateness of this exclusion was verified by fitting all following models once with and once without *OMZ*, finding it to be highly insignificant in every instance.

Secondly, we explored the influence of biogeochemical properties of the export flux (continuous predictors), that are, in turn, a result of the current state of the pelagic system. The average *sinking velocity* of each size fraction (40–100, 100–250 and 250–1000 μm) was modelled as a function of *Day* and a series of continuous fixed effects including the magnitude of the export flux (POC_{ST}), its elemental composition ($N_{ST}{:}P_{ST}$) and the contribution of biominerals (BSi_{WF} and PIC_{WF}).

Thirdly, we modelled the relationship between sinking velocity and physical particle properties. *Sinking velocity* was modelled as a function of *Day* and the continuous fixed effects particle size (*ESD*), particle porosity (P_{int}) and shape (*Aspect ratio*, i.e. length to width ratio). Here, we could use individual particles as the lowest level of replication, as the FlowCam data provided matching measures of physical properties and sinking velocity for hundreds of particles per mesocosm and day, resulting in an $N > 100{,}000$ particles. In order to account for the relatedness of particles measured within the same sample, the factor *Sample* was added as additional random effect (random intercept) nested within *Mesocosm*. Since porosity is dependent on size in Eq. 1, we assured that there was no autocorrelation between size and porosity (in a tentative model fit without interaction terms).

Statistical analysis was carried out using R (R Core Team, 2021). The packages lme4 (Bates et al., 2015) and lmerTest (Kuznetsova et al., 2017), sjstats (Lüdecke, n.d.) and performance (Lüdecke et al., 2021) were used to fit and test linear mixed effect models, calculate partial effect sizes (partial eta squared = η_p^2) and check assumptions, respectively. The normality of residuals and random effects were checked using Q-Q plots and the homogeneity of variance using residuals versus fitted plots. Data was transformed where necessary. Autocorrelation was tested for using Durbin-Watson tests. Multicollinearity was assessed by calculating the variance inflation factor and assessing the correlations between predictors. The fitted models were checked for influential data points using Cook's distance and detected outliers removed.

Results

Particle sinking velocities and phytoplankton community succession

We observed average sinking velocities of 12.8 ± 0.7 m d^{-1} (particle size: 40–100 μm), 19.4 ± 0.7 m d^{-1} (particle size: 100–250 μm), and 34.2 ± 1.5 m d^{-1} (particle size: 250–1000 μm) ($\pm$ 95% CI, **Fig. 1a–c**). Sinking velocities increased almost threefold from the smallest to the largest size class. The variability in sinking velocities of bulk sediment samples across space and time is indicated by standard deviations of 0.8, 0.9, and 1.8 m d^{-1} from the smallest to the largest size fraction, respectively. Individual particles were much more variable, however, ranging from <1 to 267 m d^{-1}.

The oxygen minimum zone (OMZ) treatment did not affect sinking velocities in any of the particle size classes over the course of the experiment (**Fig. 1** and **Table A1**). Any potential signal of the OMZ treatment (red and blue lines) must have been minor compared to the variability caused by other processes, so that mesocosms appeared to be distributed randomly around the overall mean (**Fig. 1**).
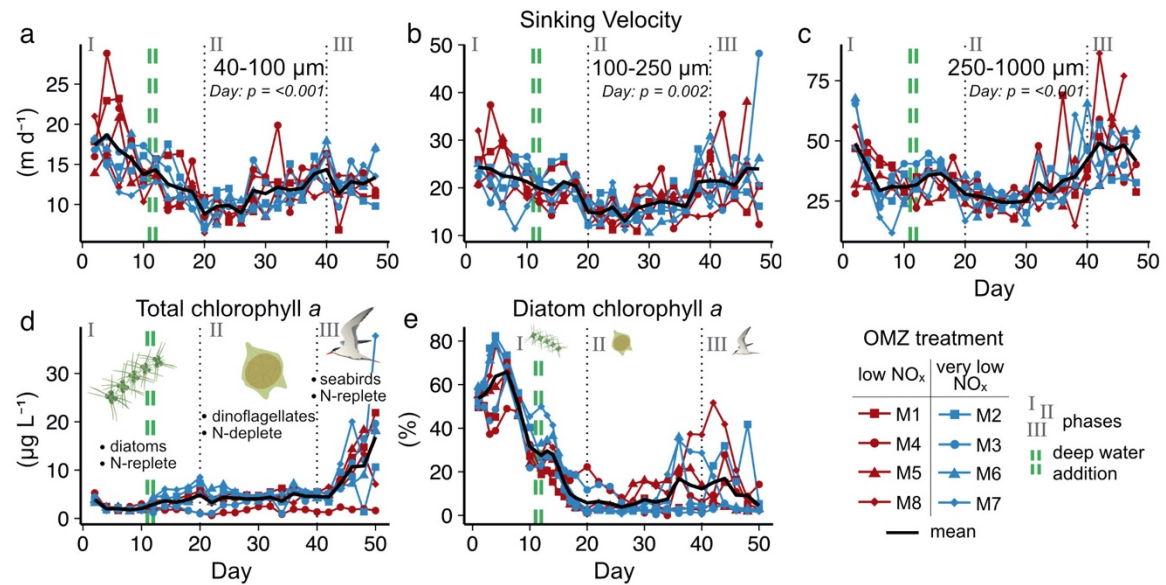
Figure 1. Temporal developments in particle sinking velocities and phytoplankton community. (**a**)–(**c**) Mean daily sinking velocities sampled from the sediment trap in three particle size classes. Significant fixed effects (*OMZ*, *Day* or *OMZ×Day*) are displayed including p-values (**Table A1**). (**d**)–(**e**) Total chlorophyll *a* and the contribution of diatoms to total chlorophyll *a* in the water column. Here, the shifts in phytoplankton and trophic state are indicated by text and symbols (Integration and Application Network; ian.umces.edu/media-library).

In contrast, pronounced temporal trends in sinking velocity were detected in all size classes, represented by the factor Day (**Fig. 1** and **Table A1**). Depending on the size class, between 42 % and 48 % of the variation in sinking velocity was explained by our models (see R^2 in **Table A1**), primarily via this temporal effect. Generally, sinking velocities started high,

progressively fell and reached their minimum in the middle of the experiment before rising again to higher levels towards the end.

We observed a distinct phytoplankton community succession, which is linked to both suspended and exported particulate matter and ultimately particle sinking velocities. Following these major biogeochemical developments, we segmented the experiment into three distinct phases: phase I (t1–t20), phase II (t20–t40) and phase III (t40–t50) (for details see Bach et al. (2020). The conditions inside the mesocosms were initially N-replete and sustained diatom-dominated communities (**Fig. 1e**). Although the OMZ water addition on t11/t12 enriched the dissolved inorganic nutrient pools slightly, these nutrients were readily taken up, and the systems became N-deplete at around t20 (see Fig. 4 in Bach et al. 2020). The decline in diatom dominance as nutrients became depleted coincided with a gradual decrease in sinking velocities of exported particles. The sinking of the smaller, yet most abundant particles slowed down in particular, with more than 50 % lower sinking velocities on t20 compared to the beginning when diatoms dominated. The community shifted towards the mixotrophic dinoflagellate *Akashiwo sanguinea*, which thrived under the regenerative conditions, and sinking velocities reached their minimum between t20 and t30. Finally, during the last ten days of the experiment (t40–t50) seabirds (Inca tern, *Larosterna inca*) started to use the mesocosm facilities as a resting place, defecating into the mesocosms and thereby providing new N and P, fueling new production (**Fig. 1d**). Simultaneously, sinking velocities reached another maximum towards t50, this time especially in the medium and large size classes.

Export flux and biomineral ballast

We could not detect an influence of particle sinking velocities on the magnitude and quality of the export flux in any of the size classes (**Fig. 2b** and **Table A2**). In this analysis, mean daily sinking velocities were neither correlated with the amount of sinking particulate organic carbon (POC) nor with the composition of the exported material, including the contribution of biominerals such as biogenic silica and calcium carbonate or the sedimented N:P ratio.

The phytoplankton community succession in the water column was, nevertheless, associated to clear temporal trends in the magnitude and elemental composition of the export flux (**Fig. 2a–b**). The period of diatom-domination (phase I) was characterized by variable daily fluxes that consisted of almost 30 % biogenic silica. The subsequent shift from diatoms to the dinoflagellate *A. sanguinea* (phase II) was apparent in a five-fold decrease of the opal weight fraction (BSi_{WF}) between t19 and t30. Intriguingly, this substantial drop in opal ballast was not reflected by a concomitant decrease in sinking velocities (compare **Fig. 2a** and **1a–c**). During phase II the mean POC_{ST} flux became temporally more stable while it differed substantially between mesocosms, as did the sedimented N:P ratios. The 'orni-eutrophication' in phase III was accompanied by a slight increase in POC_{ST} and a marked increase of TPP_{ST} (see Fig. 7 in Bach et al. 2020) with consequently decreasing sinking matter N:P ratios. All the while, the *A. sanguinea* bloom remained suspended in the water column until the end of the experiment, and did thus probably not contribute much to the sinking flux (Bach et al., 2020).
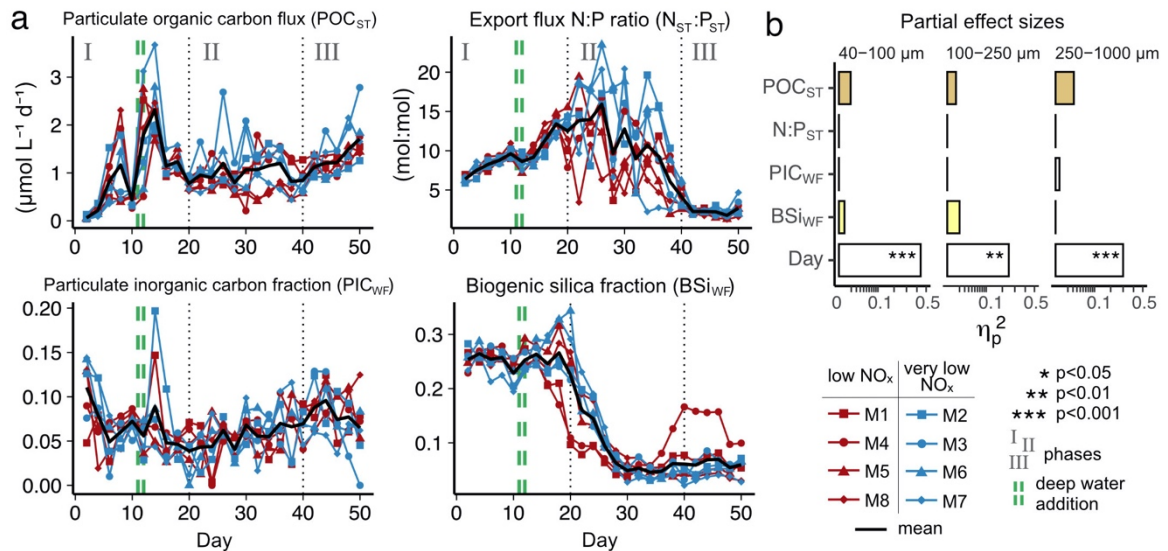
Figure 2. (**a**) Temporal development of key export parameters including absolute flux, elemental stoichiometry and mineral ballast (POC_{ST} and $N_{ST}:P_{ST}$ modified from Bach et al. 2020). (**b**) Modelled effects of these parameters on particle sinking velocity (η_p^2: partial effect size).

Physical particle properties

The physical properties of individual particles were clearly linked to their sinking velocities (**Table A3** and **Fig. 3b**). The most important property was size (ESD), which correlated positively with sinking velocity (see **Fig. B2** in the Appendix). Porosity (P_{int}), as the second most influential property, was associated with a decrease in sinking velocity. Particle shape (aspect ratio) on the other hand, had only a comparably minor effect, which was nevertheless still detectable. Rounder particles (high aspect ratio) tended to sink slightly faster than elongated ones. Finally, time (Day) showed the weakest effect here, unlike for the bulk biogeochemical export flux parameters presented before. Altogether, these physical particle properties explained a quarter of the variation in the sinking velocity at the level of the individual particle ($R^2_{marginal} = 0.25$, **Table A3**). Whilst we detected interactions between the physical particle properties and time, overarching patterns concerning the development of the relationships over time could not be identified (**Fig. B2–4**). The variation explained by these interactions was negligible compared to the main effects (**Table A3**).

Particle size, shape and porosity were relatively similar between mesocosms and OMZ treatments (**Fig. 3a**). M3 and M4 however, slightly stood out from the rest. During phase II, exported particles in M4 were bigger and more porous compared to the other mesocosms, especially on t30 and t32. M4 also had the highest sinking velocities on t32 in all size classes and among the highest on t30 (**Fig. 1a–c**). Similarly, in M3 bigger, more porous and slightly more elongated particles sank compared to the other mesocosms. Interestingly, these two mesocosms also showed a distinct phytoplankton community succession. In M4, the community shift from diatoms to dinoflagellates did not happen before the very end of the experiment, while in M3 it occurred ~10 days later than in the other mesocosms (see Fig. 6 in Bach et al. 2020). This is also apparent in the delayed decrease of diatom chlorophyll *a* at around t20 in M3 and M4 (**Fig. 1e**). The initial diatom communities of M3 and M4 were instead replaced by cryptophytes, and in M4 those were subsequently succeeded by chlorophytes,

before *A. sanguinea* finally took over. The deviations in physical particle properties in M3 and M4 might hence be connected to their peculiarities in terms of community succession.
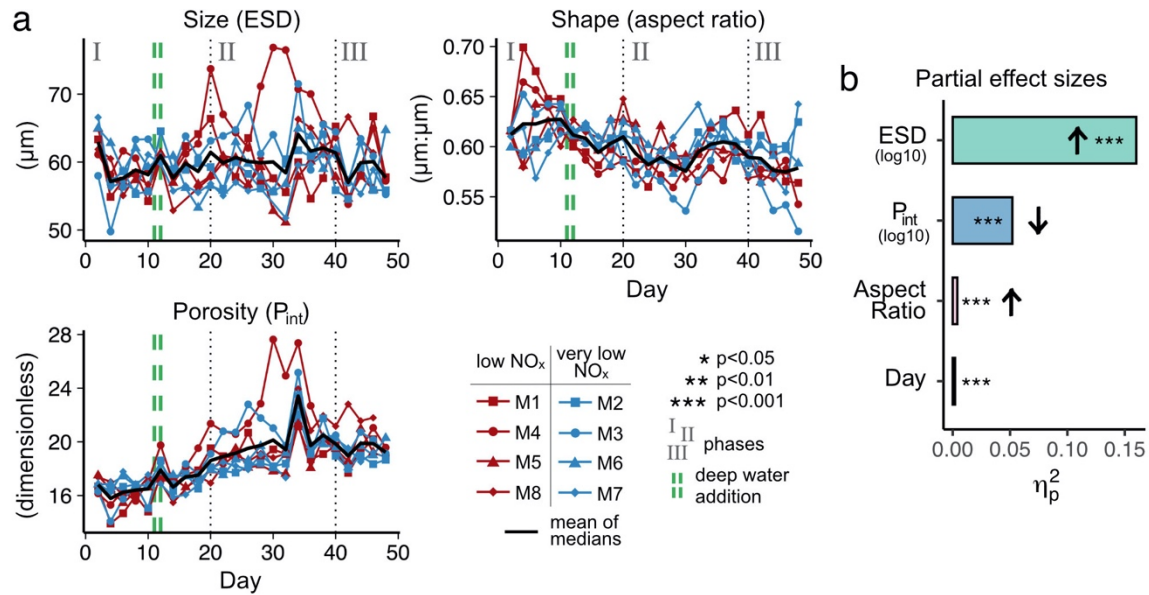
Figure 3. (**a**) Temporal development of physical particle properties and (**b**) their effect on particle sinking velocity with effect directions indicated by arrows (up = positive, down = negative). The full statistical result, including interactions between the properties and day, are given in **Table A3**. Note that (**a**) shows daily median particle properties.

Apart from these two deviations, the median particle size remained relatively stable over time in all mesocosms (**Fig. 3a**), which implies that the particle size spectrum did not change much throughout the experiment. In contrast, porosities increased slightly and aspect ratios tended to decrease from the beginning to the middle of the experiment (around t30). This implies that particles became less spherical and more porous, which would in theory be associated with decreased sinking velocities. This was reflected relatively well by our data, with decreasing sinking velocities until around t25 (**Fig. 1a–c**).

Discussion

Our mean sinking velocities ranged from 12.8 m d^{-1} in the smallest to 34.2 m d^{-1} in the largest particle size class, which is well in the range of previously published sinking velocities from around the world (size range 40–1000 µm, McDonnell and Buesseler, 2010; Bach et al., 2016, 2019; Iversen and Lampitt, 2020). In Eastern Boundary Upwelling Systems however, direct measurements of sinking velocity are scarce. Reports are restricted to the California Current (Alldredge and Gotschalk, 1988; Ploug et al., 1999) and zooplankton and fish fecal pellets in the Benguela (Ploug et al., 2008) and the Peruvian Upwelling System (Staresinic et al., 1983), respectively.

The sinking rates of aggregates sampled in the Southern California Bight by Ploug et al. (1999) were similar to our largest size fraction (mean ± SD: 31 ± 18 m d^{-1}), although their covered particle size range was significantly larger (~ 1.15 to 6 mm). In the same region, Alldredge and Gotschalk (1988) sampled aggregates that sank more than twice as fast (74 ± 39 m d^{-1}) but also

spanned an even larger size range (0.5–25.5 mm). The reported fecal pellets sinking rates were about an order of magnitude higher than our measured sinking velocities. The copepod and appendicularian fecal pellets at Cape Blanc, Mauritania sank at rates of 199 ± 92 and 732 ± 153 m d^{-1}, respectively (Ploug et al., 2008), while the anchovy fecal pellets off the coast of Peru sank at mean rates of 1100 m d^{-1} (691–1987 m d^{-1}, Staresinic et al., 1983). This is not very surprising, as densely packed fecal pellets can reach very high sinking velocities (Steinberg and Landry, 2017). Fischer and Karakas (2009) calculated particle sinking velocities for the Benguela and Canary Current Upwelling Systems by comparing flux data at two different sediment trap sampling depths. Their estimates are high compared to ours (~240 ± 57 m d^{-1} in the Canary Upwelling System and 117 m d^{-1} in the Benguela Upwelling System). However, they covered a different particle size range and it is unclear how well their sediment trap-method compares to our approach.

More comparable to our study are sinking velocity measurements by Cavan et al. (2017) using the same FlowCam method on particles sampled near the coast of Guatemala in the Eastern Tropical North Pacific. Although this system is not an EBUS (Kämpf and Chapman, 2016), it is also characterized by an extensive subsurface oxygen minimum zone (Cavan et al., 2017). The authors measured average sinking velocities of 113.6 m d^{-1} for particles of 489 ± 14 µm size, which is more than three times faster than the 34.2 ± 1.5 m d^{-1} of particles in the 250–1000 µm size range in this study (average size: 420 ± 51.4 µm). Sinking particles in the Peruvian system are thus exposed to more prolonged degradation in the subsurface than those in the Guatemalan region, resulting in increased nitrogen loss through anammox and denitrification (Karthäuser et al., 2021b) and enhanced POC attenuation. It has to be noted, though, that Cavan et al. (2017) collected their particles at greater depths than we did (40–350 m compared to 19 m). As sinking velocities increase with depth due to heterotrophic modifications (Berelson, 2001; Villa-Alfageme et al., 2016), this might be a reason for their higher estimates. Besides, seasonal dynamics and a different state of plankton community succession can cause substantial temporal variability in sinking velocities (e.g. Villa-Alfageme et al., 2016; Bach et al., 2019). The comparison of single measurements from different locations (and depths) should thus be conducted with care. That being said, the sinking velocities of our largest particles were generally low compared to other studies from EBUSs or similar systems.

Role of phytoplankton community succession and export flux

Due to the time lag between organic matter production and its sinking, it is difficult to analyze the effects of the water column plankton community on the velocity of sinking particles. Therefore, instead of comparing sinking velocities with community composition proxies, we correlated them with export flux parameters, namely the POC flux, sedimented N:P ratio and biogenic mineral fractions (PIC, BSi). These were assessed from bulk sediment trap samples and reflected community composition-related changes in the water column well.

The gradual cease of diatoms and the accompanying decrease in BSi export during phase I was accompanied by decreasing particle sinking velocities in the small and medium size fractions, while at the same time porosities increased (compare **Fig. 1a–c, 2a** and **3a**). While diatoms declined, small particles thus became less compact and sank slower. This is somewhat surprising, as particles originating from diatom communities are often relatively porous, slow

sinking and inefficient in terms of POC transfer to depth (Lam et al., 2011; Puigcorbé et al., 2015; Bach et al., 2019; Baumann et al., 2021). On the other hand, this finding stands in line with Laurencaeu-Cornec et al. (2020), who found that minerals (calcite in their case) can decrease a particle's porosity. The mechanism is thereby possibly a decrease in stickiness of calcite loaded particles, which can lead to the aggregation of more compact particles (Ball et al., 1987). Perhaps, the same happened here, with non-diatom-derived sinking matter being less opal-rich and more porous, which resulted in slower sinking velocities (see Section 4.2).

The orni-eutrophication at the end of the experiment and the resulting phytoplankton bloom likely induced the strong decrease in sedimented N:P ratios and the noticeable increase in POC export. At the same time, particle porosities decreased and sinking velocities increased in the medium and large size fractions (**Fig. B1**). The fertilization of the N-depleted system and the consequent export-related changes seem to have affected the properties of sinking particles leading to increased sinking velocities. Interestingly, M4, the mesocosm that differed the most from the others in terms of community composition and succession, did not show an increase in phytoplankton biomass (chlorophyll *a*) during phase III. Yet, the changes in the sedimented N:P ratio and POC flux were similar to the other mesocosms. The reason for this might be that the chlorophyll *a* concentration in M4 was lower than in all other mesocosms during phases II and III. Perhaps, the phytoplankton community was not able to capitalize on the provided nutrients, as opposed to the communities in the other mesocosms. It is conceivable that the bird feces partly sank to the sediment trap directly, instead of fully dissolving in the water column. There, they might have caused the observed shifts in POC and TPP export and particle properties in all mesocosms, including M4, in addition to fueling the overlaying water column productivity in most mesocosms.

Another indication for the importance of the community composition dynamics on sinking particle properties lies in the comparison of M3 and M4 to the other mesocosms. Particle sizes and porosities in M3 and especially in M4 were higher than in the other mesocosms during phase II, which was, to a certain degree, reflected by higher sinking velocities. There was a higher contribution of crypto- and chlorophytes in both mesocosms during that time, while the others were dominated by *A. sanguinea* (see Fig. 6 in Bach et al. 2020). At the same time, M4 and especially M3 were among the mesocosms with the highest POC export flux during phase II. This constitutes further evidence for an interaction between the phytoplankton community composition, the resulting export flux and the properties and sinking velocities of settling particles.

Influence of opal ballast on sinking velocity

We did not find a correlation between mean particle sinking velocities in any size class and the opal weight fraction of the export flux in our experiment. We assume this was due to the relatively small variability in sinking velocity and opal weight fraction between mesocosms on a specific measurement day. In other words, there were no consistent differences between mesocosms on the same day, from which correlations could be detected. Most of the variation occurred over time, which the model attributed to the time effect (factor "Day"). This made the detection of a potential effect of the opal weight fraction difficult. Nonetheless, we would have expected the 5-fold drop in the opal fraction between t18 and t30 to be paralleled by a

substantial decrease in sinking velocities. Although mean sinking velocities did initially decrease during this time period, the decrease was relatively moderate (from t18 to t20: 24 %, 27 % and 14 % in the small, medium and large size fraction, respectively) compared to the drop in opal content and sinking velocities remained stable thereafter.

The theoretical effect that a 5-fold drop in the opal weight fraction should have on sinking velocities is substantial. Using Stokes' law (Stokes, 1851), we calculated the effect of different opal ballasting on the sinking velocity of idealized particles. We assumed two spherical particles with 100 μm diameter to consist of POC and BSi exclusively (densities of 1.06 and 2.1 g cm^{-3}, respectively, Klaas and Archer, 2002). One had an opal contribution of 25 %, the other of 5 %, which represents values from before and after the opal drop during phase II. We calculated sinking velocities of 137 and 40 m d^{-1} for the 25 % and 5 % opal particle, respectively. According to this calculation, the observed drop in BSi should have theoretically decreased particle sinking velocities by a factor of 3.4.

One possible explanation could be concurring effects, which changed in parallel with opal ballasting and had opposing (i.e. positive) effects on sinking velocity. Conceivably, there could have been an increase in particle size or compactness due to the phytoplankton community shift or zooplankton repackaging, respectively. However, neither size increased nor porosity decreased while the opal contribution to the export flux declined. On the contrary, porosity even increased in the small and medium particle size classes, mirroring the temporal pattern of the BSi drop (compare **Fig. 2a** and **Fig. B1**).

These findings suggest that in a close-to-natural plankton community, the velocities of sinking particles are either not substantially affected by their opal fraction, or other factors balance out its potential influence. This stands in contrast to the "ballast hypothesis", which states that ballasting minerals (opal, calcium carbonate and lithogenic material) enhance the export of organic matter, partly via enhancing particle sinking velocities (Francois et al., 2002; Klaas and Archer, 2002; Armstrong et al., 2002). Although opal is considered a weaker driver of sinking velocity than calcium carbonate, a higher proportion of it should theoretically nonetheless increase sinking velocity (Francois et al., 2002; Klaas and Archer, 2002; Lee et al., 2009; Iversen and Ploug, 2010). Apparently, the idealized opal-sinking velocity relationship does not necessarily hold true in a plankton community in the surface ocean. The reason for this is likely the complexity of pelagic systems, in which numerous physical and biological drivers affect particle sinking velocities, such as size and porosity, particle type (McDonnell and Buesseler, 2010; Durkin et al., 2021), phytoplankton community composition via porosity and ballasting (e.g. Bach et al., 2016, 2019) or even diatom morphology (Laurenceau-Cornec et al., 2015). To disentangle this multitude of mechanisms, targeted laboratory studies are needed. Thus far however, most such studies have compared sinking velocities of aggregates formed by different algae species (e.g. Iversen and Ploug, 2010) without gaining much insight into the mechanistic relationships between sinking velocity and its individual drivers. In order to better resolve the relationship between sinking velocity and opal ballasting, a study similar to the one by Laurenceau-Cornec et al. (2020) is needed, who designed an experiment specifically to examine effects of calcite ballasting on particle sinking velocities.

Size, porosity and shape as drivers of sinking velocity

We found that among our tested physical particle properties, size had the strongest correlation with sinking velocity. This stands in contrast to a recent study, which did not detect a relationship between size and sinking velocity (Iversen and Lampitt, 2020). One reason for this might be that the effect size is small, thus requiring a large test power to detect it. While our study found a rather small effect size (partial effect size: $\eta_p^2 = 0.16$, **Table A3**) encompassing measurements of more than a hundred thousand particles, Iversen and Lampitt (2020) measured a total of 1060 particles, which was perhaps insufficient to detect a correlation. Another reason might be that they measured their particles *in situ*, in contrast to our *ex situ* measurement method. Williams and Giering (2022) recently argued that sampling marine particles can modify, damage and disaggregate them, which might cause the particle pool to become more homogeneous than in the natural environment and strengthen the relationship between particle size and sinking velocity. Finally, the size-sinking relationship is subject to large temporal and spatial variability, which is why the importance for location-specific estimates for it has often been highlighted (Laurenceau-Cornec et al., 2015; Giering et al., 2020; Cael et al., 2021). We estimated such a relationship for our data set in order to provide the first empirical size-sinking-relationship for particles from the Peruvian Upwelling System (**Fig. 4**). Our average estimates for the scaling factors α and β were well in range of Cael et al.'s estimates (2021, see their Figures 3 and 4) and might thus help modelers to optimize local particle flux parameterizations for the Peruvian Upwelling System.
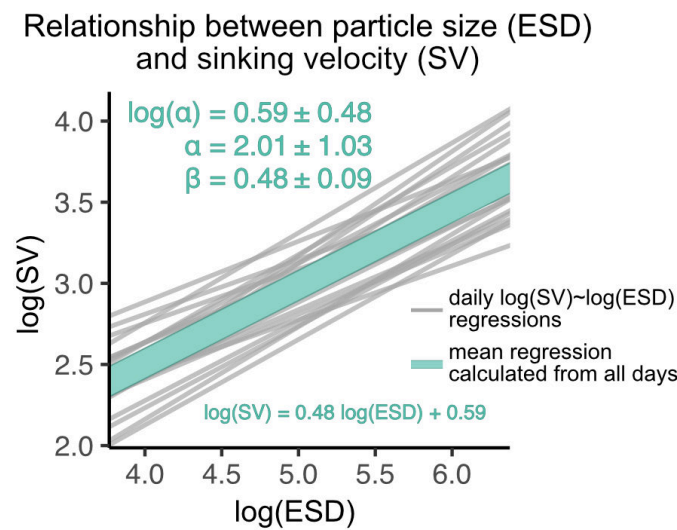
Figure 4. Size-sinking relationship of particles sampled from the sediment trap. Shown are the scaling factors α and β ± SD, as well as the mean regression model formula according to Eq. 3. This relationship was calculated in the 40–630 μm size range (see Sect. 2.3.1).

Particle porosity was the second most important driver of sinking velocity. Surprisingly, the correlation between sinking velocity and porosity was three times weaker than the one with size. So although porosity has repeatedly been reported as an important driver of sinking velocity (Alldredge and Crocker, 1995; Giering et al., 2020; Laurenceau-Cornec et al., 2020), it seems that in the size range of 40–1000 μm particle size is the more influential property. Our study is, to the best of our knowledge, the first to directly compare the size-sinking and

porosity-sinking relationships in a marine particle dataset, providing insight into the relative importance of these two drivers on sinking velocity.

The third assessed particle property, shape, was inconsequential compared to the former two, both in comparison and in absolute terms. Although rounder particles tended to sink faster than elongated ones, the aspect ratio was not overly important in driving sinking velocities. Although particle shape has been found to influence the sinking behavior (e.g. Laurenceau-Cornec et al., 2015, 2020), it is not considered as important a driver as particle size or compactness. Our results concur with this, indicating that although the aspect ratio of a particle matters, it is not a major driver of sinking velocity. Multiple times more important seem to be porosity and size, with size being the predominant driver.

Conclusions

We provide the first empirical data on particle sinking velocities in the small to medium size range (40–1000 μm) in the coastal Peruvian Upwelling System. Our data fit relatively well into the range of previously published estimates of equally-sized particles from around the world. However, particles in our largest size fraction (~0.4 mm diameter) sank slower than those in some other EBUSs and comparable systems.

We found indications that sinking velocities were connected to the phytoplankton community composition and succession and to the nutritional system status. Which species make up the base of the food web in the Peruvian Upwelling System seems to influence how fast particles sink and hence how much POC is remineralized in the subsurface OMZ. Our results further show that when a system shifts away from a diatom-based community, opal ballast does not seem to be a major driver of sinking velocity in the surface ocean. In order to disentangle the mechanisms driving particle sinking velocity under such a community shift, laboratory studies are needed that can isolate the effects of the potential drivers such as opal ballast, particle size and compactness.

Our results suggest that sinking velocity parameterizations in numerical models should include particle size and porosity as physical particle properties, with size as the more influential driver. The provided metrics of a size-sinking relationship could help to further optimize local particle flux parameterizations. Since sinking velocity determines for how long particles are exposed to degradation processes on their way to depth, it is a crucial parameter for assessing carbon sequestration and changes in subsurface oxygen concentrations. This is especially important for a region that is highly susceptible to climate-driven changes. Our study might thus help to better estimate the strength and efficiency of the biological carbon pump in the Peruvian Upwelling System and hence project the expansion of the local oxygen-deficient waters.

Additional Information

Author contributions

LTB, AJP and UR designed the experiment. PS, LTB, FM, AJP and UR contributed to the sampling. MB, LTB, SG, AJP and JT analyzed the data. MB wrote the manuscript with comments from all co-authors.

Competing interests

The authors declare that the research was conducted in the absence of any commercial or financial relationships that could be construed as a potential conflict of interest.

Special issue statement

This article is part of the special issue "Ecological and biogeochemical functioning of the coastal upwelling system off Peru: an in situ mesocosm study". It is not associated with a conference.

Acknowledgements

Financial support

Appendix A: Tables

Response variable	Source of variation	df	MS	F-value	$R^2_{marginal}$	p-value
a) Sinking velocity 40–100μm	OMZ	1	0.065	0.02	0.42	0.904
	Day	18	20.172	4.93		**<0.0001**
	OMZ × Day	18	4.702	1.15		0.318
b) log10(sinking velocity 100–250μm)	OMZ	1	0.006	0.67	0.42	0.416
	Day	18	0.040	4.74		**<0.0001**
	OMZ × Day	18	0.008	1.00		0.465
c) log10(sinking velocity 250–1000μm)	OMZ	1	0.004	0.34	0.48	0.559
	Day	18	0.070	6.07		**<0.0001**
	OMZ × Day	18	0.012	1.08		0.383

Table A1. Linear mixed models for the effects of oxygen minimum zone (OMZ) treatment across time on averaged sinking velocity per size class. Shown are the ANOVA output (df: degrees of freedom, MS: mean squares), R^2 of fixed effects ($R^2_{marginal}$) and partial effect sizes (η_p^2). Measurement days before the OMZ water addition (sampling days t2–t10) were excluded. Model diagnostics: Raw data of a) met the assumptions for normality and homogeneity. For b) and c) the response variable was log10-transformed to meet the assumptions for normality and homogeneity.

Response variable	Source of variation	df	MS	F-value	η_p^2	$R^2_{marginal}$	p-value
a) Sinking velocity 40–100 μm	Day	23	29.971	5.27	0.436	0.50	**<0.0001**
	BSi_{WF}	1	1.730	0.30	0.001		0.582
	PIC_{WF}	1	0.412	0.07	0.000		0.788
	POC_{ST}	1	7.624	1.34	0.005		0.249
	$N_{ST}{:}P_{ST}$	1	0.279	0.05	0.000		0.825
b) log10(sinking velocity 100–250 μm)	Day	23	0.020	2.29	0.246	0.39	**0.002**
	BSi_{WF}	1	0.014	1.64	0.008		0.202
	PIC_{WF}	1	0.000	0.03	0.000		0.866
	POC_{ST}	1	0.007	0.84	0.004		0.361
	$N_{ST}{:}P_{ST}$	1	0.000	0.03	0.000		0.871
c) log10(sinking velocity 250–1000 μm)	Day	23	0.036	2.88	0.300	0.41	**<0.0001**
	BSi_{WF}	1	0.000	0.02	0.000		0.884
	PIC_{WF}	1	0.002	0.17	0.001		0.682
	POC_{ST}	1	0.043	3.43	0.015		0.066
	$N_{ST}{:}P_{ST}$	1	0.001	0.06	0.000		0.811

Table A2. Linear mixed models for the relationships between averaged sinking velocities per size class and biogeochemical particle properties and time. Shown are the ANOVA output (df: degrees of freedom, MS: mean squares), R^2 of fixed effects ($R^2_{marginal}$) and partial effect sizes (η_p^2). Model diagnostics: Raw data of a) met the assumptions for normality and homogeneity. For b) and c) the response variable was log10-transformed to meet the assumptions for normality and homogeneity.

Response variable	Source of variation	df	MS	F-value	η_p^2	$R^2_{marginal}$	p-value
log10(sinking velocity)	log10(ESD)	1	1274.95	19500.45	0.160	0.25	**<0.0001**
	log10(P_{int})	1	368.41	5634.81	0.052		**<0.0001**
	Aspect Ratio	1	28.05	429.10	0.004		**<0.0001**
	Day	23	0.51	7.77	0.002		**<0.0001**
	log10(ESD) × Day	23	0.51	7.83	0.002		**<0.0001**
	log10(P_{int}) × Day	23	0.52	7.99	0.002		**<0.0001**
	Aspect Ratio × Day	23	1.25	19.06	0.004		**<0.0001**

Table A3. Linear mixed models for the relationships between sinking velocity and physical particle properties (size, porosity and shape) across time. Shown are the ANOVA output (df: degrees of freedom, MS: mean squares), R^2 of fixed effects ($R^2_{marginal}$) and partial effect sizes (η_p^2). The analysis is based on N > 100,000 particles. Model diagnostics: The right-skewed sinking velocity, ESD and P_{int} data were log10-transformed, after which only slight deviations from normality remained. Particles within one measurement were correlated with each other. The reason might be that fast sinking particles were generally measured at the beginning of a measurement, while more slow particles were measured towards the end. We nevertheless **a**rgue that our model results are interpretable due to the high significance of our correlations (all p-values < 10^{-24}).

Appendix B: Figures
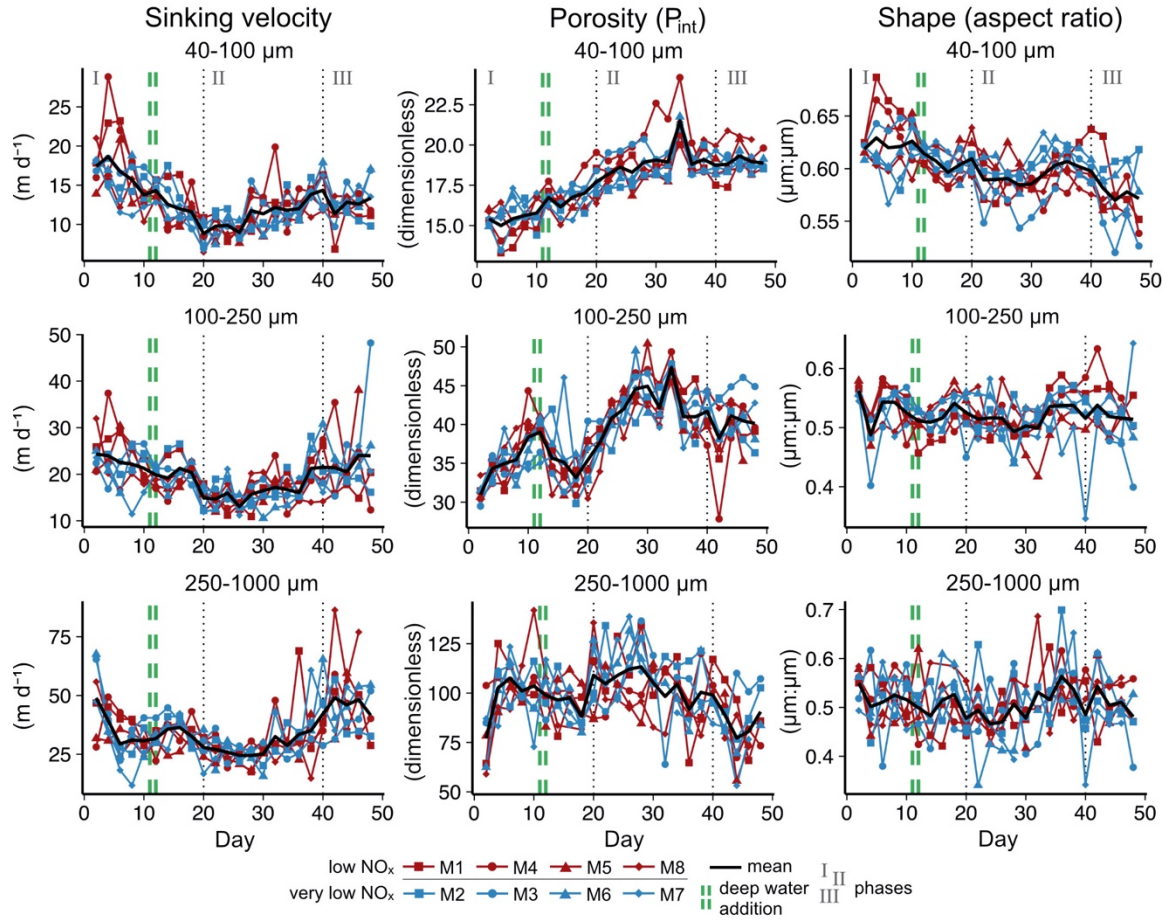
Figure B1. Temporal developments of particle sinking velocities, porosities and shapes per size class. Note that sinking velocities are also shown in **Fig. 1**, but are replicated here to facilitate the comparison with other particle properties.

Daily relationships between Sinking Velocity and Size
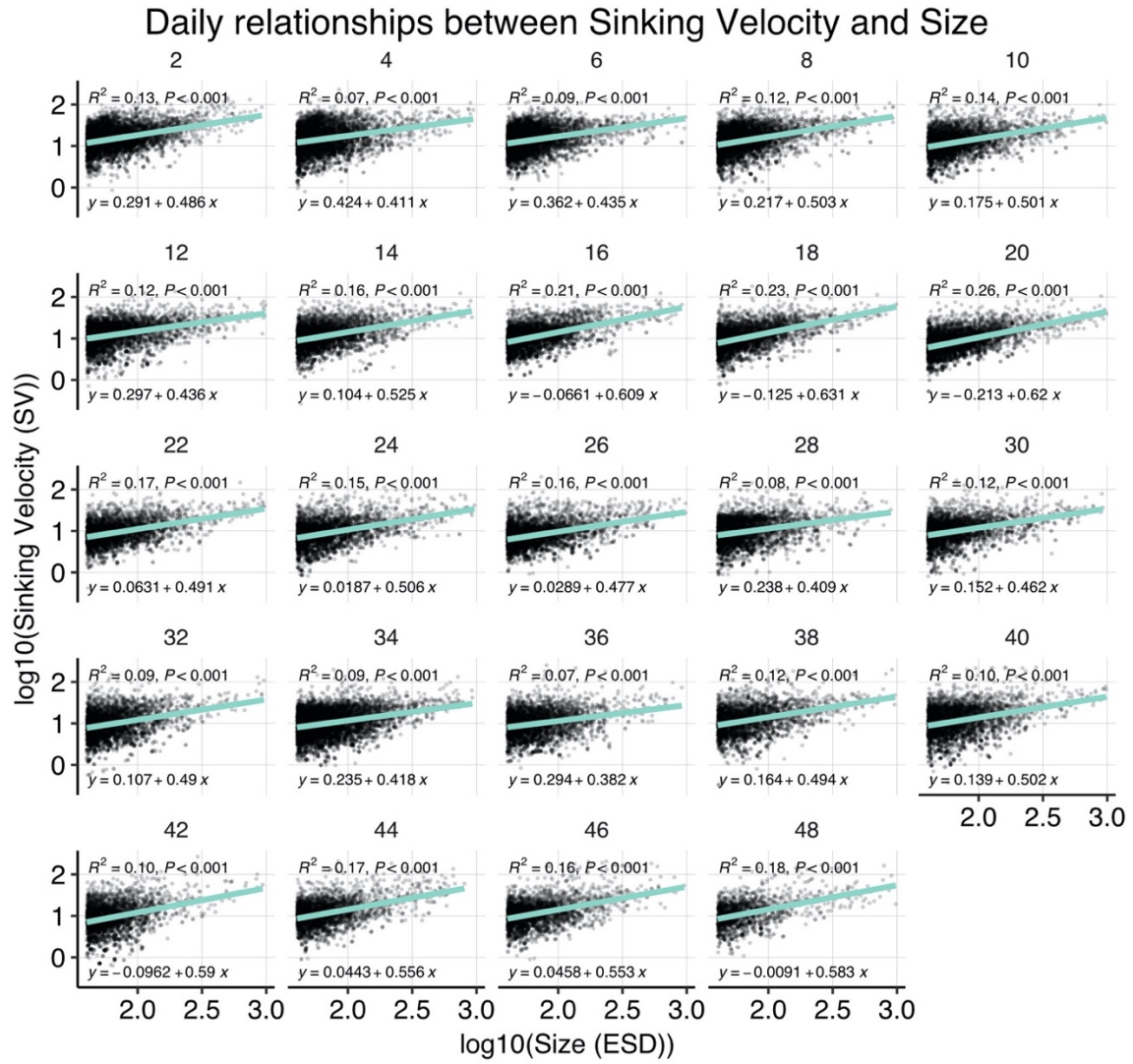
Figure B2. Correlations between sinking velocity and particle size over time. Each panel shows data of all mesocosms for one experimental day, including a linear regression with test statistics and model formula, and each black dot corresponds to one particle. Related model output: **Table A3** and **Fig. 3b**.
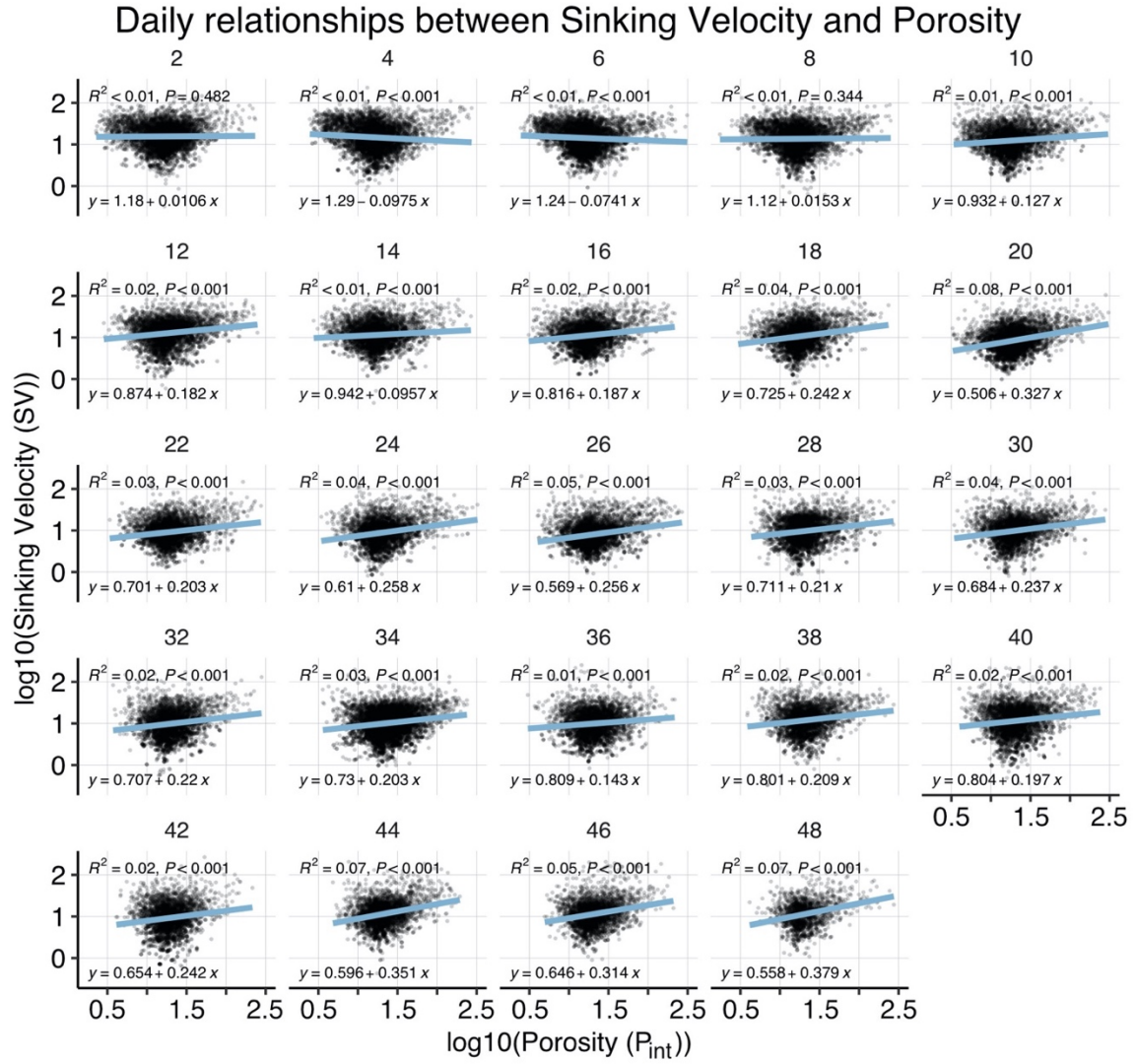
Figure B3. Correlations between sinking velocity and particle porosity over time. Each panel shows data of all mesocosms for one experimental day, including a linear regression with test statistics and model formula. Related model output: **Table A3** and **Fig. 3b**.
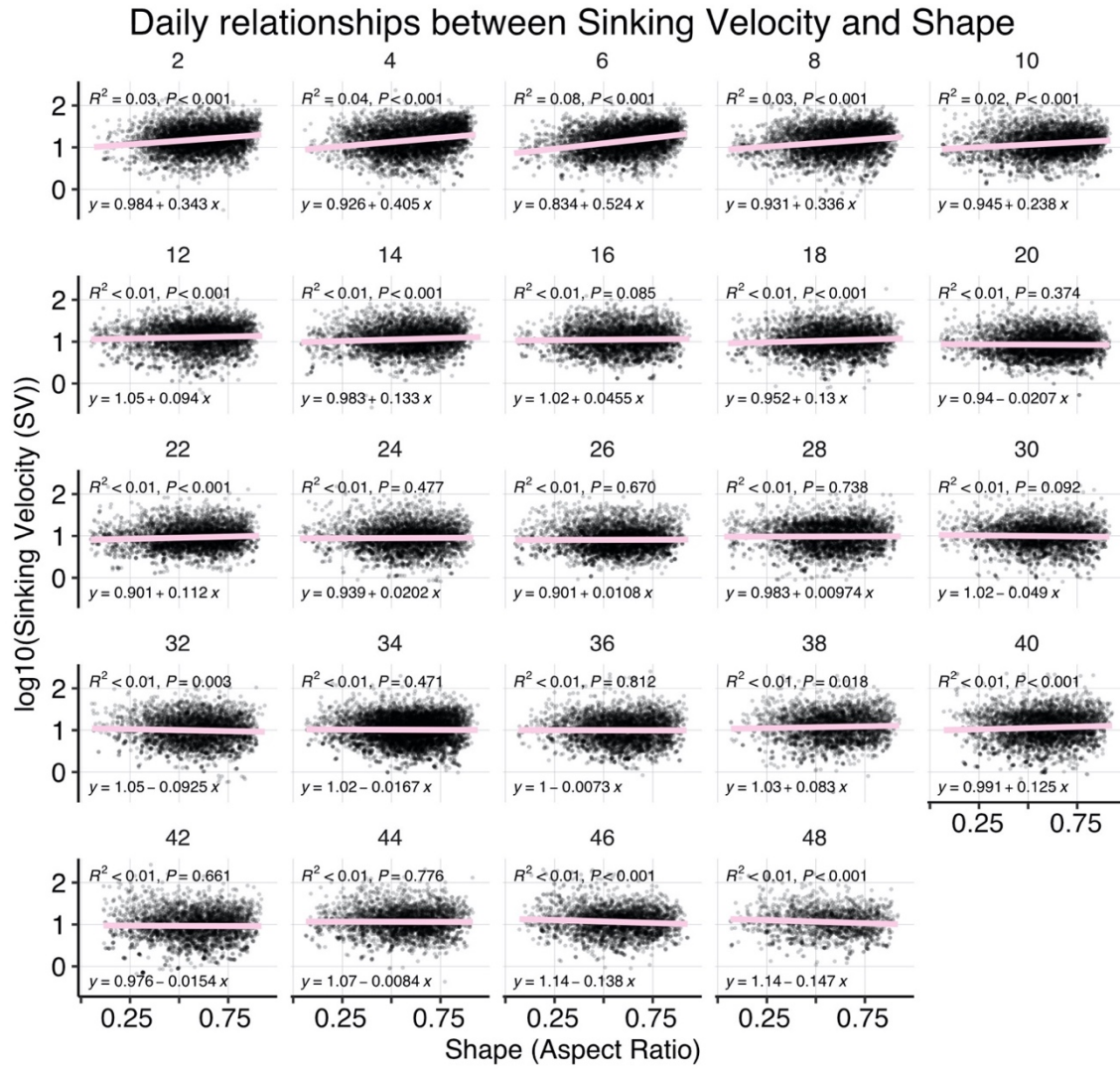
Figure B4. Correlations between sinking velocity and particle size over time. Each panel shows data of all mesocosms for one experimental day, including a linear regression with test statistics and model formula. Related model output: **Table A3** and **Fig. 3b**.

References

Alldredge, A.L., Crocker, K.M., 1995. Why do sinking mucilage aggregates accumulate in the water column? Science of The Total Environment 165, 15–22. https://doi.org/10.1016/0048-9697(95)04539-D

Alldredge, A.L., Gotschalk, C., 1988. In situ settling behavior of marine snow. Limnol. Oceanogr. 33, 339–351. https://doi.org/10.4319/lo.1988.33.3.0339

Armstrong, R.A., Lee, C., Hedges, J.I., Honjo, S., Wakeham, S.G., 2002. A new, mechanistic model for organic carbon fluxes in the ocean based on the quantitative association of POC with ballast minerals. Deep Sea Research Part II: Topical Studies in Oceanography. https://doi.org/10.1016/s0967-0645(01)00101-1

Armstrong, R.A., Peterson, M.L., Lee, C., Wakeham, S.G., 2009. Settling velocity spectra and the ballast ratio hypothesis. Deep Sea Research Part II: Topical Studies in Oceanography 56, 1470–1478. https://doi.org/10.1016/j.dsr2.2008.11.032

Bach, L.T., Boxhammer, T., Larsen, A., Hildebrandt, N., Schulz, K.G., Riebesell, U., 2016. Influence of plankton community structure on the sinking velocity of marine aggregates: Sinking velocity of marine aggregates. Global Biogeochem. Cycles 30, 1145–1165. https://doi.org/10.1002/2016GB005372

Bach, L.T., Paul, A.J., Boxhammer, T., von der Esch, E., Graco, M., Schulz, K.G., Achterberg, E., Aguayo, P., Arístegui, J., Ayón, P., Baños, I., Bernales, A., Boegeholz, A.S., Chavez, F., Chavez, G., Chen, S.-M., Doering, K., Filella, A., Fischer, M., Grasse, P., Haunost, M., Hennke, J., Hernández-Hernández, N., Hopwood, M., Igarza, M., Kalter, V., Kittu, L., Kohnert, P., Ledesma, J., Lieberum, C., Lischka, S., Löscher, C., Ludwig, A., Mendoza, U., Meyer, Jana, Meyer, J., Minutolo, F., Ortiz Cortes, J., Piiparinen, J., Sforna, C., Spilling, K., Sanchez, S., Spisla, C., Sswat, M., Zavala Moreira, M., Riebesell, U., 2020. Factors controlling plankton community production, export flux, and particulate matter stoichiometry in the coastal upwelling system off Peru. Biogeosciences 17, 4831–4852. https://doi.org/10.5194/bg-17-4831-2020

Bach, L.T., Riebesell, U., Sett, S., Febiri, S., Rzepka, P., Schulz, K.G., 2012. An approach for particle sinking velocity measurements in the 3–400 µm size range and considerations on the effect of temperature on sinking rates. Mar Biol 159, 1853–1864. https://doi.org/10.1007/s00227-012-1945-2

Bach, L.T., Stange, P., Taucher, J., Achterberg, E.P., Algueró-Muñiz, M., Horn, H., Esposito, M., Riebesell, U., 2019. The Influence of Plankton Community Structure on Sinking Velocity and Remineralization Rate of Marine Aggregates. Global Biogeochem. Cycles 33, 971–994. https://doi.org/10.1029/2019GB006256

Ball, R.C., Weitz, D.A., Witten, T.A., Leyvraz, F., 1987. Universal kinetics in reaction-limited aggregation. Phys. Rev. Lett. 58, 274–277. https://doi.org/10.1103/PhysRevLett.58.274

Barlow, R.G., Cummings, D.G., Gibb, S.W., 1997. Improved resolution of mono- and divinyl chlorophylls a and b and zeaxanthin and lutein in phytoplankton extracts using reverse phase C-8 HPLC. Marine Ecology Progress Series 161, 303–307. https://doi.org/10.3354/meps161303

Bates, D., Mächler, M., Bolker, B., Walker, S., 2015. Fitting Linear Mixed-Effects Models Using **lme4**. J. Stat. Soft. 67. https://doi.org/10.18637/jss.v067.i01

Baumann, M., Taucher, J., Paul, A.J., Heinemann, M., Vanharanta, M., Bach, L.T., Spilling, K., Ortiz, J., Arístegui, J., Hernández-Hernández, N., Baños, I., Riebesell, U., 2021. Effect of Intensity and Mode of Artificial Upwelling on Particle Flux and Carbon Export. Front. Mar. Sci. 8, 742142. https://doi.org/10.3389/fmars.2021.742142

Berelson, W.M., 2001. Particle settling rates increase with depth in the ocean. Deep-sea Research Part Ii-topical Studies in Oceanography. https://doi.org/10.1016/s0967-0645(01)00102-3

Boxhammer, T., Bach, L.T., Czerny, J., Riebesell, U., 2016. Technical note: Sampling and processing of mesocosm sediment trap material for quantitative biogeochemical analysis. Biogeosciences 13, 2849–2858. https://doi.org/10.5194/bg-13-2849-2016

Cael, B.B., Cavan, E.L., Britten, G.L., 2021. Reconciling the Size-Dependence of Marine Particle Sinking Speed. Geophys Res Lett 48. https://doi.org/10.1029/2020GL091771

Cavan, E.L., Trimmer, M., Shelley, F., Sanders, R., 2017. Remineralization of particulate organic carbon in an ocean oxygen minimum zone. Nat Commun 8, 14847. https://doi.org/10.1038/ncomms14847

Chavez, F.P., Messié, M., 2009. A comparison of Eastern Boundary Upwelling Ecosystems. Progress in Oceanography 83, 80–96. https://doi.org/10.1016/j.pocean.2009.07.032

DiTullio, G.R., Geesey, M.E., Maucher, J.M., Alm, M.B., Riseman, S.F., Bruland, K.W., 2005. Influence of iron on algal community composition and physiological status in the Peru upwelling system. Limnology and Oceanography 50, 1887–1907. https://doi.org/10.4319/lo.2005.50.6.1887

Durkin, C.A., Buesseler, K.O., Cetinić, I., Estapa, M.L., Kelly, R.P., Omand, M.M., 2021. A Visual Tour of Carbon Export by Sinking Particles. Global Biogeochemical Cycles. https://doi.org/10.1029/2021gb006985

Fischer, G., Karakas, G., 2009. Sinking rates and ballast composition of particles in the Atlantic Ocean: implications for the organic carbon fluxes to the deep ocean. Biogeosciences. https://doi.org/10.5194/bg-6-85-2009

Francois, R., Honjo, S., Krishfield, R., Manganini, S., 2002. Factors controlling the flux of organic carbon to the bathypelagic zone of the ocean: Factors controlling organic

carbon flux. Global Biogeochem. Cycles 16, 34-1-34–20.
https://doi.org/10.1029/2001GB001722

Giering, S.L.C., Cavan, E.L., Basedow, S.L., Briggs, N., Burd, A.B., Darroch, L.J., Guidi, L., Irisson, J.-O., Iversen, M.H., Kiko, R., Lindsay, D., Marcolin, C.R., McDonnell, A.M.P., Möller, K.O., Passow, U., Thomalla, S., Trull, T.W., Waite, A.M., 2020. Sinking Organic Particles in the Ocean—Flux Estimates From in situ Optical Devices. Front. Mar. Sci. 6, 834. https://doi.org/10.3389/fmars.2019.00834

Guidi, L., Stemmann, L., Jackson, G.A., Ibanez, F., Claustre, H., Legendre, L., Picheral, M., Gorskya, G., 2009. Effects of phytoplankton community on production, size, and export of large aggregates: A world-ocean analysis. Limnol. Oceanogr. 54, 1951–1963. https://doi.org/10.4319/lo.2009.54.6.1951

Hansen, H.P., Koroleff, F., 1999. Determination of nutrients, in: Methods of Seawater Analysis, Third, Completely Revised and Extended Edition. WILEY-VCH, pp. 159–228.

Iversen, M.H., Lampitt, R.S., 2020. Size does not matter after all: No evidence for a size-sinking relationship for marine snow. Progress in Oceanography. https://doi.org/10.1016/j.pocean.2020.102445

Iversen, M.H., Ploug, H., 2010. Ballast minerals and the sinking carbon flux in the ocean: carbon-specific respiration rates and sinking velocity of marine snow aggregates. Biogeosciences 7, 2613–2624. https://doi.org/10.5194/bg-7-2613-2010

Kalvelage, T., Lavik, G., Lam, P., Contreras, S., Arteaga, L., Löscher, C.R., Oschlies, A., Paulmier, A., Stramma, L., Kuypers, M.M.M., 2013. Nitrogen cycling driven by organic matter export in the South Pacific oxygen minimum zone. https://doi.org/10.1594/pangaea.843461

Kämpf, J., Chapman, P., 2016. Upwelling Systems of the World. Springer International Publishing, Cham. https://doi.org/10.1007/978-3-319-42524-5

Karstensen, J., Stramma, L., Visbeck, M., 2008. Oxygen minimum zones in the eastern tropical Atlantic and Pacific oceans. Progress in Oceanography 77, 331–350. https://doi.org/10.1016/j.pocean.2007.05.009

Karthäuser, C., Ahmerkamp, S., Marchant, H.K., Bristow, L.A., Hauss, H., Iversen, M.H., Kiko, R., Maerz, J., Lavik, G., Kuypers, M.M.M., 2021a. Small sinking particles control anammox rates in the Peruvian oxygen minimum zone. Nature Communications. https://doi.org/10.1038/s41467-021-23340-4

Karthäuser, C., Ahmerkamp, S., Marchant, H.K., Bristow, L.A., Hauss, H., Iversen, M.H., Kiko, R., Maerz, J., Lavik, G., Kuypers, M.M.M., 2021b. Small sinking particles control anammox rates in the Peruvian oxygen minimum zone. Nature Communications. https://doi.org/10.1038/s41467-021-23340-4

Khatiwala, S., Tanhua, T., Mikaloff Fletcher, S., Gerber, M., Doney, S.C., Graven, H.D., Gruber, N., McKinley, G.A., Murata, A., Ríos, A.F., Sabine, C.L., 2013. Global ocean storage of anthropogenic carbon. Biogeosciences 10, 2169–2191. https://doi.org/10.5194/bg-10-2169-2013

Klaas, C., Archer, D., 2002. Association of sinking organic matter with various types of mineral ballast in the deep sea: Implications for the rain ratio. Global Biogeochemical Cycles. https://doi.org/10.1029/2001gb001765

Kuznetsova, A., Brockhoff, P.B., Christensen, R.H.B., 2017. lmerTest Package: Tests in Linear Mixed Effects Models. J. Stat. Soft. 82. https://doi.org/10.18637/jss.v082.i13

Lam, P.J., Doney, S.C., Bishop, J.K.B., 2011. The dynamic ocean biological pump: Insights from a global compilation of particulate organic carbon, $CaCO_3$, and opal concentration profiles from the mesopelagic: The dynamic ocean biological pump. Global Biogeochem. Cycles 25, n/a-n/a. https://doi.org/10.1029/2010GB003868

Laurenceau-Cornec, E.C., Le Moigne, F.A.C., Gallinari, M., Moriceau, B., Toullec, J., Iversen, M.H., Engel, A., De La Rocha, C.L., 2020. New guidelines for the application of Stokes' models to the sinking velocity of marine aggregates. Limnology and Oceanography 65, 1264–1285. https://doi.org/10.1002/lno.11388

Laurenceau-Cornec, E.C., Trull, T.W., Davies, D.M., Bray, S.G., Doran, J., Planchon, F., Carlotti, F., Jouandet, M.-P., Cavagna, A.-J., Waite, A.M., Blain, S., 2015. The relative importance of phytoplankton aggregates and zooplankton fecal pellets to carbon export: insights from free-drifting sediment trap deployments in naturally iron-fertilised waters near the Kerguelen Plateau. Biogeosciences 12, 1007–1027. https://doi.org/10.5194/bg-12-1007-2015

Lee, C., Peterson, M.L., Wakeham, S.G., Armstrong, R.A., Cochran, J.K., Miquel, J.C., Fowler, S.W., Hirschberg, D., Beck, A., Xue, J., 2009. Particulate organic matter and ballast fluxes measured using time-series and settling velocity sediment traps in the northwestern Mediterranean Sea. Deep Sea Research Part II: Topical Studies in Oceanography 56, 1420–1436. https://doi.org/10.1016/j.dsr2.2008.11.029

Lüdecke, D., n.d. Statistical Functions for Regression Models (Version 0.18.1). https://doi.org/10.5281/zenodo.1284472

Lüdecke, D., Ben-Shachar, M., Patil, I., Waggoner, P., Makowski, D., 2021. performance: An R Package for Assessment, Comparison and Testing of Statistical Models. JOSS 6, 3139. https://doi.org/10.21105/joss.03139

Mackey, M.D., Mackey, D.J., Higgins, H.W., Wright, S.W., 1996. CHEMTAX - a program for estimating class abundances from chemical markers: application to HPLC measurements of phytoplankton. Marine Ecology Progress Series 144, 265–283. https://doi.org/10.3354/meps144265

Marsay, C.M., Sanders, R.J., Henson, S.A., Pabortsava, K., Achterberg, E.P., Lampitt, R.S., 2015. Attenuation of sinking particulate organic carbon flux through the mesopelagic ocean. Proc. Natl. Acad. Sci. U.S.A. 112, 1089–1094. https://doi.org/10.1073/pnas.1415311112

McDonnell, A.M.P., Boyd, P.W., Buesseler, K.O., 2015. Effects of sinking velocities and microbial respiration rates on the attenuation of particulate carbon fluxes through the mesopelagic zone. Global Biogeochemical Cycles. https://doi.org/10.1002/2014gb004935

McDonnell, A.M.P., Buesseler, K.O., 2010. Variability in the average sinking velocity of marine particles. Limnol. Oceanogr. 55, 2085–2096. https://doi.org/10.4319/lo.2010.55.5.2085

Paul, A.P., Bach, L.T., Schulz, K.G., Boxhammer, T., Czerny, J., Achterberg, E.P., Hellemann, D., Trense, Y., Nausch, M., Sswat, M., Riebesell, U., 2015. Effect of elevated CO_2 on organic matter pools and fluxes in a summer Baltic Sea plankton community. Biogeosciences 12, 6181–6203. https://doi.org/10.5194/bg-12-6181-2015

Pennington, J.T., Mahoney, K.L., Kuwahara, V.S., Kolber, D.D., Calienes, R., Chavez, F.P., 2006. Primary production in the eastern tropical Pacific: A review. Progress in Oceanography. https://doi.org/10.1016/j.pocean.2006.03.012

Ploug, H., Grossart, H.-P., Azam, F., Jørgensen, B.B., 1999. Photosynthesis, respiration, and carbon turnover in sinking marine snow from surface waters of Southern California Bight: implications for the carbon cycle in the ocean. Marine Ecology Progress Series. https://doi.org/10.3354/meps179001

Ploug, H., Iversen, M.H., Fischer, G., 2008. Ballast, sinking velocity, and apparent diffusivity within marine snow and zooplankton fecal pellets: Implications for substrate turnover by attached bacteria. Limnology and Oceanography. https://doi.org/10.4319/lo.2008.53.5.1878

Puigcorbé, V., Benitez-Nelson, C.R., Masqué, P., Verdeny, E., White, A.E., Popp, B.N., Prahl, F.G., Lam, P.J., 2015. Small phytoplankton drive high summertime carbon and nutrient export in the Gulf of California and Eastern Tropical North Pacific. Global Biogeochem. Cycles 29, 1309–1332. https://doi.org/10.1002/2015GB005134

R Core Team, 2021. R: A Language and Environment for Statistical Computing.

Riebesell, U., Czerny, J., von Bröckel, K., Boxhammer, T., Büdenbender, J., Deckelnick, M., Fischer, M., Hoffmann, D., Krug, S.A., Lentz, U., Ludwig, A., Muche, R., Schulz, K.G., 2013. Technical Note: A mobile sea-going mesocosm system – new opportunities for ocean change research. Biogeosciences 10, 1835–1847. https://doi.org/10.5194/bg-10-1835-2013

Riley, J.S., Sanders, R., Marsay, C.M., Le Moigne, F.A.C., Achterberg, E.P., Poulton, A.J., 2012. The relative contribution of fast and slow sinking particles to ocean carbon export. Global Biogeochemical Cycles. https://doi.org/10.1029/2011gb004085

Ristow, G.H., 1997. Wall correction factor for sinking cylinders in fluids. Phys. Rev. E 55, 2808–2813. https://doi.org/10.1103/PhysRevE.55.2808

Sharp, J.H., 1974. Improved analysis for "particulate" organic carbon and nitrogen from seawater. Limnol. Oceanogr. 19, 984–989. https://doi.org/10.4319/lo.1974.19.6.0984

Smetacek, V., Klaas, C., Strass, V., Assmy, P., Montresor, M., Cisewski, B., Savoye, N., Webb, A., d'Ovidio, F., Arrieta, J.M., Bathmann, U., Bellerby, R.G.J., Berg, G.M., Croot, P., Gonzalez, S.F., Henjes, J., Herndl, G.J., Hoffmann, L.J., Leach, H., Losch, M., Mills, M.M., Neill, C., Peeken, I., Röttgers, R., Sachs, O., Sauter, E., Schmidt, M.M., Schwarz, J.N., Terbrüggen, A., Wolf-Gladrow, D., 2012. Deep carbon export from a Southern Ocean iron-fertilized diatom bloom. Nature 487, 313–319. https://doi.org/10.1038/nature11229

Staresinic, N., Farrington, J.W., Gagosian, R.B., Clifford, C.H., Hulburt, E.M., 1983. Downward Transport of Particulate Matter in the Peru Coastal Upwelling: Role of the Anchoveta, Engraulis Ringens. https://doi.org/10.1007/978-1-4615-6651-9_12

Steinberg, D.K., Landry, M.R., 2017. Zooplankton and the Ocean Carbon Cycle. Annu. Rev. Mar. Sci. 9, 413–444. https://doi.org/10.1146/annurev-marine-010814-015924

Stokes, G.G., 1851. On the Effect of the Internal Friction of Fluids on the Motion of Pendulums. Transactions of the Cambridge Philosophical Society 9, 8–106.

Turner, J.T., 2015. Zooplankton fecal pellets, marine snow, phytodetritus and the ocean's biological pump. Progress in Oceanography 130, 205–248. https://doi.org/10.1016/j.pocean.2014.08.005

Villa-Alfageme, M., de Soto, F.C., Ceballos, E., Giering, S.L.C., Le Moigne, F.A.C., Henson, S., Mas, J.L., Sanders, R.J., 2016. Geographical, seasonal, and depth variation in sinking particle speeds in the North Atlantic. Geophys. Res. Lett. 43, 8609–8616. https://doi.org/10.1002/2016GL069233

Wickham, H., Averick, M., Bryan, J., Chang, W., D'Agostino McGowan, L., François, R., Grolemund, G., Hayes, A., Henry, L., Hester, J., Kuhn, M., Pedersen, T.L., Miller, E., Bache, S.M., Müller, K., Ooms, J., Robinson, D., Seidel, D.P., Spinu, V., Takahashi, K., Vaughan, D., Wilke, C., Woo, K., Hiroaki, Y., 2019. Welcome to the tidyverse. Journal of Open Source Software 4, 1686. https://doi.org/10.21105/joss.01686

Williams, J.R., Giering, S.L.C., 2022. In situ Particle Measurements Deemphasize the Role of Size in Governing Particle Sinking Velocity (preprint). Oceanography. https://doi.org/10.1002/essoar.10511459.1

4 Manuscript III

Counteracting effects of nutrient composition (Si:N) on export flux under artificial upwelling

Moritz Baumann[1]*, Silvan Goldenberg[1], Jan Taucher[1], Mar Fernández-Méndez[2], Joaquin Ortiz[1], Jacqueline Haussmann[1], Ulf Riebesell[1]

[1]Biological Oceanography, GEOMAR Helmholtz Centre for Ocean Research, Kiel, Germany
[2]Polar Biological Oceanography, Alfred-Wegener-Institut Helmholtz-Zentrum für Polar- und Meeresforschung, Bremerhaven, Germany

Abstract. In order to keep global warming below 1.5 °C, technologies removing carbon from the atmosphere will be needed. Artificial upwelling of nutrient-rich water stimulates primary productivity and could enhance the vertical carbon flux to the deep sea, thus increasing the oceanic uptake of atmospheric carbon. The efficiency of this CO_2 removal technique is affected by the nutrient composition of the upwelled water, which determines the resulting phytoplankton community and thus the carbon sequestration potential. We tested the effect of nutrient composition (Si relative to N) in artificially upwelled waters on export flux parameters in a mesocosm experiment. We enclosed an oligotrophic plankton community in the subtropical North Atlantic for 35 days and constantly fertilized it with nutrient-rich deep water composed of different Si:N ratios (gradient from 0.07–1.33 mol:mol). Artificial upwelling led to a doubling of exported particulate matter (1.0 to 2.2 µmol POC L^{-1} d^{-1}) with increased C:N ratios (9.5 to 11.1 mol:mol). Elevated Si:N ratios additionally enhanced POC export (effect size: 1.5 µmol POC L^{-1} d^{-1} per 1 mol:mol Si:N) and associated C:N ratios (effect size: 1.8 mol:mol per 1 mol:mol Si:N), however, the over-consumed carbon was only partly channeled into the export flux. The BSi fraction of the export flux increased more than 3.5-fold over the gradient of the Si:N nutrient composition (0.10 to 0.36). However, heavier ballasted particles were not respired less or sank faster. On the contrary, sinking velocity significantly decreased under high Si:N, most likely due to decreased particle size. Respiration rates remained similar across all treatments, thus not indicating any protection of Si content against degradation. The nutrient composition under artificial upwelling thus led to counteracting effects on the carbon sequestration potential. On the one hand, it increased the magnitude of carbon export and associated C:N ratios, on the other, it retained parts of the overconsumed carbon in the surface and decreased the efficiency with which carbon is transported to depth.

Introduction

In order to keep global warming below 1.5 °C, a massive reduction of anthropogenic CO_2 emissions is inevitable. In addition however, carbon dioxide removal (CDR) on a grand scale will be required in order to compensate unavoidable future emissions (IPCC, 2018). The oceanic realm constitutes the biggest non-geological carbon reservoir of our planet, and it offers vast space for carbon dioxide removal techniques to be deployed. Artificial upwelling is one such technology, which aims to enhance biological productivity in the surface ocean by transporting nutrient-rich water from deeper layers to the oligotrophic surface (Pan et al., 2016). The increase in primary productivity should theoretically cause an enhanced vertical export flux of sinking particulate organic matter, which transports organically bound carbon to depth. Once the carbon reaches the deep ocean (generally 1,000 m), it is regarded as sequestered on the time scale of up to centuries (Siegel et al., 2021). This natural process is called the "biological carbon pump", whose strength might be enhanced using artificial upwelling.

The carbon sequestration potential of artificial upwelling via the biological carbon pump is mainly determined by (a) how much material starts to sink out of the surface ocean and (b) the efficiency with which it is transferred to depth, i.e. the vertical attenuation of carbon flux (Henson et al., 2012a). The latter is controlled by the rate with which the exported material sinks and the rate at which it is remineralized back to the dissolved inorganic carbon (DIC) pool (McDonnell et al., 2015). Additionally, the amount of carbon relative to the limiting nutrient (usually nitrate or phosphate) plays a role. The carbon to nutrient ratio of sequestered particulate matter needs to be higher than that of the upwelled inorganic nutrients for artificial upwelling to sequester carbon efficiently (Baumann et al., 2021).

The nutrient composition of the upwelled water also determines the structure and composition of the phytoplankton community. By shaping the base of the food web, it thus affects the whole food web structure and ultimately the resulting ecosystem services, such as carbon export. The amount of dissolved silicate (orthosilicic acid, $Si(OH)_4$) is perhaps the most important characteristic when it comes to defining the phytoplankton community structure under meso- or eutrophic conditions. Under abundant silicate, diatoms (*Bacillariophyceae*) thrive, whereas under Si scarcity phyto-flagellates usually dominate (Sommer, 1994).

Diatoms are important players in the ocean carbon cycle (Field et al., 1998), contributing 40 % to the global particulate organic carbon (POC) export (Jin et al., 2006). They are chain-forming organisms, which constitute the yearly spring blooms at high latitudes and seasonal blooms in coastal upwelling regions (Smetacek, 1985, 1999). When the limiting nutrient is exhausted (usually nitrate or silicic acid), they form aggregates and export large amounts of biogenic carbon from the euphotic zone to the deep sea (Honjo and Manganini, 1993). Diatom blooms are short-lived, but can be sustained by recurring silicic acid fertilization and the associated carbon sequestration upheld on time scales of weeks to months (Dugdale and Wilkerson, 1998; Allen et al., 2005). They incorporate the silicic acid into their cell walls as biogenic silica (BSi), a biomineral two times heavier than particulate organic carbon (Klaas and Archer, 2002). As biogenic ballast material, it is considered to increase particle sinking velocities (Armstrong et al., 2009), and it might as well act as a protective barrier against microbial remineralization (Armstrong et al., 2002; Klaas and Archer, 2002). Furthermore,

aggregation processes can be facilitated by the exudation of transparent exopolymer particles (TEP), which are often exuded at the termination of a bloom (Obernosterer and Herndl, 1995) and promote the formation of larger marine snow particles.

However, diatoms do not necessarily promote efficient carbon export. In fact, their blooms can result in relatively inefficient transfer of particulate organic matter from the surface ocean to depth (Guidi et al., 2009; Henson et al., 2012b; Maiti et al., 2013). Exuded TEP itself are positively buoyant and can thus decrease the density of particulate matter in aggregates, thereby leading to its retention in the surface (Mari et al., 2017). Furthermore, diatom-originated aggregates are usually relatively porous, which can reduce sinking velocities and facilitate bacterial remineralization rates (Lam et al., 2011; Puigcorbé et al., 2015; Bach et al., 2019b). The diatom type and its physiological traits influence how much a population contributes to carbon export (Tréguer et al., 2018). It is thus important to characterize the plankton community and its structure in concert with the resulting carbon export and carbon sequestration potential.

We here tested the effect of nutrient composition (Si relative to N) in artificially upwelled waters on the quantity and stoichiometry of sinking matter, as well as on particle sinking velocities and remineralization rates. We enclosed a natural oligotrophic plankton community in the subtropical North Atlantic inside a mesocosm facility for 35 days. The mesocosms were fertilized every second day with nutrient-rich deep water composed of different Si:N ratios (gradient from 0.07–1.33 mol:mol). We anticipated that artificial upwelling would increase the export flux and remineralization rates of the relatively fresh exported matter (Baumann et al., 2021). We further expected the silification of diatom cells to increase with Si:N ratios, resulting in a higher BSi export flux and enhanced biogenic ballasting of exported matter, potentially enhancing particle sinking velocities.

Materials and Methods

Experimental setup

The mesocosm experiment was carried out in autumn 2019 in the subtropical North Atlantic. We used eight *in situ* mesocosms, which are the shorter equivalents of the KOSMOS mesocosm design (Riebesell et al., 2013) and have already successfully been deployed (Bach et al., 2019a). They are 2 m in diameter, 4 m long and possess a bag made of transparent polyurethane. At the bottom, the bag tapers off into a conical sediment trap, from which sinking material can regularly be sampled. They were filled simultaneously with ~8 m^3 of oligotrophic water from outside the harbor on the 6th of September (experimental day 0). During the filling, a 3 mm mesh at the water inlet kept larger organisms from entering the mesocosms.

During the 35 day-long experiment, the enclosed plankton communities were subjected to recurring additions of nutrient-rich deep water. The water was collected west of Gran Canaria at ~120-160 m depth. Before the addition of deep water to the mesocosms, inorganic nutrients were added to reach our desired nutrient levels. Thereby, C, N and P were supplied at Redfield

ratios (C:N:P = 106:16:1), reaching nitrate concentrations of 30 µmol L^{-1} with corresponding 1.9 µmol L^{-1} of phosphate and 199 µmol L^{-1} of dissolved inorganic carbon. Nitrate thereby served as the reference for the Si:N treatment. Silicic acid (Si(OH)$_4$) was added in different amounts (between 2 and 40 µmol L^{-1}, **Fig. 1a**) to achieve the specific treatment levels. These were chosen to mimic the different stoichiometries of potential source waters from different locations (Sarmiento et al., 2004; Griffiths et al., 2013) and depths (Sarmiento et al., 2007; Llinás et al., 1994). The first upwelling treatment was carried out on day 6, and was repeated every other day until day 32 (**Fig. 1b**).

Midway through the experiment, two more manipulations were carried out in order to assess the trophic transfer. On day 15, small pelagic fish were introduced to the mesocosms and on day 16 an isotopic tracer (^{13}C) was added. This allowed us to trace the path of matter through the pelagic food web up to the trophic level of small pelagic fish. In order to maintain the pelagic quality of the enclosed ecosystems, the mesocosm bags were regularly cleaned to prevent the attachment of fouling organisms. Therefore, the inside and outside walls were cleaned regularly using a ring-shaped wiper or by divers equipped with brushes, respectively (**Fig. 1b**). For more information on the experimental setup, the mesocosm maintenance and the deep water collection see Goldenberg et al. (to be submitted).
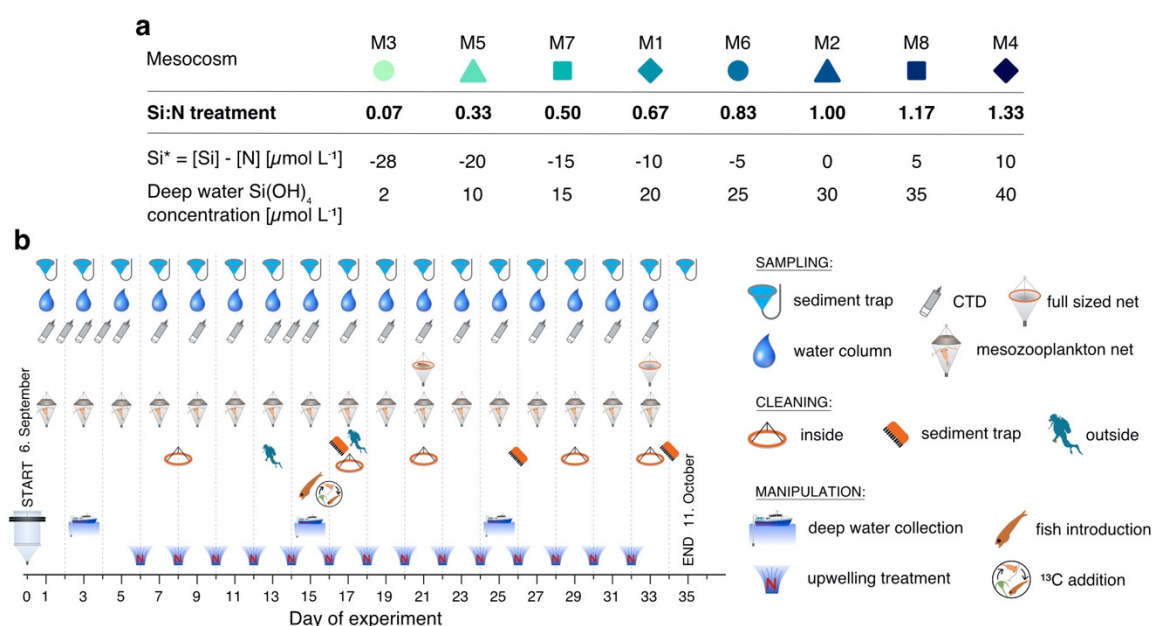
Figure 1. Experimental timeline with sampling, cleaning and manipulation schedule.

Sampling procedure

Water column and sediment trap samples were taken every to every second experimental day for the analysis of various biogeochemical and ecological parameters. The samples were analyzed in the nearby laboratory facilities of the Plataforma Oceánica de Canarias (PLOCAN) and the University of Las Palmas de Gran Canaria (ULPGC). Integrated water column samples were taken using submersible, 2 m long plastic tubes. They were transferred to 10 L carboys and stored dark and cold until arrival in the laboratory. There, they were subsampled for the analysis of phytoplankton abundances, composition and biomass and concentrations of

particulate biogenic matter. Sedimented material was sampled every second day through the hose attached to the sediment traps by means of a manual vacuum pump (<0.3 bar). It was collected in 5 L glass bottles (Schott Scandinavia, Denmark) and stored dark until further processing. In the lab, the sediment bottles were gently rotated to homogenize the material, and subsequently subsampled for measurements of sinking velocity and remineralization rates. The remainder of the material was prepared for the analysis of particulate biogenic matter, including particulate organic carbon, nitrogen and phosphorus (POC, PON, POP) and biogenic silica (BSi).

Sample processing and measurement

Sediment trap material

After the subsampling the settled biogenic matter first had to be separated from sea water (see Boxhammer et al., 2016). 3 mol L^{-1} of ferric chloride ($FeCL_3$) were added to the sediment bottles to make the material flocculate, followed by 3 mol L^{-1} of NaOH as a pH buffer, after which the bottles were left alone for 1 h to let the material settle. Subsequently, the supernatant sea water was carefully decanted. The sediment suspension was then centrifuged at ~5,200 g for 10 min in a 6–16KS centrifuge (Sigma Laborzentrifugen, Germany), and then again at ~5,000 g for 10 min in a 3K12 centrifuge (Sigma). This yielded sediment pellets, which were frozen at –20 °C and transported to Kiel, where their elemental composition was analyzed. In Kiel, the pellets were freed of any leftover moisture by freeze-drying and ground in a cell mill (Edmund Bühler, Germany), to obtain fine and homogeneous sediment powder. This powder was weighed and then then subsampled for POC, PON, BSi and POP measurements. Particulate organic carbon and nitrogen subsamples were transferred into tin cups and their contents measured after Sharp (1974) in duplicates on a Euro EA-CN analyzer (HEKAtech, Germany). POC subsamples were additionally fumed with 1 mol L^{-1} HCl and dried at 50 °C overnight before the measurement to remove the particulate inorganic carbon fraction, while PON was measured directly. Biogenic silica and particulate organic phosphorus concentrations were measured spectrophotometrically following Hansen and Koroleff (1999). The mass fluxes to the sediment trap were calculated by upscaling the measured C, N, Si and P concentrations in the subsamples to the total sample weight. The mass fluxes were then normalized to the time between sample collection (48 h) and to the mesocosm volume to obtain daily mass fluxes in $\mu mol\ L^{-1}\ d^{-1}$. The relative contribution of BSi to the total export flux as a proxy for BSi ballasting was calculated according to Bach et al. (2016).

$$BSi\ fraction = \frac{2.1*BSi}{1.06*POC+2.1*BSi+2.7*PIC} \qquad (1)$$

where the daily export fluxes of BSi, POC and PIC are multiplied with their respective densities (Klaas and Archer, 2002).

Water column samples

The integrated water samples were analyzed for their POC, PON and total particulate carbon (TPC) concentrations. Therefore, subsamples were taken in our on-shore labs and the suspended particulate material was collected on pre-combusted glass fiber filters (0.7 μm, Whatman). Filters for POC and PON analyses were acidified for ~2 h with 1 mol L^{-1} HCl to

remove the inorganic carbon fraction. Filters for POC/N and TPC were then dried for 24 h at 60 °C in pre-combusted glass petri dishes. They were packed into tin cups (8 × 8 × 15 mm, LabNeed, Germany) and transported back to Kiel, where their carbon and nitrogen contents were measured on a CN analyzer, as described for sedimented matter above. The particulate inorganic carbon content was estimated as the difference between TPC and POC. Since we did not find consistent evidence for the presence of particulate inorganic carbon (Goldenberg et al., to be submitted), we pooled the TPC and POC/N filters to obtain POC and PON duplicates.

Diatom biovolume was estimated using the Utermöhl method (Edler and Elbrächter, 2010). Water samples were fixed with Lugol's iodine (final concentration of 1 %) and stored inside 250 mL brown glass bottles. Subsamples were transferred to settling chambers (20–50 mL), from which cells were counted after 24 h using inverse light microscopy. A minimum of 500 phytoplankton cells per taxa were counted and identified to the lowest possible taxonomic level. Due to the high phytoplankton abundances, not all cells per subsample were counted, but a minimum of 500 cells across all taxa. The dimensions of the dominant taxa were regularly measured, and, based on average sizes, their specific biovolumes were calculated (Olenina et al., 2006). Total diatom biovolume was calculated from cell abundances and per capita biovolume.

Sinking velocity of sediment trap particles

In order to assess the potential transfer efficiency of sinking particles, we measured sinking velocities (SV) of particles in the 40–1000 μm size spectrum. We therefore used a video microscopy method, which was developed by Bach et al. (2012) and further reworked by Bach et al. (2019b) and Baumann et al. (2021). Diluted sediment subsamples were transferred to a sinking chamber (1 x 1 cm edge length), which was vertically mounted on a FlowCam device (Fluid Imaging Technologies, United States). Settling particles were therein recorded for 20 min at ~7 fps. Particle sinking velocities were calculated by fitting a linear model to the y-positions of multiple captures of the same particle and their respective time stamps. The calculations were carried out using the MATLAB software (version R2018b). Particles out of focus were excluded from the analysis based on the blurriness of their contour lines. Wall effects of the sinking chamber were corrected for using the equation in Ristow et al. (1997). Because of the temperature-dependence of sinking velocity measurements (Bach et al., 2012), our laboratory was temperature-controlled and set to 22–23 °C, depending on the daily *in situ* mesocosm temperatures.

Alongside sinking velocity, particle size as equivalent spherical diameter (ESD) and porosity (i.e. compactness) as a size-normalized measure for particle intensity (P_{int}) were measured. The underlying assumption of our porosity-proxy was that porous particles appear brighter (translucent) whereas more compact ones appear darker (opaque). High intensity values (i.e. brighter images) thus resulted in high porosities and vice versa. As large particles are generally more porous than small ones (Laurenceau-Cornec et al., 2020), our porosity-proxy is size-dependent, and was calculated following Bach et al. (2019b):

$$P_{int} = (intensity/255)^2 * ESD \qquad (2)$$

We analyzed sinking velocity and particle properties in four different particle classes: small (40–100 μm), medium (100–250 μm) and large particles (250–1000 μm), as well as the fastest 10 % of sinking particles across the three size fractions. As fast sinking particles are particularly important for carbon sequestration processes (see Section 4.1) and since we detected the strongest treatment effects in this particle class, we mainly focus on the fast sinking particle class in our later analysis.

Remineralization rates of sinking particles

The other factor that determines the transfer efficiency of particulate matter exported via the biological carbon pump is its remineralization rate. The higher it is, the lower the efficiency of carbon transfer to depth. Here, we measured the carbon-specific remineralization rate of sedimented material every 4 days via the oxygen depletion rate in dark-incubated sediment. Therefore, seven 330 mL glass bottles (Schott) were sampled headspace-free from the water column of each mesocosm. Four of these were used as replicates and three as controls ((4 + 3) bottles × 8 mesocosms = 56 bottles in total). They were transported dark and cool to the temperature-controlled lab (daily *in situ* temperature), where they acclimatized for 2 h in a water bath. There, between 0.5–3 mL of sediment suspension from sediment subsamples of the respective mesocosm was carefully added to the replicate bottles, while the controls were left untreated. A plastic pipette with a widened tip was used for the sediment addition to keep aggregates intact. All bottles were then incubated in darkness on a rotating plankton wheel (~1 rpm), and oxygen depletion over time was measured. O_2 measurements were carried out non-invasively on PSt3 optodes (PreSens Precision Sensing, Germany) mounted inside the bottles using a handheld optical measurement device (Fibox4 Trace, PreSens). They were automatically corrected for temperature, which was measured in a dummy bottle, and for atmospheric pressure measured by the Fibox4. Salinity was corrected for using the respective mesocosm salinity, measured by CTD casts on the respective day. The eight incubations lasted on average ~27 h, during which 5–8 O_2 measurement were carried out in intervals of 2–6 h. After the incubations the particulate matter inside the bottles was collected on pre-combusted glass fiber filters (0.7 μm, Whatman) and their POC contents analyzed similarly as for the water column filters.

Carbon-specific remineralization rates (C_{remin}, d^{-1}) were calculated by dividing the O_2 depletion rate (r in μmol O_2 L^{-1} d^{-1}) of the sediment material by its measured POC content (μmol C L^{-1}) at the end of the incubation:

$$C_{remin} = \frac{(r*RQ)}{(POC + r*RQ*\Delta t)} \qquad (3)$$

Thereby, RQ is the respiratory quotient (μmol C μmol O_2^{-1}), commonly regarded as 1, i.e. 1 mol CO_2 produced : 1 mol O_2 consumed (Ploug and Grossart, 2000; Iversen and Ploug, 2013; Bach et al., 2019b), and the time interval between the start of the incubation and the filtration start is factored in as Δt (d). C-specific remineralization rates were calculated for both sediment-containing bottles and blank bottles with only mesocosm water. The remineralization rates of the sedimented particulate matter were calculated by correcting the rates of the sediment-containing bottles for the rates in the blank bottles.

Finally, we calculated the remineralization length scale (RLS, m) as the quotient of sinking velocity (SV, m d^{-1}) and carbon-specific remineralization rates (C$_{remin}$, d^{-1}). It resembles the vertical distance over which 63 % of the sinking POC flux are being remineralized back to inorganic carbon (Cavan et al., 2017).

$$RLS = \frac{SV}{C_{remin}} \qquad (4)$$

Data analysis

The eight mesocosms constituted individual replicates along the established Si:N artificial upwelling gradient, and were sampled repetitively throughout the experiment. Linear mixed effects models with random intercept were used to detect effects of the upwelled Si:N ratio and its change over time on export parameters. Si:N was employed as continuous explanatory variable, experimental day as categorical fixed effect and mesocosm as categorical random effect. In order to assess the effect of silicon-associated export mechanisms (e.g. BSi ballasting) more directly, the exported Si:N ratio (i.e. exported BSi to exported PON, **Fig. S1**) was established as continuous explanatory variable for some parameters. The models were fit using restricted maximum likelihood and a type III test with Satterthwaite's approximation. All data analyses were carried out with the R software (version 4.1.2, R Core Team, 2021; RStudio Team, 2022). For data exploration and visualization the "tidyverse" package was used (Wickham et al., 2019). Statistical testing was performed using "lme4" (Bates et al., 2015) and "lmerTest" (Kuznetsova et al., 2017), always employing a significance level of $\alpha = 0.05$. The package "performance" (Lüdecke et al., 2021) was used to check assumptions. Normality of residuals and random effects were checked with Q-Q plots, homogeneity of variance with residuals versus fitted plots. Data was transformed where necessary. In addition, the temporal development of the Si:N effect was examined. Therefore, linear regressions for each sampling day were computed and their slopes ± 95 % confidence intervals were plotted over time.

Based on the daily export fluxes and stoichiometric ratios (see **Fig. 2b–e** and **Fig. S1**), we segmented the experiment into three phases to be able to discuss our results more comprehensively: oligotrophic baseline (days 3–9), initial response (days 11–21) and longer term response (days 23–35).

Results

Diatom community and particulate matter export

Artificial upwelling fueled diatom blooms in all mesocosms. High Si fertilization additionally accelerated bloom development during the initial growth phase (Goldenberg et al., to be submitted). The diatom blooms consisted mainly of the chain-forming *Leptocylindrus* and the pennate *Pseudo-nitzschia* genera (Ortiz et al., to be submitted). Throughout the treatment application, diatom biovolume was higher under Si-rich upwelling than under Si scarcity (**Fig. 2a**), indicating that abundant Si promoted plenty of material for building cell structures.

In all mesocosms the diatom blooms resulted in increased export fluxes of freshly produced particulate matter to the sediment trap (**Fig. 2b**). This material was characterized by elevated C:N ratios compared to pre-upwelling conditions (**Fig. 2c**). The Si:N ratio further enhanced both particulate organic carbon export and exported C:N ratios during the initial treatment response phase (days 11–21). Actively managing silicon to nutrient ratios thus enhanced the export of organically bound carbon during the system's adjustment to artificial upwelling.
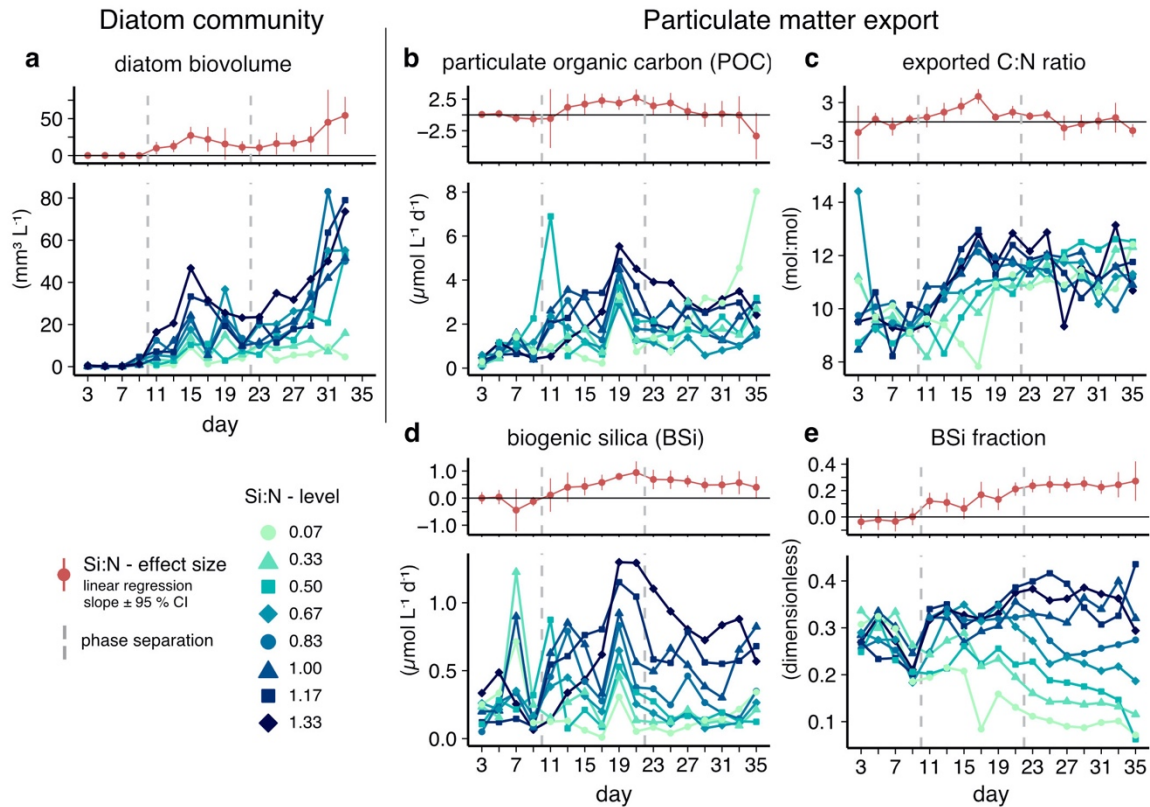
Figure 2. Suspended diatoms and particulate matter export under varying Si:N of artificially upwelled water. Daily Si:N effects are shown in red.

Increased export fluxes as a response to upwelling and to high Si:N ratios were primarily observed for carbon, nitrogen and silicon pools (see **Fig. 2b,d** and **Fig. S1**). Particulate organic carbon and nitrogen export increased on average 3- and 2.5-fold from the pre-treatment (days 3–9) to the initial response phase (days 11–21), respectively, while biogenic silica export increased 1.7-fold. In contrast, the export of total particulate phosphorus did not increase (**Fig. S1**). The peak in the export flux parameters on day 19 was likely a consequence of the cleaning of the inside mesocosm walls and the sediment traps on day 17 (compare **Fig. 1** and **Fig. 2b–e**). The Si:N treatment was mirrored most clearly in the biogenic silica flux, the BSi fraction of the total flux (**Fig. 2d–e**) and the exported Si:N ratio (**Fig. S1**). Si-rich upwelling did thus not only cause a higher BSi flux, but also increased the BSi ballasting of sinking particles (**Table S1**). Both effects persisted throughout the initial and long-term response phases. In contrast, the positive Si:N effect on POC export and exported C:N ratios disappeared during the longer-term response phase.

Sinking particle characteristics

The nutrient composition in the upwelled water affected the properties of sinking particles. Surprisingly, high Si:N in upwelled waters temporarily decreased sinking velocity and size of the fastest sinking particles (**Fig. 3b–c**). The effect was similar, although slightly weaker, for sinking velocities classified by particle size (**Fig. S2** and **Table S2**). The relationship between the Si:N ratio of exported matter and sinking velocity (/particle size) yielded similar results (**Fig. 3d,h**, **Table S2f–i**). This shows that a high proportion of biogenic silica ballast correlated with smaller sizes and lower sinking speeds of fast sinking particles. Moreover, the reduced sinking speeds in the high Si:N treatments were not only associated with smaller sizes, but also with lower particle porosities (**Fig. 3g**).

The remineralization rates of sinking particulate matter increased when freshly produced material sank to the sediment traps at the onset of the upwelling treatment and subsequently decreased again towards the end of the experiment. In contrast to sinking velocities, remineralization rates were however not affected by the upwelled Si:N ratio (**Table S2**), except for day 15, on which there was a small positive effect (**Fig. 3a**).
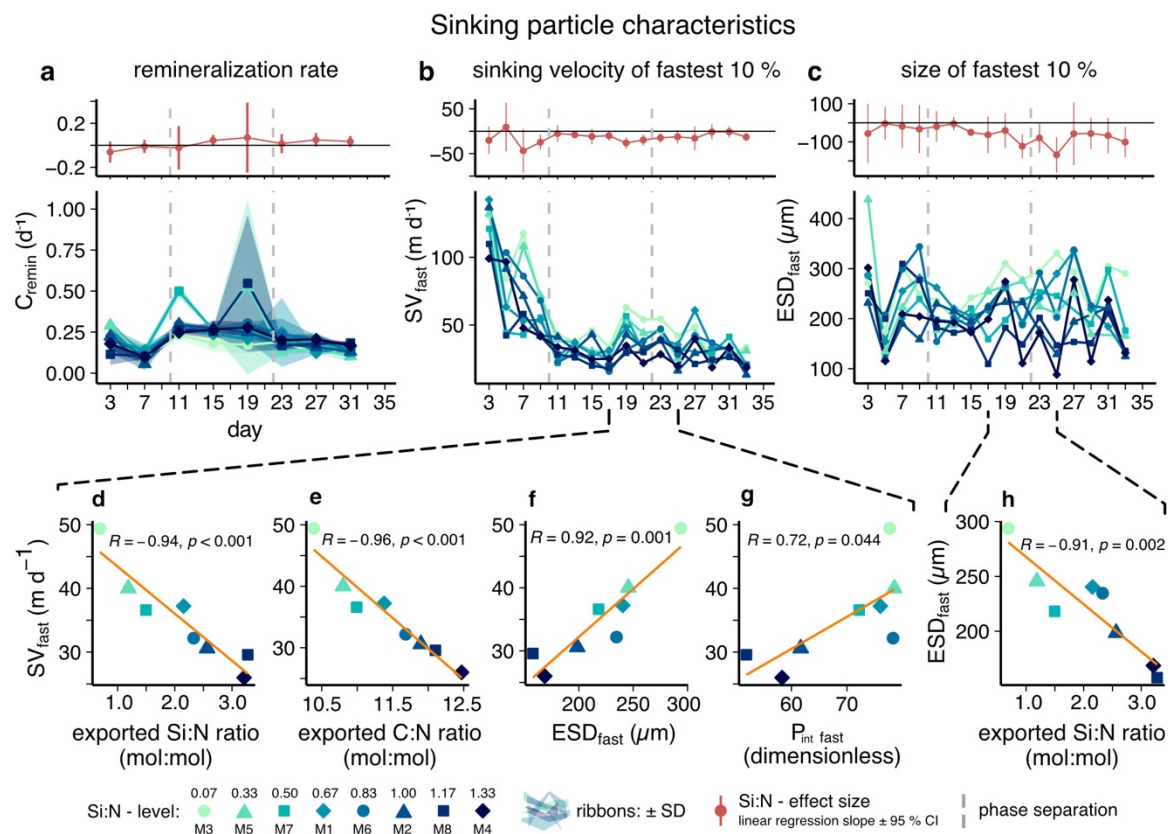
Figure 3. Sinking particle characteristics and daily Si:N effect sizes. Particle sinking velocities, sizes and porosities in (**b–h**) are means of the fastest 10 % of sinking particles. (**d–h**) give further evidence on potential drivers of the negative Si:N effect on sinking velocities (/particle sizes), and include mean data from days 17 to 25.

The Si:N ratio of upwelled water and resulting differences in diatom occurrence led to distinct biogeochemical responses in export-related parameters. We found increased sinking velocities

of fast sinking particles only under low to moderate diatom presence (**Fig. 4a**). In the Si-rich upwelling treatments, in which diatoms occurred aplenty (**Fig. 2a**), particle sinking velocities were rather low. It thus seems like high diatom abundances did not allow for fast sinking particles. Likewise, fast sinking particles and high C:N ratios did not occur simultaneously during the times of a positive Si:N effect on exported C:N ratios (**Fig. 3e** and **Fig. 4b**). The exported particles in between days 17 and 25 were either fast sinking, or carbon-rich, but not both. Finally, only a part of the over-consumed carbon under high Si:N upwelling was exported (**Fig. 4c**). Under low Si:N, C:N ratios in the water column were relatively low (~5–12 mol:mol), and exported matter was carbon-enriched compared to the suspended material (retention of N in the water column, **Fig. 4c**). In contrast, under high Si:N, the C:N ratios in the water column were much higher (~10–17.5 mol:mol), however, the exported matter was carbon-depleted relative to the suspended material (indicating retention of C in the water column). This indicates that the additionally taken-up carbon under high Si:N was partly retained as POC (i.e. non-sinking particles) in the water column instead of being channeled into export production. The amount of silicon relative to nitrogen in artificially upwelled water thus affected export-related parameters in counteracting ways.
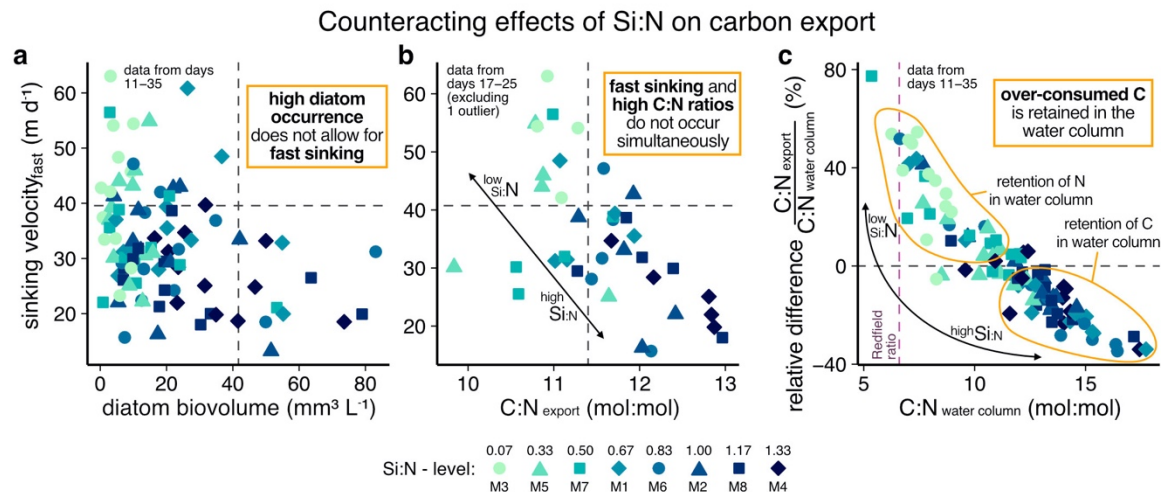
Figure 4. Summary figure displaying the counteracting effects of Si:N on export related parameters. Note that (**b**) excludes the data point M3 on day 17 (exported C:N ratio: 7.8 mol:mol, sinking velocity of fastest 10%: 33.4 m d^{-1}).

Discussion

Counteracting effects of Si:N upwelling

POC export and associated C:N ratios increased after the onset of artificial upwelling. This finding is similar to an earlier artificial upwelling mesocosm study (Baumann et al., 2021). The Si:N composition in the artificially upwelled water had positive effects on the quantity and stoichiometry of the export flux. Si-rich upwelling led to a temporarily enhanced particulate organic carbon flux with elevated C:N ratios, both of which is beneficial for potential carbon sequestration. The reason for this is that during the adjustment phase diatom abundances and C:N ratios of suspended particulate matter were higher under Si-rich compared to Si-scarce

upwelling (Goldenberg et al. to be submitted). This enhanced biomass production and the elevated C:N ratios were in time reflected by the export flux. Furthermore, the Si:N ratio had a lasting positive effect on biogenic silica export and hence on the relative contribution of BSi ballast to sedimented matter. High Si:N ratios in upwelled water thus promoted the carbon sequestration potential in several ways.

Curiously though, the more than 3-fold increase in BSi ballast under Si-rich upwelling did not result in higher particle sinking velocities. On the contrary, sinking velocities temporarily decreased under enhanced ballasting. The reason for this was most likely that particles under Si-replete conditions were ~100 μm smaller than the ones experiencing Si-scarce upwelling. Apparently, the decreased particle size outweighed the positive effect of enhanced BSi ballast. Although we found this negative Si:N effect on sinking velocities for almost all considered particle size classes, it was most prominent for those particles that sank fastest (**Table S2**). These fast sinking particles can be considered the most important contributor to the biological pump as they reach the sequestration depth most rapidly and spend the least amount of time in the mesopelagic zone, where the majority of remineralization occurs (Mayor et al., 2014; García-Martín et al., 2021). Furthermore, as sinking velocity is positively affected by particle size (Cael et al., 2021), fast sinking particles are often large and hence incorporate high amounts of organic carbon. The speed with which the fastest particles sink is thus an important predictor for carbon sequestration processes (Riley et al., 2012). Another counterintuitive finding was the positive correlation between sinking velocity and particle porosity at the end of the adjustment phase. Theoretically, porosity should negatively affect a particle's sinking velocity by lowering its density (Laurenceau-Cornec et al., 2020). Here, however, the opposite was observed. The reason for this is that the fast sinking, porous particles were also large, and porosity is size-dependent (Laurenceau-Cornec et al., 2020). Additionally, the correlation between sinking velocity and size was a lot stronger than the one with porosity (compare **Fig. 3f** and **g**), suggesting that particle size – again – overruled the negative effect of porosity. This is in line with a recent study, in which we observed the same particle size spectrum as here and found particle size to be a stronger predictor for sinking velocity than porosity (Baumann et al., submitted). Consequently, it seems that the large sizes of fast sinking particles increased their sinking velocities over the combined negative effects of lower BSi ballast and higher porosities.

The remaining question is, what the reason for the decreased particle sizes and sinking velocities under Si-rich upwelling was. To try and answer it, a look at the sediments from the time period in question (end of the adjustment phase) is helpful. **Figure 5** shows pictures of a subsample of sedimented material from day 21 of each mesocosm, aligned along the Si:N upwelling gradient. There are apparent differences between the high and low Si:N treatments: under Si scarcity particles were relatively large, distinct, and contrasted strongly with the background, whereas under abundant Si, single particles were smaller and hardly distinguishable. In fact, in the two highest treatments it seems like tiny specks were loosely connected to each other in some sort of matrix. We argue that the reason for this impression, and hence the underlaying mechanism in question, were transparent exopolymer particles (TEP), which were increasingly exuded under Si-rich upwelling.

Although we did not measure TEP in this experiment, the enhanced C:N ratios both in suspended and exported particulate matter indicate its occurrence. TEP are exuded primarily under nutrient limitation (Mari et al., 2017; Obernosterer and Herndl, 1995). In our experiment the added nitrate was always fully taken up after each deep water addition (Goldenberg et al., to be submitted). There was thus recurring nutrient limitation, which could have promoted TEP production. Since diatoms were more dominant in the high Si:N treatments, one would expect higher TEP formation in there (as suggested by **Fig. 5**). TEP can act as "biological glue" and promote aggregation, but it can also retain suspended matter in the surface layer due to its positive buoyancy (Mari et al., 2017). Aggregates that are composed of a high fraction of TEP have a high C:N ratio and elevated buoyancy. They only start sinking once they incorporate enough dense, non-TEP particles, which decreases their buoyancy and their C:N ratio (Azetsu-Scott and Passow, 2004). This might be the reason for why high C:N ratios of sinking matter and high sinking velocities were mutually exclusive in our experiment (**Fig. 4b**). It could also explain why the high particulate matter C:N ratios were retained in the water column and the over-consumed carbon under abundant Si only partly reached the sediment trap (**Fig. 4c**). This stands in line with an earlier mesocosm experiment, during which TEP concentration increased sharply following a simulated artificial upwelling event, and was highlighted as the reason for the decrease of sinking velocities (Bach et al., 2019b).
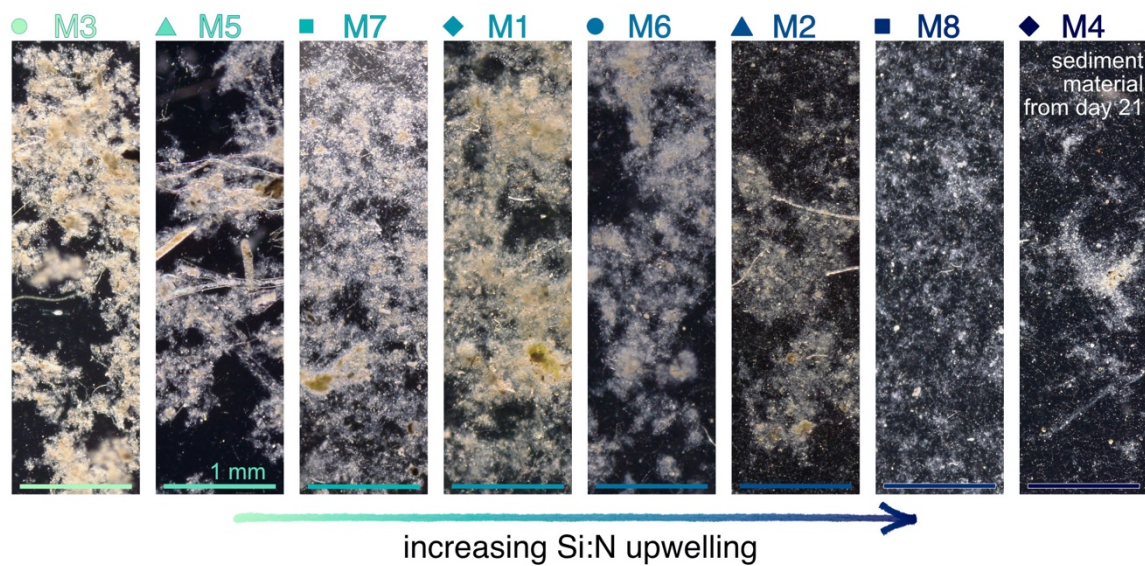
Figure 5. Material sampled from the sediment trap of each mesocosm on day 21. Pictures were taken on a stereo microscope (Stemi 305, ZEISS) using a 10X magnification.

Summing up, enhancing the proportion of Si in artificially upwelled water increased BSi ballasting of sinking particles but also decreased their sizes and ultimately resulted in lower sinking velocities. Furthermore, sediment remineralization did not change with upwelled Si:N ratio, hence opal did not seem to shield organic matter from respiration (Boyd and Trull, 2007). A high contribution of opal did thus not go hand in hand with particle properties that are beneficial for transfer efficiency. When considering the correlations between BSi and POC fluxes in the deep ocean (Klaas and Archer, 2002), our findings suggest that in the surface ocean the positive effects of opal ballasting on POC fluxes are superimposed by other drivers. For example, the enhanced formation of positively buoyant TEP could exert a negative control

on sinking velocities (Azetsu-Scott and Passow, 2004) and retain carbon-rich material in the surface (Mari et al., 2017). As particles sink through the epi- and mesopelagic zones, the preferential remineralization of organic material, including TEP, might leave a higher fraction of opal behind and could thus be the reason for the observed correlations between POC and BSi fluxes (Sanders et al., 2010).

Implications for artificial upwelling as negative emission technology

The various Si:N effects on export parameters in our study were of counteracting nature. Some imply an increased potential for carbon sequestration and thus carbon removal from the atmosphere, others are unfavorable in that aspect (**Table 1**). In the following, we will discuss the relative importance of our findings in respect to the carbon removal potential of artificial upwelling.

export response variable	Si:N effect short term	Si:N effect long term	implication for C sequestration
Quantity:			
POC export	↑	—	⊕ higher export production
relative difference C:N export / C:N water column	↓	↓	⊖ retention of carbon in the water column
Quality:			
exported C:N ratio	↑	—	⊕ balances upwelled DIC:NO_3^-
BSi ballast	↑	↑	⊕ increases sinking velocity
remineralization rate	—	—	⊜ no effect on transfer efficiency
particle size	↓	—	⊖ decreases sinking velocity
sinking velocity	↓	—	⊖ decreases transfer efficiency

⊕ / ⊖ / ⊜: positive / negative / no effect on carbon sequestration potential

Table 1. Summary of Si:N effects under artificial upwelling on export-related parameters and their implications for the carbon sequestration potential. Short term (initial response phase) and long term (longer term response phase) effects are displayed.

The key Si:N effects concerning the carbon sequestration potential are the positive effects on daily POC fluxes, exported matter C:N ratios and BSi ballasting on the one side, and the negative effects on sinking velocities and the relative difference between suspended and exported C:N ratios on the other (**Table 1**). Si-replete conditions temporarily caused more material to be exported from the surface and positively affected the C:N ratio of exported matter, both of which strengthens the biological carbon pump. However, the C:N effect was buffered by the retention of parts of the over-consumed carbon in the water column, and additionally, sinking velocities decreased, which hampered the potential for efficient organic carbon transfer to depth.

The question is whether the increased POC flux and elevated C:N ratios, or the decreased sinking velocities would have had a larger impact on the realized carbon deep export. The remineralization length scale (RLS), a proxy for the POC transfer efficiency, helps to get an

understanding of the relative importance of flux quantity versus quality. **Figure 6** shows the RLS, surface POC fluxes and theoretical attenuated POC fluxes at the respective RLS depth for the lowest and highest Si:N treatments on day 21. On this day, there were pronounced and rather linear Si:N effects, making this comparison representative of the range of Si:N ratios tested here. Due to the 2.5-fold higher particle sinking velocities under low Si:N, the transfer of organic carbon to depth would have very likely been more efficient in the lowest compared to the highest treatment (RLS depth more than 2-fold deeper). Nonetheless, the 6-fold higher POC flux under the highest Si availability would have probably led to more POC sinking out of the euphotic zone (50–100 m depth) in this treatment. We can, however, not say whether the enhanced flux attenuation under high Si:N would ultimately lead to less POC reaching the deep ocean than under Si-scarcity. For this, a sophisticated flux attenuation model would be needed, which is beyond the scope of this study. We hence emphasize the importance of incorporating our experimental findings into biogeochemical models. This would help to resolve the relative importance of counteracting effects of artificial upwelling as a carbon removal technique.
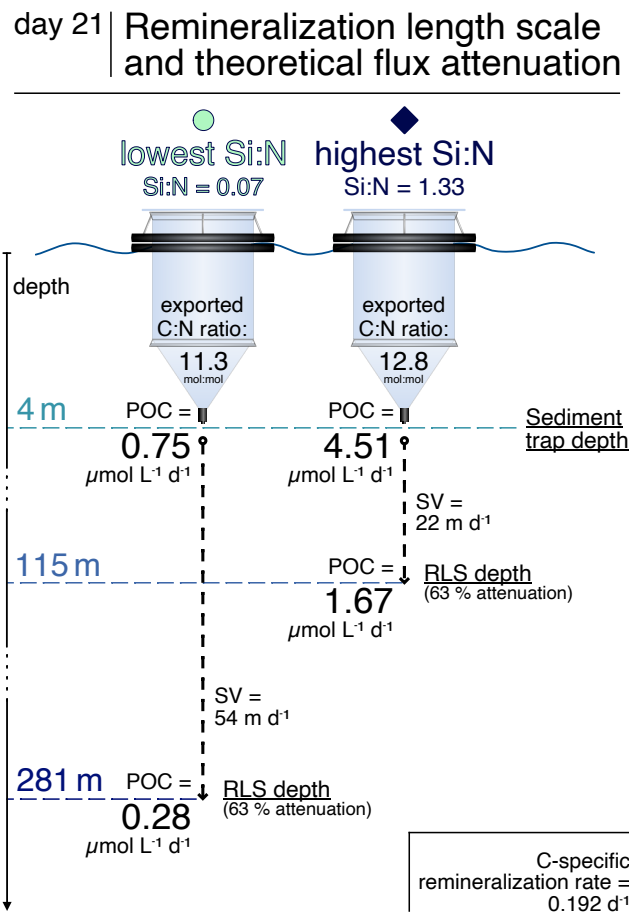
Figure 6. Remineralization length scale (RLS) and resulting flux attenuation for highest and lowest Si:N treatment on day 21. RLSs were calculated from sinking velocities (SV) of the fastest sinking particles on day 21 and remineralization rates averaged across mesocosms from day 23.

When discussing the implications of these results, it is important to differentiate between short and long term effects. The observed short term Si:N effects carry more weight for stationary artificial upwelling applications, which result in one-time fertilization of water patches, e.g. a

moored wave pump (Liu et al., 1999; Fan, 2016). Also the remineralization rates, which increased after the onset of artificial upwelling, subsequently decreased again towards the end of the experiment, and thus only temporarily hampered the efficiency of particle transfer. The longer term effects are more important regarding the application of drifting artificial upwelling devices, which fertilize the same patch of water over longer time periods. Concerning recurring upwelling, most of the Si:N effects are thus not crucial, and instead the benefit of increased POC fluxes and enhanced sinking matter C:N ratios would come into play. Those elevated carbon to nutrient ratios would, however, be buffered under Si-rich upwelling by the retention of over-consumed carbon in the water column.

In summary, artificial upwelling enhanced POC fluxes and associated C:N ratios, and did so on the time scale of multiple weeks. Additionally, the upwelled Si:N ratio temporarily enhanced carbon assimilation and consequently the POC flux and exported matter C:N ratios. However, the over-consumed carbon was partly retained in the water column, possibly due to the enhanced formation of positively buoyant TEP under high diatom abundances. Furthermore, although Si-rich upwelling enhanced BSi ballasting manifold, changes in particle properties led to temporarily decreased sinking velocities and hence less efficient particle export. In a next step, modelling approaches could help to resolve the relative importance of these findings by incorporating them into POC flux attenuation simulations.

Bibliography

Allen, J.T., Brown, L., Sanders, R., Mark Moore, C., Mustard, A., Fielding, S., Lucas, M., Rixen, M., Savidge, G., Henson, S.A., Mayor, D., 2005. Diatom carbon export enhanced by silicate upwelling in the northeast Atlantic. Nature 437, 728–732. https://doi.org/10.1038/nature03948

Armstrong, R.A., Lee, C., Hedges, J.I., Honjo, S., Wakeham, S.G., 2002. A new, mechanistic model for organic carbon fluxes in the ocean based on the quantitative association of POC with ballast minerals. Deep Sea Research Part II: Topical Studies in Oceanography. https://doi.org/10.1016/s0967-0645(01)00101-1

Armstrong, R.A., Peterson, M.L., Lee, C., Wakeham, S.G., 2009. Settling velocity spectra and the ballast ratio hypothesis. Deep Sea Research Part II: Topical Studies in Oceanography 56, 1470–1478. https://doi.org/10.1016/j.dsr2.2008.11.032

Azetsu-Scott, K., Passow, U., 2004. Ascending marine particles: Significance of transparent exopolymer particles (TEP) in the upper ocean. Limnol. Oceanogr. 49, 741–748. https://doi.org/10.4319/lo.2004.49.3.0741

Bach, L.T., Boxhammer, T., Larsen, A., Hildebrandt, N., Schulz, K.G., Riebesell, U., 2016. Influence of plankton community structure on the sinking velocity of marine aggregates: Sinking velocity of marine aggregates. Global Biogeochem. Cycles 30, 1145–1165. https://doi.org/10.1002/2016GB005372

Bach, L.T., Hernández-Hernández, N., Taucher, J., Spisla, C., Sforna, C., Riebesell, U., Arístegui, J., 2019a. Effects of Elevated CO_2 on a Natural Diatom Community in the Subtropical NE Atlantic. Front. Mar. Sci. 6, 75. https://doi.org/10.3389/fmars.2019.00075

Bach, L.T., Riebesell, U., Sett, S., Febiri, S., Rzepka, P., Schulz, K.G., 2012. An approach for particle sinking velocity measurements in the 3–400 µm size range and considerations on the effect of temperature on sinking rates. Mar Biol 159, 1853–1864. https://doi.org/10.1007/s00227-012-1945-2

Bach, L.T., Stange, P., Taucher, J., Achterberg, E.P., Algueró-Muñiz, M., Horn, H., Esposito, M., Riebesell, U., 2019b. The Influence of Plankton Community Structure on Sinking Velocity and Remineralization Rate of Marine Aggregates. Global Biogeochem. Cycles 33, 971–994. https://doi.org/10.1029/2019GB006256

Bates, D., Mächler, M., Bolker, B., Walker, S., 2015. Fitting Linear Mixed-Effects Models using lme4. Journal of Statistical Software 67, 1–48. https://doi.org/10.18637/jss.v067.i01

Baumann, M., Taucher, J., Paul, A.J., Heinemann, M., Vanharanta, M., Bach, L.T., Spilling, K., Ortiz, J., Arístegui, J., Hernández-Hernández, N., Baños, I., Riebesell, U., 2021. Effect of Intensity and Mode of Artificial Upwelling on Particle Flux and Carbon Export. Front. Mar. Sci. 8, 742142. https://doi.org/10.3389/fmars.2021.742142

Boxhammer, T., Bach, L.T., Czerny, J., Riebesell, U., 2016. Technical note: Sampling and processing of mesocosm sediment trap material for quantitative biogeochemical analysis. Biogeosciences 13, 2849–2858. https://doi.org/10.5194/bg-13-2849-2016

Boyd, P.W., Trull, T.W., 2007. Understanding the export of biogenic particles in oceanic waters: Is there consensus? Progress in Oceanography 72, 276–312. https://doi.org/10.1016/j.pocean.2006.10.007

Cael, B.B., Cavan, E.L., Britten, G.L., 2021. Reconciling the Size-Dependence of Marine Particle Sinking Speed. Geophys Res Lett 48. https://doi.org/10.1029/2020GL091771

Cavan, E.L., Trimmer, M., Shelley, F., Sanders, R., 2017. Remineralization of particulate organic carbon in an ocean oxygen minimum zone. Nat Commun 8, 14847. https://doi.org/10.1038/ncomms14847

Dugdale, R.C., Wilkerson, F.P., 1998. Silicate regulation of new production in the equatorial Pacific upwelling. Nature 391, 270–273. https://doi.org/10.1038/34630

Edler, L., Elbrächter, M., 2010. The Utermöhl method for quantitative phytoplankton analysis, in: Microscopic and Molecular Methods for Quantitative Phytoplankton Analysis. UNESCO, Paris, pp. 13–20.

Fan, W., 2016. Experimental study on the performance of a wave pump for artificial upwelling. Ocean Engineering 10.

Field, C.B., Behrenfeld, M.J., Randerson, J.T., Falkowski, P., 1998. Primary Production of the Biosphere: Integrating Terrestrial and Oceanic Components. Science 281, 237–240. https://doi.org/10.1126/science.281.5374.237

García-Martín, E.E., Davidson, K., Davis, C.E., Mahaffey, C., McNeill, S., Purdie, D.A., Robinson, C., 2021. Low Contribution of the Fast-Sinking Particle Fraction to Total Plankton Metabolism in a Temperate Shelf Sea. Global Biogeochem Cycles 35. https://doi.org/10.1029/2021GB007015

Griffiths, J.D., Barker, S., Hendry, K.R., Thornalley, D.J.R., van de Flierdt, T., Hall, I.R., Anderson, R.F., 2013. Evidence of silicic acid leakage to the tropical Atlantic via Antarctic Intermediate Water during Marine Isotope Stage 4. Paleoceanography 28, 307–318. https://doi.org/10.1002/palo.20030

Guidi, L., Stemmann, L., Jackson, G.A., Ibanez, F., Claustre, H., Legendre, L., Picheral, M., Gorskya, G., 2009. Effects of phytoplankton community on production, size, and export of large aggregates: A world-ocean analysis. Limnol. Oceanogr. 54, 1951–1963. https://doi.org/10.4319/lo.2009.54.6.1951

Hansen, H.P., Koroleff, F., 1999. Determination of nutrients, in: Methods of Seawater Analysis, Third, Completely Revised and Extended Edition. WILEY-VCH, pp. 159–228.

Henson, S.A., Lampitt, R.S., Johns, D., 2012a. Variability in phytoplankton community structure in response to the North Atlantic Oscillation and implications for organic carbon flux. Limnol. Oceanogr. 57, 1591–1601. https://doi.org/10.4319/lo.2012.57.6.1591

Henson, S.A., Sanders, R., Madsen, E., 2012b. Global patterns in efficiency of particulate organic carbon export and transfer to the deep ocean: Export and Transfer Efficiency. Global Biogeochem. Cycles 26. https://doi.org/10.1029/2011GB004099

Honjo, S., Manganini, S.J., 1993. Annual biogenic particle fluxes to the interior of the North Atlantic Ocean; studied at 34°N 21°W and 48°N 21°W. Deep Sea Research Part II: Topical Studies in Oceanography 40, 587–607. https://doi.org/10.1016/0967-0645(93)90034-K

Iversen, M.H., Ploug, H., 2013. Temperature effects on carbon-specific respiration rate and sinking velocity of diatom aggregates – potential implications for deep ocean export processes. Biogeosciences 10, 4073–4085. https://doi.org/10.5194/bg-10-4073-2013

Jin, X., Gruber, N., Dunne, J.P., Sarmiento, J.L., Armstrong, R., 2006. Diagnosing the contribution of phytoplankton functional groups to the production and export of particulate organic carbon, CaCO3, and opal from global nutrient and alkalinity

distributions. Global Biogeochemical Cycles 20. https://doi.org/10.1029/2005gb002532

Klaas, C., Archer, D., 2002. Association of sinking organic matter with various types of mineral ballast in the deep sea: Implications for the rain ratio. Global Biogeochemical Cycles. https://doi.org/10.1029/2001gb001765

Kuznetsova, A., Brockhoff, P.B., Christensen, R.H.B., 2017. lmerTest Package: Tests in Linear Mixed Effects Models. J. Stat. Soft. 82. https://doi.org/10.18637/jss.v082.i13

Lam, P.J., Doney, S.C., Bishop, J.K.B., 2011. The dynamic ocean biological pump: Insights from a global compilation of particulate organic carbon, $CaCO_3$, and opal concentration profiles from the mesopelagic: The dynamic ocean biological pump. Global Biogeochem. Cycles 25, n/a-n/a. https://doi.org/10.1029/2010GB003868

Laurenceau-Cornec, E.C., Le Moigne, F.A.C., Gallinari, M., Moriceau, B., Toullec, J., Iversen, M.H., Engel, A., De La Rocha, C.L., 2020. New guidelines for the application of Stokes' models to the sinking velocity of marine aggregates. Limnology and Oceanography 65, 1264–1285. https://doi.org/10.1002/lno.11388

Liu, C.C.K., Dai, J.J., Lin, H., Guo, F., 1999. Hydrodynamic Performance of Wave-Driven Artificial Upwelling Device. J. Eng. Mech. 125, 728–732.

Llinás, O., Rodríguez de León, A., Siedler, G., Wefer, G., 1994. ESTOC Data Report 1994 77.

Lüdecke, D., Ben-Shachar, M., Patil, I., Waggoner, P., Makowski, D., 2021. performance: An R Package for Assessment, Comparison and Testing of Statistical Models. JOSS 6, 3139. https://doi.org/10.21105/joss.03139

Maiti, K., Charette, M.A., Buesseler, K.O., Kahru, M., 2013. An inverse relationship between production and export efficiency in the Southern Ocean. Geophys. Res. Lett. 40, 1557–1561. https://doi.org/10.1002/grl.50219

Mari, X., Passow, U., Migon, C., Burd, A.B., Legendre, L., 2017. Transparent exopolymer particles: Effects on carbon cycling in the ocean. Progress in Oceanography 151, 13–37. https://doi.org/10.1016/j.pocean.2016.11.002

Masson-Delmotte, V., Zhai, P., Pörtner, H.-O., Roberts, D., Skea, J., Shukla, P.R., Pirani, A., Moufouma-Okia, W., Péan, C., Pidcock, R., Connors, S., Matthews, J.B.R., Chen, Y., Zhou, X., Gomis, M.I., Lonnoy, E., Maycock, T., Tignor, M., Waterfield, T., 2018. IPCC, 2018: Summary for Policymakers. Global Warming of 1.5°C. An IPCC Special Report on the impacts of global warming of 1.5°C above pre-industrial levels and related global greenhouse gas emission pathways, in the context of strengthening the global response to the threat of climate change, sustainable development, and efforts to eradicate poverty.

Mayor, D.J., Sanders, R., Giering, S.L.C., Anderson, T.R., 2014. Microbial gardening in the ocean's twilight zone: Detritivorous metazoans benefit from fragmenting, rather than ingesting, sinking detritus: Fragmentation of refractory detritus by zooplankton beneath the euphotic zone stimulates the harvestable production of labile and nutritious microbial. BioEssays 36, 1132–1137. https://doi.org/10.1002/bies.201400100

McDonnell, A.M.P., Boyd, P.W., Buesseler, K.O., 2015. Effects of sinking velocities and microbial respiration rates on the attenuation of particulate carbon fluxes through the mesopelagic zone. Global Biogeochemical Cycles. https://doi.org/10.1002/2014gb004935

Obernosterer, I., Herndl, G.J., 1995. Phytoplankton extracellular release and bacterial growth: dependence on the inorganic N: P ratio. Mar. Ecol. Prog. Ser. 116, 247–257. https://doi.org/10.3354/meps116247

Olenina, I., Hajdu, S., Edler, L., Andersson, A., Wasmund, N., Busch, S., Göbel, J., Gromisz, S., Huseby, S., Huttunen, M., Jaanus, A., Kokkonen, P., Ledaine, I., Niemkiewicz, E., 2006. Biovolumes and size-classes of phytoplankton in the Baltic Sea (No. 106), Baltic Sea Environment Proceedings. HELCOM.

Pan, Y., Fan, W., Zhang, D., Chen, J.W., Huang, H., Liu, S., Jiang, Z., Di, Y., Tong, M., Chen, Y., 2016. Research progress in artificial upwelling and its potential environmental effects. Sci. China Earth Sci. 59, 236–248. https://doi.org/10.1007/s11430-015-5195-2

Ploug, H., Grossart, H.-P., 2000. Bacterial growth and grazing on diatom aggregates: Respiratory carbon turnover as a function of aggregate size and sinking velocity. Limnol. Oceanogr 45, 1467–1475. https://doi.org/10.4319/lo.2000.45.7.1467

Puigcorbé, V., Benitez-Nelson, C.R., Masqué, P., Verdeny, E., White, A.E., Popp, B.N., Prahl, F.G., Lam, P.J., 2015. Small phytoplankton drive high summertime carbon and nutrient export in the Gulf of California and Eastern Tropical North Pacific. Global Biogeochem. Cycles 29, 1309–1332. https://doi.org/10.1002/2015GB005134

R Core Team, 2021. R: A Language and Environment for Statistical Computing.

Riebesell, U., Czerny, J., von Bröckel, K., Boxhammer, T., Büdenbender, J., Deckelnick, M., Fischer, M., Hoffmann, D., Krug, S.A., Lentz, U., Ludwig, A., Muche, R., Schulz, K.G., 2013. Technical Note: A mobile sea-going mesocosm system – new opportunities for ocean change research. Biogeosciences 10, 1835–1847. https://doi.org/10.5194/bg-10-1835-2013

Riley, J.S., Sanders, R., Marsay, C.M., Le Moigne, F.A.C., Achterberg, E.P., Poulton, A.J., 2012. The relative contribution of fast and slow sinking particles to ocean carbon export. Global Biogeochemical Cycles. https://doi.org/10.1029/2011gb004085

Ristow, G.H., 1997. Wall correction factor for sinking cylinders in fluids. Phys. Rev. E 55, 2808–2813. https://doi.org/10.1103/PhysRevE.55.2808

RStudio Team, 2022. RStudio: Integrated Development Environment for R.

Sanders, R., Morris, P.J., Poulton, A.J., Stinchcombe, M.C., Charalampopoulou, A., Lucas, M., Thomalla, S.J., 2010. Does a ballast effect occur in the surface ocean. Geophysical Research Letters. https://doi.org/10.1029/2010gl042574

Sarmiento, J.L., Gruber, N., Brzezinski, M.A., Dunne, J.P., 2004. High-latitude controls of thermocline nutrients and low latitude biological productivity. Nature 427, 56–60. https://doi.org/10.1038/nature02127

Sarmiento, J.L., Simeon, J., Gnanadesikan, A., Gruber, N., Key, R.M., Schlitzer, R., 2007. Deep ocean biogeochemistry of silicic acid and nitrate. Global Biogeochem. Cycles 21. https://doi.org/10.1029/2006GB002720

Sharp, J.H., 1974. Improved analysis for "particulate" organic carbon and nitrogen from seawater. Limnol. Oceanogr. 19, 984–989. https://doi.org/10.4319/lo.1974.19.6.0984

Siegel, D.A., DeVries, T., Doney, S.C., Bell, T., 2021. Assessing the sequestration time scales of some ocean-based carbon dioxide reduction strategies. Environ. Res. Lett. 16, 104003. https://doi.org/10.1088/1748-9326/ac0be0

Smetacek, V., 1999. Diatoms and the ocean carbon cycle. Protist 150, 25–32. https://doi.org/10.1016/s1434-4610(99)70006-4

Smetacek, V., 1985. Role of sinking in diatom life-history cycles: ecological, evolutionary and geological significance. Marine Biology. https://doi.org/10.1007/bf00392493

Sommer, U., 1994. Are marine diatoms favoured by high Si:N ratios? Marine Ecology Progress Series 115, 309–315. https://doi.org/10.3354/meps115309

Tréguer, P., Bowler, C., Moriceau, B., Dutkiewicz, S., Gehlen, M., Aumont, O., Bittner, L., Dugdale, R.C., Finkel, Z.V., Iudicone, D., Jahn, O., Guidi, L., Lasbleiz, M., Leblanc, K., Lévy, M., Pondaven, P., 2018. Influence of diatom diversity on the ocean biological carbon pump. Nature Geoscience 11, 27–37. https://doi.org/10.1038/s41561-017-0028-x

Wickham, H., Averick, M., Bryan, J., Chang, W., D'Agostino McGowan, L., François, R., Grolemund, G., Hayes, A., Henry, L., Hester, J., Kuhn, M., Pedersen, T.L., Miller, E., Bache, S.M., Müller, K., Ooms, J., Robinson, D., Seidel, D.P., Spinu, V., Takahashi, K., Vaughan, D., Wilke, C., Woo, K., Hiroaki, Y., 2019. Welcome to the tidyverse. Journal of Open Source Software 4, 1686. https://doi.org/10.21105/joss.01686

Supplement
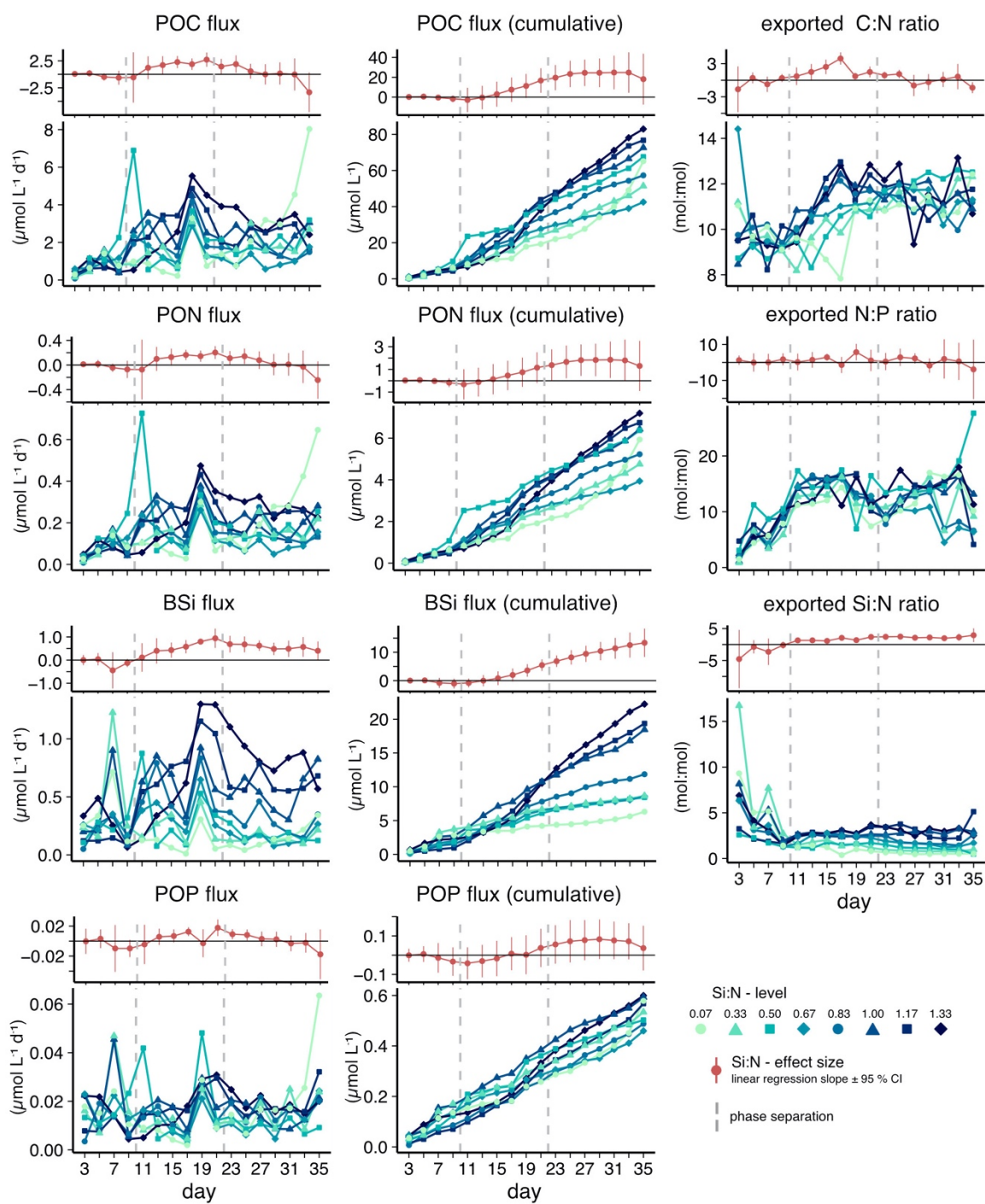
Figure S1. Particulate matter export flux (daily flux, cumulative flux and elemental ratios) and daily Si:N effect sizes.
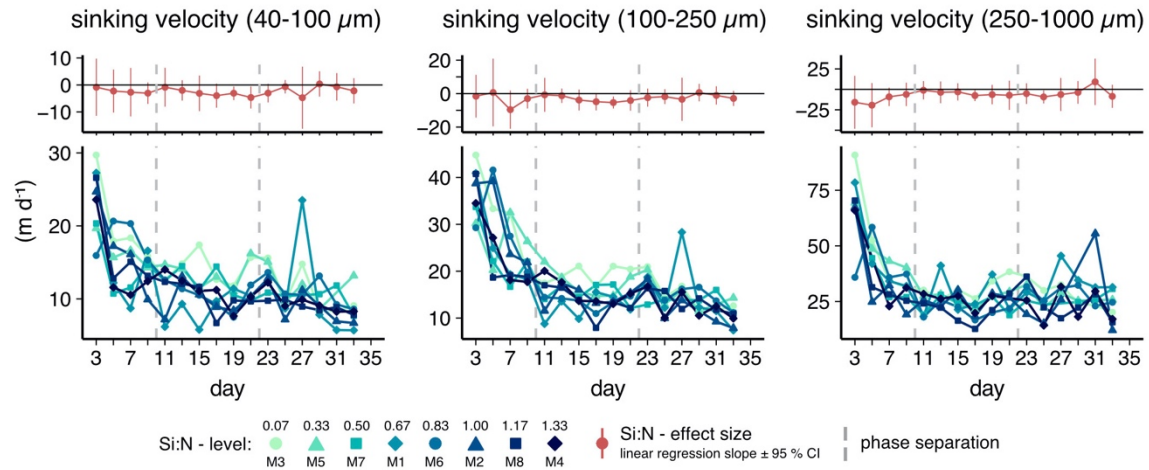
Figure S2. Sinking velocities and daily Si:N effect sizes for different size fractions of the 40–1000 μm size spectrum.

Response variable	Fixed effect	MS	df$_{Num}$	df$_{Den}$	F-value	p-value	R²$_{marginal}$
a) Particulate organic carbon flux (POC)	Si:N	3.676	1	6	3.6	0.1064	0.43
	Day	4.041	12	72	3.96	0.0001	
	Si:N × Day	3.254	12	72	3.19	**0.0011**	
b) Particulate organic nitrogen flux (PON)	Si:N	0.026	1	6	2.83	0.1434	0.375
	Day	0.026	12	72	2.9	0.0025	
	Si:N × Day	0.019	12	72	2.11	**0.0269**	
c) Biogenic silica flux (BSi)	Si:N	1.933	1	6	69.67	0.0002	0.692
	Day	0.043	12	72	1.54	0.1291	
	Si:N × Day	0.055	12	72	1.99	**0.0373**	
d) Particulate organic phosphorus flux (POP)	Si:N	0	1	6	2.15	0.1932	0.483
	Day	0	12	72	4.74	<0.0001	
	Si:N × Day	0	12	72	2.08	**0.0288**	
e) Particulate inorganic carbon flux (PIC)	Si:N	0.015	1	6	4.35	0.0821	0.693
	Day	0.022	12	72	6.59	**<0.0001**	
	Si:N × Day	0.006	12	72	1.82	0.0609	
f) Exported Si:N ratio	Si:N	25.263	1	6	155.12	<0.0001	0.801
	Day	0.471	12	72	2.89	0.0026	

		MS	df_Num	df_Den	F	p	R²marginal
	Si:N × Day	0.39	12	72	2.39	**0.0115**	
g) Exported C:N ratio	Si:N	12.027	1	78	30.49	<0.0001	0.663
	Day	3.12	12	78	7.91	<0.0001	
	Si:N × Day	2.472	12	78	6.27	**<0.0001**	
h) Exported Si:C ratio	Si:N	0.161	1	6	150.41	<0.0001	0.814
	Day	0.006	12	72	5.62	<0.0001	
	Si:N × Day	0.004	12	72	3.59	**0.0003**	
i) Exported N:P ratio	Si:N	4.803	1	6	0.49	0.5106	0.229
	Day	10.832	12	72	1.1	0.3715	
	Si:N × Day	7.555	12	72	0.77	0.6795	
j) Exported PIC:POC (rain) ratio	Si:N	0	1	6	0.92	0.3747	0.692
	Day	0.003	12	72	4.97	**<0.0001**	
	Si:N × Day	0	12	72	0.62	0.8176	
k) BSi fraction of total flux	Si:N	0.138	1	6	131.31	<0.0001	0.846
	Day	0.006	12	72	8.5	<0.0001	
	Si:N × Day	0.009	12	72	5.46	**<0.0001**	

MS: mean squares; df_{Num} and df_{Den}: numerator and denominator degrees of freedom; $R^2_{marginal}$: proportion of variation explained by all fixed effects

Table S1. Linear mixed models showing the effects of artificial upwelling on particulate matter flux and stoichiometries. Si:N, Day (day 11–33) and Si:N × Day were deployed as fixed effects and Mesocosm as random effect. Significant fixed effects to be interpreted are displayed in bold.

Response variable	Fixed effect	MS	df_{Num}	df_{Den}	F-value	p-value	$R^2_{marginal}$
a) Sinking velocity (fastest 10 % of particles)	**Si:N**	2011.613	1	69	45.03	**<0.0001**	0.628
	Day	215.873	11	69	4.83	**<0.0001**	
	Si:N × Day	64.594	11	69	1.45	0.1728	
b) Sinking velocity (40–100 μm size fraction)	**Si:N**	72.263	1	6	12.25	**0.0131**	0.392
	Day	11.177	11	63	1.9	0.0567	
	Si:N × Day	3.406	11	63	0.58	0.8399	
c) Sinking velocity (100–250 μm size fraction)	**Si:N**	101.653	1	69	11.68	**0.0011**	0.398
	Day	12.206	11	69	1.4	0.1919	
	Si:N × Day	4.066	11	69	0.47	0.9173	
d) Sinking velocity (250–1000 μm size fraction)	Si:N	222.494	1	6	5.61	0.0534	0.301
	Day	20.888	11	63	0.53	0.8781	
	Si:N × Day	27.532	11	63	0.69	0.7391	
e) Carbon-specific remineralization rate	Si:N	0.008	1	36	1.37	0.249	0.447
	Day	0.011	5	36	1.87	0.1242	
	Si:N × Day	0.001	5	36	0.24	0.9424	
f) Sinking velocity (fastest 10 % of particles)	**exported Si:N ratio**	1437.807	1	9	33.9	**0.0002**	0.633
	Day	223.136	11	65	5.26	**<0.0001**	
	exported Si:N ratio × Day	80.847	11	65	1.91	0.0547	
g) Sinking velocity (40–100 μm size fraction)	**exported Si:N ratio**	112.339	1	69	20.43	**<0.0001**	0.435
	Day	14.105	11	69	2.57	**0.0087**	
	exported Si:N ratio × Day	4.821	11	69	0.88	0.5664	
h) Sinking velocity (100–250 μm size fraction)	**exported Si:N ratio**	146.11	1	69	18.35	**<0.0001**	0.442
	Day	16.789	11	69	2.11	**0.0309**	
	exported Si:N ratio × Day	6.395	11	69	0.8	0.6367	

i) Sinking velocity (250–1000 µm size fraction)	exported Si:N ratio	116.466	1	10	3.32	0.0976	0.349
	Day	29.585	11	64	0.84	0.5989	
	exported Si:N ratio × Day	49.29	11	64	1.4	0.1931	

MS: mean squares; df_{Num} and df_{Den}: numerator and denominator degrees of freedom; $R^2_{marginal}$: proportion of variation explained by all fixed effects

Table S2. (**a**)–(**e**): Linear mixed models showing the effects of artificial upwelling on sinking velocities and carbon-specific remineralization rate. (**f**)–(**i**): Linear mixed models showing the relationship between sinking velocities and the Si:N ratio of the particulate export flux (BSi:PON). Si:N (or exported Si:N ratio for (**f**)–(**i**)), Day (day 11–33) and Si:N × Day were deployed as fixed effects and Mesocosm as random effect. Significant fixed effects to be interpreted are displayed in bold.

5   Synthesis

5.1 Carbon export under natural and artificial upwelling

This doctoral thesis compiles data of the effects of both natural (Chapter 3) and artificial (Chapters 2 and 4) upwelling on the efficiency of the biological carbon pump. In this section I describe some of the theoretical similarities and differences between the two systems and compare the export data collected in the natural Peruvian upwelling system with the results from the artificial upwelling studies carried out in the Canaries.

Artificial upwelling mimics the mechanism that drives primary productivity in natural upwelling systems. Nutrients in the upwelled deep water stimulate phytoplankton growth when they reach the euphotic zone. Artificial upwelling offers the possibility to control the amount of upwelled water and the mode with which it is translocated – within the given technical restrictions. In wind-driven coastal upwelling systems, the wind stress along the shore controls the amount of upwelled deep water and thus the input of new nutrients to the surface layer (Kämpf and Chapman, 2016). Temporal variability in wind stress on the time scales of days to seasons causes relatively variable upwelling conditions. Intermediate wind speeds, which cause enough upwelling but not too much turbulence, maximize primary production rates (Ware and Thomson, 1991). The upwelling conditions in natural upwelling systems are thus a lot less stable than they could potentially be under artificial upwelling. The increase in primary productivity during our Gran Canaria 2018 study was comparable to maximum primary production rates in Eastern Boundary Upwelling Systems (EBUS). Kämpf and Chapman report theoretical maximum primary production rates in EBUS of more than 3 g C m^{-2} d^{-1} (2016). Under recurring upwelling, we measured maximum primary production rates of more than 2 g C m^{-2} d^{-1} and more than 4.5 g C m^{-2} d^{-1} under singular upwelling (Ortiz et al., 2022). The resulting potential for export production under artificial upwelling is thus comparable to the major natural upwelling systems.

Our measured export fluxes under natural upwelling (Chapter 3) were substantially lower than the fluxes in our artificial upwelling studies (Chapters 2 and 4). This is somewhat surprising, as the chlorophyll *a* concentrations were comparable for most of the experimental duration. Additionally, in contrast to natural upwelling, artificial upwelling led to enhanced C:N ratios of exported particulate matter. To understand what the causes for these differences might have been, one needs to look at the different phytoplankton community successions. In Peru, the community was already upwelling-adapted and in the phase of shifting from diatom- to dinoflagellate-dominance. The relatively small pulse of upwelled nutrients did nothing but stall this succession for a few days. While dinoflagellates dominated, suspended matter C:N ratios increased. However, they remained suspended in the water column until the end of the experiment, which is why neither the stoichiometry shift nor their captured carbon was transferred to the sediment trap (Bach et al., 2020). In the oligotrophic Canary Island system on the other hand, upwelling led to a shift from picophytoplankton adapted to nutrient limitation and high light intensities to diatom-dominated micro- and nanophytoplankton specialized on capitalizing on new nutrients and high growth rates (Ortiz et al., 2022). The initial conditions in the subtropical waters off of Gran Canaria were very different from the conditions under the upwelling treatment. In contrast, the disturbance in the Peruvian system

was not that large and the adjustments to the new conditions were not that severe. Consequently, the grazing community was perhaps more capable of keeping the phytoplankton community in check in Peru, whereas the zooplankton under artificial upwelling did not have enough time to catch up with the much faster phytoplankton growth. Both the mismatch scenario in the Canary Island region as well as the persistence of dinoflagellates in the water column of the Peruvian system might have resulted in higher export rates under artificial compared to natural upwelling.

Although the stimulation mechanism of artificial and natural coastal upwelling is the same, they differ from each other when it comes to carbon export. When applying artificial upwelling for the sake of carbon dioxide removal (CDR), a location in the open ocean is favorable, where exported carbon can be sequestered in the deep ocean interior. Eastern Boundary Upwelling Systems (EBUS) are located along coasts, often above comparably shallow shelfs, which is not ideal for carbon sequestration. Additionally, in these systems POC is often exported to water layers, which are soon to be upwelled. Hence, the remineralized DIC may end up at the surface again rather soon. However, the vertical off-shore transport of coastal water masses can cause suspended POC to sink to the deep ocean at the shelf break (Hales et al., 2006). Furthermore, high amounts of exported biomass in the sub-surface, together with slow ventilation create oxygen-depleted sub-surface waters in EBUS (Karthäuser et al., 2021). These hamper remineralization and thus make particle export more efficient (Weber and Bianchi, 2020). This feature of subsurface oxygen minimum zones would likely not occur when applying artificial upwelling in the open ocean, because of less constricted ventilation of sub-surface waters. Artificial and natural upwelling systems are thus only to some extent comparable in terms of carbon sequestration.

5.2   Artificial upwelling and the biological carbon pump

The main scope of this doctoral thesis was to assess the effects that artificial upwelling has on the functioning of the biological carbon pump. In Chapter 2 I described the effects that the upwelling intensity and mode had on export related parameters during the Gran Canaria 2018 mesocosm campaign. In Chapter 4 I presented results from the Gran Canaria 2019 experiment, in which the effect of different Si:N ratios were tested. Overall, artificial upwelling increased the surface carbon flux while it negatively affected the efficiency with which organic matter is transferred from the surface to the ocean interior (**Table 5.2**).

We found that the absolute amount of N added as upwelled deep water caused an increase in suspended and exported C:N ratios. Average POC fluxes in response to artificial upwelling increased 3–4-fold compared to pre-upwelling conditions. At the same time, upwelling intensity increased sinking matter degradation rates and decreased particle sinking velocities. As a result, the remineralization length scale (RLS) as a proxy for POC flux attenuation decreased more than 2-fold. The temporal mode of upwelling also had counteracting effects on export related parameters. A singular pulse of upwelling increased the C:N ratio of exported matter while it simultaneously enhanced particle porosities and thereby decreased sinking velocities compared to the control treatment. Under recurring upwelling we observed no such changes. The Si:N ratio of artificially upwelled water had similar effects on particle export as

upwelling intensity. Across the Si:N gradient, the POC flux increased 3-fold while the RLS decreased more than 2-fold. However, these effects lasted only while the community adjusted to the upwelling treatment and faded over time.

Artificial upwelling

		Intensity	**Mode**		**Si:N ratio** (recurring, high intensity)	
			singular	recurring	short term	long term
Biological Carbon Pump	**C flux magnitude**	**+** higher POC export and exported C:N ratios	**+** higher exported C:N ratios	**o**	**+** higher POC export and exported C:N ratios	**o**
	transfer efficiency	**—** faster degradation of sinking matter and lower sinking velocities	**—** lower sinking velocities	**o**	**—** lower sinking velocities	**o** increased BSi ballast, unaltered sinking velocities

+ / — / o : positive / negative / no effect on strength/efficiency of biological carbon pump

Table 5.2. Effects of artificial upwelling intensity, upwelling mode and upwelled Si:N ratio on export-related parameters. The first column (Intensity) shows insights from the Gran Canaria 2018 and 2019 experiments (comparison of pre-treatment with treatment conditions).

The increasing POC fluxes and changes in particle characteristics were mainly associated with changes in the phytoplankton community. The grazer communities were not able to catch up with the phytoplankton growth in either experiment and hence likely had a limited influence on sinking particle characteristics. Generally, upwelling stimulated primary productivity and induced a shift from the oligotrophic baseline community to diatom-based communities. The upwelled Si relative to N thereby controlled the relative amount of silicon and carbon that the diatoms incorporated into organic matter per mol of nitrogen. The enhanced productivity was mainly controlled by upwelling intensity and led to stronger fluxes of organic matter to the sediment traps. When diatoms ran into nutrient limitation, they produced more carbon-rich organic matter (and likely TEP), leading to increased C:N ratios of suspended and exported particles. At the same time, the exported material was relatively fresh and porous, which was probably the reason for its quick degradation and slow sinking.

5.2.1 The importance of sinking matter elemental ratios

The fact that artificial upwelling led to enhanced C:N ratios of produced and sinking organic matter is crucial. In fact, a high ratio of carbon to limiting nutrient in the exported material is a prerequisite for artificial upwelling to achieve net CDR via the biological carbon pump. Upwelled deep water transports dissolved inorganic carbon (DIC) and associated nutrients (nitrate, phosphate and silicic acid) from a certain upwelling depth to the surface. This upwelling depth needs to be deeper than the maximum mixed layer depth at the given location, to bring up nutrients that would otherwise be locked away in the deep ocean. When transferring this water to the surface, the difference between the DIC and nutrient

concentrations in the surface compared to the upwelled deep water are defined as excess DIC and nutrients. This excess DIC would lead to increasing seawater pCO_2 and thus a loss of carbon via air-sea gas exchange. Thus, in order to achieve CDR, the uptake of carbon and its subsequent export to the upwelling depth needs to exceed the upwelled excess DIC. The upwelled nutrients are new nutrients and thus fuel new production. Usually, the surface ocean is N-depleted and hence, excess nitrate equals the total new nitrate. Assuming that new production equals export production (as proposed by Eppley and Peterson, 1979), the upwelled nutrients will completely be exported from the surface ocean. They might be cycled for days, weeks or even months above the permanent pycnocline, but will eventually be exported. If nitrogen constitutes the limiting nutrient in the surface, the C:N ratio of the exported particulate matter at the depth of upwelling needs to surpass the C:N ratio of excess nutrients in the upwelled water in order for net C sequestration to occur. In this case, more carbon is associated to the sequestered compared to the upwelled nitrogen, resulting in atmospheric CO_2 influx to the ocean (see **Fig. 5.2.1**).
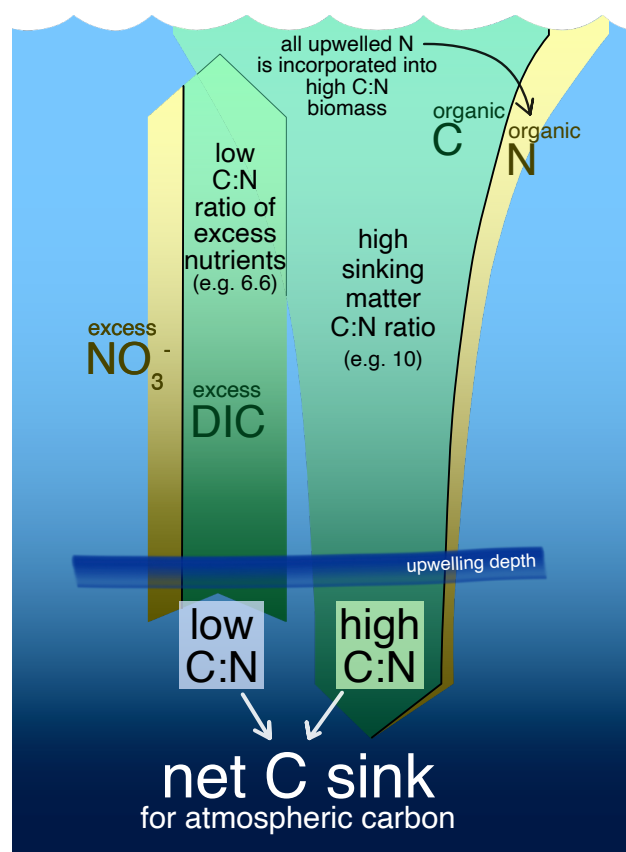
Figure 5.2.1. Importance of C:N ratios for net carbon sequestration. In this upwelling scenario, the exported organic matter C:N ratio is higher than the upwelled excess C:N ratio, which causes a net carbon sink.

The C:N ratio of sinking matter becomes a less determining factor when the upwelled water contains so called "preformed nutrients". These are nutrients that were biologically not utilized, but instead transported from the surface to the ocean interior through deep water formation (Marinov et al., 2006). Since they were not incorporated into organic matter, they do not have a biotic carbon counterpart. Hence, the incorporation of preformed nutrients into

sinking biomass would increase the biological carbon pump without the need to overcompensate for upwelled excess DIC. Preformed nutrients are mainly distributed via the formation of deep and intermediate waters in the Southern Ocean. Since the North Atlantic deep water formation supplies relatively little amounts of preformed nutrients, the upper 1000 m in the subtropical North Atlantic are scarce in preformed nutrients (Primeau et al., 2013). In the region of the Canary Islands, in which we carried out our artificial upwelling experiments, they do thus not play a major role. The enhanced sinking matter C:N ratios under artificial upwelling are hence especially important when the upwelled nutrients are not preformed but remineralized. In this case, elevated ratios are necessary to allow for net carbon drawdown – if the C:N ratio of exported matter at the upwelling depth is still high enough (i.e. exceeding the excess $DIC:NO_3^-$ ratio of upwelled water).

By increasing exported matter C:N ratios, artificial upwelling thus fulfilled the prerequisite that is required for net carbon drawdown via the biological pump. In addition, it strengthened the vertical POC flux from the surface. However, it simultaneously hampered the POC transfer efficiency through less favorable particle characteristics, meaning that potentially most of the organic carbon might be recycled in the surface ocean. The question arises, what these counteracting effects imply for the long-term carbon sequestration potential of artificial upwelling. Would the exported organic matter with its elevated C:N ratios make it to the deep sea, or would it be degraded before it reaches a meaningful sequestration depth?

5.3 Carbon sequestration potential of artificial upwelling

5.3.1 POC flux magnitude and C:N composition versus transfer efficiency

In order to answer the question which is more important for long-term carbon sequestration potential, the magnitude and stoichiometry of the initial sinking flux or the transfer efficiency, I calculated POC fluxes to depth under different surface export and flux attenuation scenarios. A simplistic one-dimensional water column model described in detail by Bach et al. (2016) was used to calculate POC flux profiles to up to 1000 m depth.

$$POC_z = POC_{z-1} - \left(POC_{z-1} * \frac{C_{model}}{SV_{model}} * (z - (z-1)) \right) \qquad (5.1)$$

POC_z is the POC flux (μmol L^{-1} d^{-1}) at depth z (m), C_{model} the temperature-dependent remineralization rate (d^{-1}) and SV_{model} the depth-dependent sinking velocity (m d^{-1}). C_{model} and SV_{model} parameterizations were adapted from the University of Victoria model by Schmittner et al. (2008). C_{model} was parameterized to decrease with depth due to decreasing temperatures according to

$$C_{model} = \frac{C}{e^{(0.0639*\Delta T)}} \qquad (5.2)$$

where C is the carbon-specific remineralization rate (d^{-1}) and ΔT the temperature difference (° C) between our measurements and the *in situ* temperature at depth z. The exponential function of the scaling factor 0.0639 corresponds to a Schmittner's b_{bio} scaling factor of 1.066 (2008) and corresponds to a Q10 value of ~2. The temperature profile originates from a CTD cast

north of Gran Canaria at the European Station for Time-Series in the Ocean (ESTOC, 29.17 N; -15.50 W) during an *RV Poseidon* cruise in March 2019 (POS 533, Quack, 2019). Since the relatively light organic fraction of sinking particles is assumed to be preferably degraded with depth (Berelson, 2001) and the average size of particles usually tends to increase with depth, sinking velocity was parameterized to slightly increase with depth.

$$SV_{model} = 0.04 * z + SV \qquad (5.3)$$

C_{model} and SV_{model} were estimated using sinking velocities and remineralization rates measured during the Gran Canaria 2018 and 2019 mesocosm campaigns reported in Chapters 2 and 4.

I carried out two sensitivity analyses for the synthesis of this doctoral thesis, in each of which I modeled POC fluxes to up to 1000 m depth under different scenarios for export flux from the surface. Essentially, the influence of the flux magnitude from the surface, the C:N ratio of the flux, and the transfer efficiency (given as RLS) were tested as drivers for POC fluxes to different depth horizons (representing different timescales of carbon sequestration).

Magnitude of export flux vs. RLS

For the first sensitivity analysis, I compared how the magnitude of export flux from the surface and RLS control POC fluxes at different depths. As pointed out earlier, artificial upwelling increased the surface POC flux, while it simultaneously decreased the transfer efficiency, i.e. the RLS, compared to the control scenario (see Section 5.2). The POC fluxes to 100, 500 and 1000 m depth are shown for different export conditions in **Fig. 5.3.1 a–c**. The contour lines were computed with the one-dimensional flux model for a range of RLS and POC fluxes from the surface layer, and calculating the remaining POC flux for the given depths. The data points in the graph depict the export observations during the Gran Canaria 2018 and 2019 mesocosm campaigns. Shown are the mean (± SD) values of the pooled singular and recurring upwelling treatments (red and blue, four mesocosms each), the experimental control from 2018 (grey, i.e. no upwelling) and the gradient of Si:N upwelling treatments (turquoise to dark blue: low to high Si:N).

The higher POC surface flux under artificial upwelling causes substantially higher POC fluxes at 100 m depth compared to the control, especially in the high Si:N treatments (**Fig. 5.3.1a**). At this depth, the surface POC flux is the more important factor compared to RLS, which is illustrated by the horizontal orientation of the contour lines. With depth, RLS becomes gradually more important and the orientation of the contour lines shifts. At 500 m depth, most of the Gran Canaria 2019 Si:N treatments result in lower POC fluxes than the control scenario, while the singular and especially the recurring upwelling treatments export considerably more carbon to depth than the control (**Fig. 5.3.1b**). At 1000 m depth the observed trends amplify. Transfer efficiency becomes more influential while the surface POC flux further loses significance. The singular and recurring upwelling modes transport the highest amounts of POC to this depth, followed by the control scenario. The 2019 Si:N treatments export the least amount of carbon to the deep ocean (**Fig. 5.3.1c**).

The low transfer efficiency in the Si:N treatments is driven by high degradation rates and low sinking velocities in response to artificial upwelling. For comparison: the average degradation and sinking rates across the Gran Canaria 2018 upwelling treatments were 0.119 ± 0.041 d^{-1}

and 53.5 $\pm$ 14.4 m d^{-1} (days 11 to 29), respectively, while they were 0.228 $\pm$ 0.094 d^{-1} and 32.8 $\pm$ 10.4 m d^{-1} (mean $\pm$ SD, days 11 to 35) across all Si:N treatments for Gran Canaria 2019. Sinking matter in the 2019 Si:N treatments was thus degraded ~1.9-fold faster and sank ~0.6-fold slower than in the 2018 upwelling treatments. One reason for this might be differences in the realized upwelling intensity. While the Si:N treatments exclusively experienced extreme upwelling intensities, the 2018 singular and recurring upwelling modes incorporate a gradient of low to extreme intensities. Since RLS decreases with upwelling intensity (see Section 5.2), the consistently extreme upwelling intensities in 2019 could explain the lower RLS. However, sinking and degradation rates already differed between the two experiments before the upwelling treatments started to affect export production, albeit less strongly (~1.5-fold higher degradation rates and ~0.9-fold lower sinking velocities in the Si:N treatments). An explanation for this could be that the 2019 mesocosms enclosed a shallower and thus much smaller water parcel than the ones used in 2018. Therefore, the exported matter in 2019 might have been generally fresher and easier degradable than in 2018.

C:N composition of export flux vs. RLS

Artificial upwelling also resulted in carbon-enriched sinking matter, which should theoretically be beneficial for increasing the carbon sequestration potential. The relative influence of artificial upwelling effects on the C:N ratio and RLS was assessed by comparing computed one-dimensional vertical carbon flux profiles with different RLS and surface C:N to a baseline scenario (C:N and RLS of the control scenario). For the baseline, the assumption is that a given amount of N input is completely taken up and converted to export flux from the surface, with the baseline C:N and RLS corresponding to that of control conditions. Contour lines for Fig. **5.3.1 d–f** were computed with the one-dimensional flux model for a range of RLS and C:N ratios of flux from the surface layer (for a fixed amount of N input), and calculating the remaining POC flux for the given depths. The C:N ratios in our control scenario (8.56 $\pm$ 0.65) were well in range of reported suspended matter C:N ratios from the Eastern North Atlantic (~9, Martiny et al., 2013), while organic matter was more carbon-rich in all upwelling treatments. Accordingly, these higher C:N ratios of the exported POM result in a higher magnitude of carbon export. For the present sensitivity analysis, I assumed RLS to be identical for C and N (i.e. no change in C:N with depth).

The analysis shows that deep POC fluxes become less dependent on exported C:N ratios with increasing depth, while the importance of RLS increases (**Fig. 5.3.1e–f**). Notably, the transfer efficiency plays a much more important role than the C:N ratio. Already at 100 m depth, the control (with lowest C:N) exports more POC than most Si:N treatments, and no upwelling scenario with high C:N transports more POC to 1000 m depth than the control. This is because the range of C:N ratios was narrower than the range of POC surface fluxes in the previous analysis, while the RLS range remained the same (C:N: 8.5–11.5, i.e. ~1.4-fold; surface POC flux: 1–3 μmol L^{-1} d^{-1}, i.e. 3-fold). Elevated C:N ratios do thus not necessarily lead to higher POC deep export, if flux attenuation increases simultaneously.
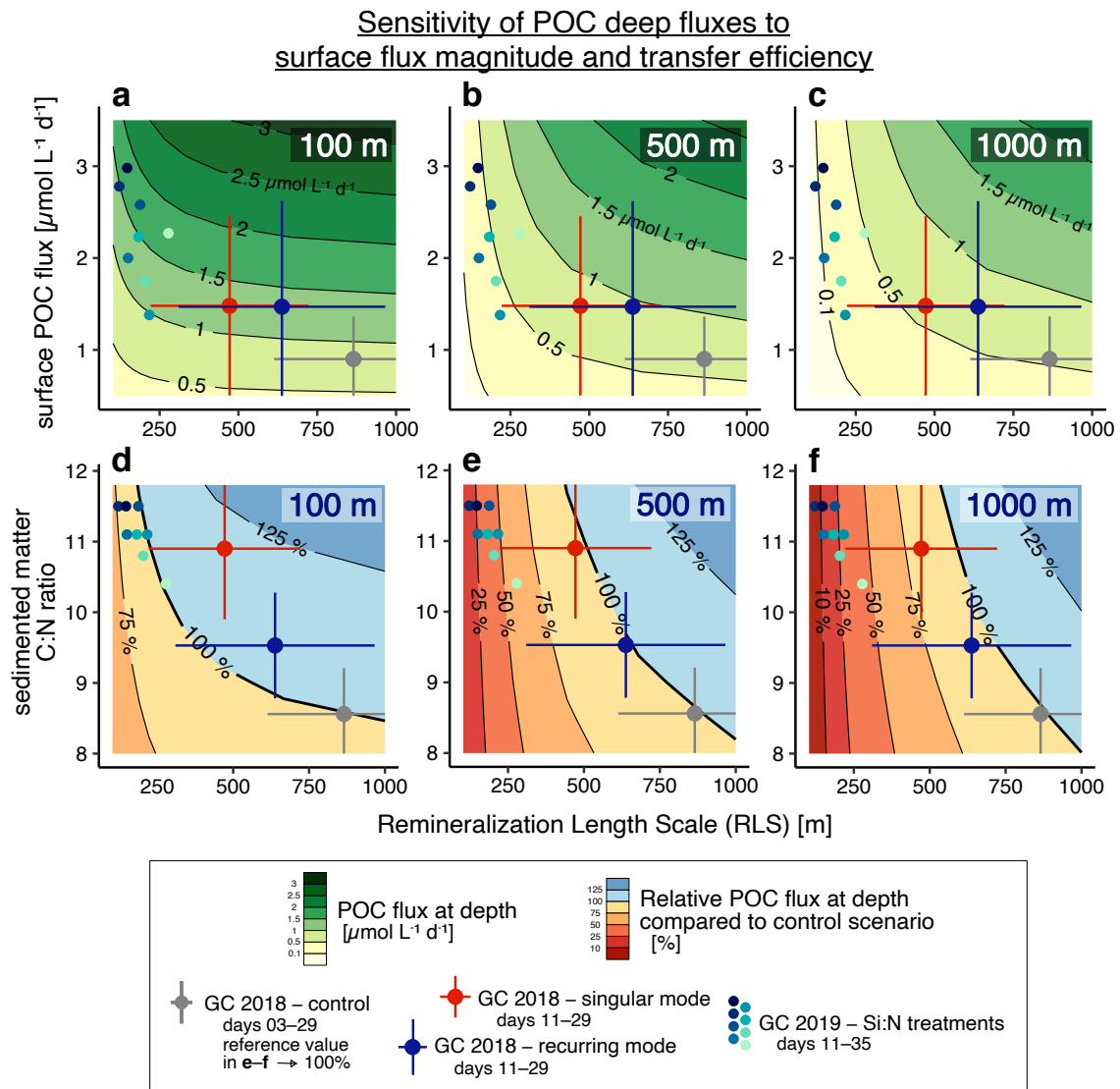
Figure 5.3.1. Sensitivity of POC fluxes at 100, 500 and 1000 m depth to surface flux magnitude and transfer efficiency. Shown are a range of combinations of remineralization length scales (RLS) with surface POC fluxes (**a**)–(**c**) and surface flux C:N ratios (**d**)–(**f**). The contour lines in (**d**)–(**f**) depict the relative POC flux compared to the control scenario (grey, baseline C:N and RLS). The data points in the graph depict the export observations during the Gran Canaria 2018 and 2019 mesocosm campaigns. Shown are the mean (± SD) values of the pooled singular and recurring upwelling treatments (red and blue, four mesocosms each), the experimental control from 2018 (grey, i.e. no upwelling) and the gradient of Si:N upwelling treatments (turquoise to dark blue: low to high Si:N). The point ranges depict mean values across time (and mesocosms, in respect of the singular and recurring scenarios) ± standard deviation (SD).

Implications for artificial upwelling as a negative emission technology

In summary, the results of the sensitivity analyses indicate that the decreased transfer efficiency under artificial upwelling counteracts the positive effect of surface flux magnitude and increased C:N ratios. Which of the drivers dominates (POC surface flux, C:N composition or RLS), depends on the depth. While flux magnitude and C:N are more important in the surface ocean, flux attenuation becomes increasingly important towards the deep ocean. The importance of RLS might be further amplified by the increase of sub-surface temperatures as

a response to upwelling. When applied in global models, artificial upwelling causes temperature increases in the sub-surface waters below 100 m (Oschlies et al., 2010). This might increase the sub-surface remineralization and thus further enhance the importance of RLS.

The fact that the POC flux to the deep ocean might ultimately be equal or higher in the control scenario compared to some of the artificial upwelling scenarios (**Fig. 5.3.1**) does not mean, that in those cases artificial upwelling would not be able to achieve CDR. Instead, it shows that most of the additional exported matter would be recycled in the surface ocean. We do not know, when or in which form this biomass (built-up from upwelled nutrients) would finally reach the upwelling depth. But if this biomass contained more carbon than the amount of initially upwelled excess DIC, this carbon would be stored somewhere between the surface layer and the upwelling depth. Hence, artificial upwelling would temporarily still act as a net carbon sink.

The flux attenuation models suggest that high upwelling intensities might be useful in areas where the sequestration depth does not need to be very deep in order to sequester carbon on meaningful time scales. Low upwelling intensities leading to lower flux attenuation might be more beneficial in areas where the organic matter needs to be exported rather deep in order to achieve sufficient sequestration times. This trade-off between enhancing the carbon flux magnitude and altering its sinking particle properties needs to be considered for the application of artificial upwelling. Changing the nutrient stoichiometry in artificially upwelled water seems to lead to a similar trade-off. Si:N ratios temporarily correlated positively with POC export and C:N ratios and negatively with sinking velocities. This mutual exclusiveness of increased flux magnitude and efficient transfer to depth seemed to cease after the initial adjustment phase. It might thus not be of great importance when applying artificial upwelling in a recurring manner by fertilizing the same water patch over time scales of weeks to months. A recurring form of upwelling seems to be generally more useful for sequestering carbon in the deep ocean than a singular upwelling pulse. Although singular upwelling causes considerably higher sinking matter C:N ratios, recurring upwelling transported slightly more carbon to depth due to its more efficient POC transfer.

5.3.2 The role of sequestration times

The CDR permanence of artificial upwelling depends on the sequestration time of the exported carbon, i.e. the time the carbon remains locked inside in the oceans' interior. Ocean circulation and mixing of water masses transports exported carbon back to the surface, where it re-equilibrates with the atmosphere and leaks out as CO_2 (Orr et al., 2001). Sequestration times can vary between a few years or decades to up to a millennium and mainly depend on the injection depth and the location of POC export (Siegel et al., 2021).

The injection depth, i.e. the depth, at which exported POC gets remineralized, has a strong influence on the sequestration time. Generally, sequestration times for organic matter exported to 500 m depth and shallower are quite short, i.e. <50 years (Siegel et al., 2021). This indicates that the RLS might be more important than the surface POC flux for permanent carbon sequestration. The injection depth is, however, location-specific. Siegel et al. (2021) tested two contrasting locations, one in the sub-Arctic North Pacific and the station BATS in the subtropical North Atlantic. A POC injection depth of 1000 m led to sequestration times of

~400 years at the Pacific site compared to ~30 years at BATS. At an injection depth of 1500 m, sequestration times increased to multi-centennial scales at both sites. Consequently, the upwelling location needs to be chosen carefully, as efficient carbon sequestration to 1000 m depth does not guarantee long-term CO_2 sequestration. The problem of CO_2 leakage could be mitigated by directly sinking the organic biomass. This would circumvent the biological carbon pump as relatively inefficient transport pathway. The combined approach of artificial upwelling and cultivation of macroalgae with direct sinking is one such approach (Wu et al., 2022), which could lead to sequestration times in the order of millennia.

Optimizing the carbon sequestration potential

How can one maximize the carbon sequestration potential of artificial upwelling? What is the ideal upwelling strategy for achieving the maximum CO_2 sequestration? This thesis has provided some insight into the mechanisms that play a role when answering these questions. By extrapolating the experimentally measured POC fluxes to depth, I was able to show that changes occurring in the relimeranization length scale become more important with depth than changes in surface POC fluxes. The need for high transfer efficiencies in order to achieve efficient CDR is highlighted by the short sequestration times at shallow POC injection depths (<500 m). This suggests that forms of upwelling, which imply relatively efficient carbon transfer, are needed to achieve the maximum net carbon sequestration. Our empirical data suggests that, in order to achieve the highest possible transfer efficiency (i.e. RLS), a recurring mode of upwelling, low to medium upwelling intensities and deep water Si:N ratios not above 1:1 are favorable. Furthermore, locations characterized by long sequestration times at relatively shallow injection depths are useful to achieve longer CDR permanence. Tropical regions offer such conditions, especially in the Eastern Pacific and Indian Ocean. In the eastern tropical Pacific, for example, sequestration times of carbon exported to 500 m depth lie within 100–150 years (Siegel et al., 2021). Such sequestration times could help to mitigate climate change by buying more time to reduce anthropogenic emissions and actively sequester atmospheric carbon in long-term reservoirs.

5.4   Difficulties assessing artificial upwelling CDR

When trying to assess the carbon dioxide removal of artificial upwelling in an open ocean scenario, the vast temporal and spatial scales, in which the biological carbon pump operates, become a problem. As pointed out above, one important requirement to accurately assess the net CDR of artificial upwelling would be monitoring the sinking matter carbon to nutrient ratios at the depth from which deep water was originally upwelled. The difficulty is following that particle flux in the open ocean. First of all, the produced organic matter might not readily sink out, but instead be trapped in the surface mixed layer for time scales of multiple weeks (see Chapter 2) or even months. Secondly, by the time the produced particles sink, they might have laterally moved away from the area where the nutrients were artificially upwelled, making them harder to follow and to relate them to the artificial upwelling site. They might also have been dispersed through mixing with surrounding water masses, further enlarging the area that needs to be observed. Finally, subsurface ocean currents will cause horizontal drifting of sinking matter, potentially moving it further away from the upwelling site. On top of that,

organic matter can not only reach depth via gravitational sinking, but also via other "particle injection pumps" (Boyd et al., 2019). These come with their own difficulties and add to the complexity of following the organic matter flux originating from a fertilized water parcel in the surface ocean. Precisely assessing, how much CDR is achieved with artificial upwelling, thus requires rigorous observational effort.

In order to cope with the problem of monitoring our oceans in four dimensions – three in space and one in time –, one has to follow the organic matter flux into the ocean interior. This could be achieved by combining multiple oceanographic observational tools, such as biogeochemical ARGO floats or gliders, moorings equipped with sensors and/or neutrally buoyant sediment traps. This, however, would be costly, require lots of manpower and would thus be ineffective to do on a regular basis, e.g. while employing upwelling devices as means of generating negative carbon emissions on the time scale of years and decades. The impracticability of following carbon fluxes to the deep ocean thus represents a major problem for CDR crediting (National Academies of Sciences, Engineering, and Medicine, 2021), as it will not be feasible for companies to regularly and reliably assess the accurate carbon sequestration achieved by their artificial upwelling devices. This problem could be tackled by carrying out sophisticated open-ocean experiments, which accurately assess POC fluxes and flux attenuation with depth resulting from artificial upwelling. These case studies could act as a guideline. They could inform about the CDR potential of artificial upwelling under certain circumstances (oceanic region, upwelling intensity, mode, depth, etc.) and enable a better evaluation of case-specific artificial upwelling scenarios, e.g. by later on feeding the collected data into models for CDR crediting.

5.5 Next steps in artificial upwelling research

The findings of this doctoral thesis suggest three important next steps of future research concerning the carbon dioxide removal potential of artificial upwelling. First of all, longer experimental durations are needed in order to study long-term adjustments of plankton communities to artificial upwelling. Secondly, open ocean trials are needed that incorporate close monitoring of the changes related to the biological carbon pump. Thirdly, modeling approaches need to incorporate experimental findings into global ocean models in order to test their relevance and to extrapolate the resulting changes to the earth system.

5.5.1 Long-term studies

There were indications that the upwelling durations of 5–6 weeks in our experiments described in Chapters 2 and 4 were not long enough to allow for match conditions between predator and prey. The zooplankton was not able to catch up with the enhanced phytoplankton growth and large amounts of produced organic matter were retained in the water column as suspended matter in both experiments. Apparently, shifting an oligotrophic to a meso- or eutrophic system requires more than a month to allow for the food web and particle export to properly adapt to the altered conditions, especially if the community is diluted with deep water. Seasonal experimental durations (3–6 months) seem to be necessary to study the long-term adaptions of the surface community to artificial upwelling and to reliably assess the resulting export

efficiency (export production over primary production). This would also allow for a more accurate modeling of POC fluxes and could answer the question if enhanced sinking matter C:N ratios would remain elevated in the long-term, or if this is a temporarily occurring effect.

5.5.2 Open ocean trials

This thesis incorporates findings of the effects of artificial upwelling on the POC export flux and other export-related parameters. However, our experiments were restricted to the very surface ocean. In order to assess the CO_2 sequestration potential of artificial upwelling more realistically, open ocean trials are needed. These would allow for measurements of the export flux at the depths necessary for a proper CDR assessment. They would also diminish experimental artifacts, such as the lack of migrating zooplankton, the exclusion of large pelagic organisms and restricted vertical mixing of water masses.

Open ocean trials will require sophisticated POC flux monitoring in order to assess the CO_2 removal potential via the biological carbon pump (National Academies of Sciences, Engineering, and Medicine, 2021). First of all, one would need to track the water masses on which upwelled waters had an imprint. Tracers could be mixed into the upwelled water, which allow for the pursue of upwelled nutrients. Other than that, one could try to contain the upwelled water in a relatively confined horizontal space, e.g. by placing an upwelling device inside an eddy that forms a secluded water parcel in the open ocean (see e.g. Lovecchio et al., 2022). Following and characterizing the community responses in the surface layer would require ship-based operations including water sampling and CTD-casts with high temporal and spatial resolution. Much like the iron fertilization experiments carried out in the 90s and early 2000s (de Baar et al., 2005). Ship-based observations alone would, however, be insufficient to monitor the sinking particle flux. In order to cover a wide and deep section of the water column underneath the fertilized water patch (i.e. hundreds of meters deep and kilometers wide), automatically operating gliders equipped with optical particle flux measurement devices (e.g. biogeochemically equipped ARGO floats) would be inevitable. In addition, neutrally buoyant, free-drifting sediment traps could follow sinking particles within the sub-surface ocean currents and assess the sinking matter C:N ratio (McDonnell et al., 2015), which is needed to assess the net carbon sequestration. Ideally, multiple such experiments would be carried out, covering multiple seasons and oceanographic provinces. The results of such studies could help to inform society and stakeholders about the real potential of artificial upwelling as negative emission technology.

5.5.3 Refining modeling approaches

One of the main findings of this doctoral thesis is that artificial upwelling changes export characteristics in counteracting ways. It enhances the magnitude and C:N ratios of sinking matter and weakens the potential transfer efficiency (via altered sinking velocity and respiration rates). We analyzed the sensitivity of the POC flux to changes in exported matter C:N ratio and changes in RLS in Section 5.3 using a simplistic one-dimensional model. While this exercise provides interesting insights into the relative importance of different controlling factors for carbon flux to the deep ocean, more sophisticated modeling approaches are needed to quantitatively assess the impacts of these findings under different artificial upwelling scenarios. So far, global models testing artificial upwelling have assumed (a) constant

stoichiometries, meaning that only upwelled preformed nutrients can lead to carbon sequestration via the biological pump, and (b) no changes in sinking velocities or particle degradation rates. Future modeling approaches should thus parameterize artificial upwelling to enhance sinking matter carbon to nutrient ratios while at the same time enhancing degradation rates. Implementing such changes of the biological carbon pump in earth system models will likely alter the outcome of previously estimated CDR rates and result in distinct effects on the global carbon cycle and climate-related changes. The consequences of applying artificial upwelling regionally or globally need to be re-assessed in order to refine our knowledge about potential environmental risks and benefits.

In summary, the next steps in artificial upwelling research are thus open ocean trials, ideally with long experimental durations, and refined modelling approaches incorporating current and future insights from empirical studies. This will create a more thorough understanding of how artificial upwelling affects the biological carbon pump and enable a realistic assessment of its CDR potential.

References

Bach, L.T., Boxhammer, T., Larsen, A., Hildebrandt, N., Schulz, K.G., Riebesell, U., 2016. Influence of plankton community structure on the sinking velocity of marine aggregates: Sinking velocity of marine aggregates. Global Biogeochem. Cycles 30, 1145–1165. https://doi.org/10.1002/2016GB005372

Bach, L.T., Paul, A.J., Boxhammer, T., von der Esch, E., Graco, M., Schulz, K.G., Achterberg, E.P., Aguayo, P., Arístegui, J., Ayón, P., Baños, I., Bernales, A., Boegeholz, A.S., Chavez, F., Chavez, G., Chen, S.-M., Doering, K., Filella, A., Fischer, M., Grasse, P., Haunost, M., Hennke, J., Hernández-Hernández, N., Hopwood, M., Igarza, M., Kalter, V., Kittu, L., Kohnert, P., Ledesma, J., Lieberum, C., Lischka, S., Löscher, C., Ludwig, A., Mendoza, U., Meyer, J., Meyer, J., Minutolo, F., Ortiz Cortes, J., Piiparinen, J., Sforna, C., Spilling, K., Sanchez, S., Spisla, C., Sswat, M., Zavala Moreira, M., Riebesell, U., 2020. Factors controlling plankton community production, export flux, and particulate matter stoichiometry in the coastal upwelling system off Peru. Biogeosciences 17, 4831–4852. https://doi.org/10.5194/bg-17-4831-2020

Berelson, W.M., 2001. Particle settling rates increase with depth in the ocean. Deep-sea Research Part Ii-topical Studies in Oceanography. https://doi.org/10.1016/s0967-0645(01)00102-3

Boyd, P.W., Claustre, H., Levy, M., Siegel, D.A., Weber, T., 2019. Multi-faceted particle pumps drive carbon sequestration in the ocean. Nature 568, 327–335. https://doi.org/10.1038/s41586-019-1098-2

de Baar, H.J.W., Boyd, P.W., Coale, K.H., Landry, M.R., Tsuda, A., Assmy, P., Bakker, D.C.E., Bozec, Y., Barber, R.T., Brzezinski, M.A., Buesseler, K.O., Boyé, M., Croot, P.L., Gervais, F., Gorbunov, M.Y., Harrison, P.J., Hiscock, W.T., Laan, P., Lancelot, C., Law, C.S., Levasseur, M., Marchetti, A., Millero, F.J., Nishioka, J., Nojiri, Y., van Oijen, T., Riebesell, U., Rijkenberg, M.J.A., Saito, H., Takeda, S., Timmermans, K.R., Veldhuis, M.J.W., Waite, A.M., Wong, C.-S., 2005. Synthesis of iron fertilization experiments: From the Iron Age in the Age of Enlightenment. J. Geophys. Res. 110, C09S16. https://doi.org/10.1029/2004JC002601

Eppley, R.W., Peterson, B.J., 1979. Particulate organic matter flux and planktonic new production in the deep ocean. Nature 282, 677–680. https://doi.org/10.1038/282677a0

Hales, B., Karp-Boss, L., Perlin, A., Wheeler, P.A., 2006. Oxygen production and carbon sequestration in an upwelling coastal margin. Global Biogeochem. Cycles 20, n/a-n/a. https://doi.org/10.1029/2005GB002517

Kämpf, J., Chapman, P., 2016. Upwelling Systems of the World. Springer International Publishing, Cham. https://doi.org/10.1007/978-3-319-42524-5

Karthäuser, C., Ahmerkamp, S., Marchant, H.K., Bristow, L.A., Hauss, H., Iversen, M.H., Kiko, R., Maerz, J., Lavik, G., Kuypers, M.M.M., 2021. Small sinking particles control anammox rates in the Peruvian oxygen minimum zone. Nature Communications. https://doi.org/10.1038/s41467-021-23340-4

Lovecchio, E., Gruber, N., Münnich, M., Frenger, I., 2022. On the Processes Sustaining Biological Production in the Offshore Propagating Eddies of the Northern Canary Upwelling System. JGR Oceans 127. https://doi.org/10.1029/2021JC017691

Marinov, I., Gnanadesikan, A., Toggweiler, J.R., Sarmiento, J.L., 2006. The Southern Ocean biogeochemical divide. Nature 441, 964–967. https://doi.org/10.1038/nature04883

Martiny, A.C., Vrugt, J.A., Primeau, F.W., Lomas, M.W., 2013. Regional variation in the particulate organic carbon to nitrogen ratio in the surface ocean. Global Biogeochem. Cycles 27, 723–731. https://doi.org/10.1002/gbc.20061

McDonnell, A.M.P., Lam, P.J., Lamborg, C.H., Buesseler, K.O., Sanders, R., Riley, J.S., Marsay, C.M., Smith, H.E.K., Sargent, E.C., Lampitt, R.S., Bishop, J.K.B., 2015. The oceanographic toolbox for the collection of sinking and suspended marine particles. Progress in Oceanography. https://doi.org/10.1016/j.pocean.2015.01.007

National Academies of Sciences, Engineering, and Medicine, 2021. A Research Strategy for Ocean-based Carbon Dioxide Removal and Sequestration. National Academies Press, Washington, D.C. https://doi.org/10.17226/26278

Orr, J.C., Aumont, O., Yool, A., Plattner, K., Joos, F., Maier-Reimer, E., 2001. Ocean CO_2 sequestration efficiency from 3-D ocean model comparison. CSIRO 469–474.

Ortiz, J., Arístegui, J., Hernández-Hernández, N., Fernández-Méndez, M., Riebesell, U., 2022. Oligotrophic Phytoplankton Community Effectively Adjusts to Artificial Upwelling Regardless of Intensity, but Differently Among Upwelling Modes. Front. Mar. Sci. 9, 880550. https://doi.org/10.3389/fmars.2022.880550

Oschlies, A., Pahlow, M., Yool, A., Matear, R.J., 2010. Climate engineering by artificial ocean upwelling: Channelling the sorcerer's apprentice. Geophys. Res. Lett. 37. https://doi.org/10.1029/2009GL041961

Primeau, F.W., Holzer, M., DeVries, T., 2013. Southern Ocean nutrient trapping and the efficiency of the biological pump. J. Geophys. Res. Oceans 118, 2547–2564. https://doi.org/10.1002/jgrc.20181

Quack, B., 2019. Atmosphere-Ocean-Islands-Biogeochemical interactions in the Macaronesian Archipelagos of Cabo Verde, the Canaries and Madeira. POSEIDON Cruise Report POS533, Mindelo (Cabo Verde) to Las Palmas (Spain), 28.02. – 22.03.2019 (Cruise report No. POS533). GEOMAR Helmholtz-Centre for Ocean Research Kiel.

Schmittner, A., Oschlies, A., Matthews, H.D., Galbraith, E.D., 2008. Future changes in climate, ocean circulation, ecosystems, and biogeochemical cycling simulated for a business-as-usual CO_2 emission scenario until year 4000 AD. Global Biogeochem. Cycles 22, n/a-n/a. https://doi.org/10.1029/2007GB002953

Siegel, D.A., DeVries, T., Doney, S.C., Bell, T., 2021. Assessing the sequestration time scales of some ocean-based carbon dioxide reduction strategies. Environ. Res. Lett. 16, 104003. https://doi.org/10.1088/1748-9326/ac0be0

Ware, D.M., Thomson, R.E., 1991. Link Between Long-Term Variability in Upwelling and Fish Production in the Northeast Pacific Ocean. Can. J. Fish. Aquat. Sci. 48, 2296–2306. https://doi.org/10.1139/f91-270

Weber, T., Bianchi, D., 2020. Efficient Particle Transfer to Depth in Oxygen Minimum Zones of the Pacific and Indian Oceans. Front. Earth Sci. 8, 376. https://doi.org/10.3389/feart.2020.00376

Wu, J., Keller, D.P., Oschlies, A., 2022. Carbon Dioxide Removal via Macroalgae Open-ocean Mariculture and Sinking: An Earth System Modeling Study (preprint). Management of the Earth system: carbon sequestration and management. https://doi.org/10.5194/esd-2021-104

6   Danksagung

Wundervollerweise gibt es zahlreiche Menschen, die mich beim Schreiben dieser Thesis in den letzten vier Jahren begleitet und unterstützt haben. Ulf Riebesell gebührt dabei besonderer Dank. Zum einen danke ich ihm dafür, dass er mir als Dozent die faszinierende Welt des Planktons nahegelegt und meine Faszination für die marine Biogeochemie geschürt hat. Zum anderen dafür, dass er mir die Möglichkeit gegeben hat in seiner Arbeitsgruppe als KOSMO(S)naut so manches Abenteuer zu erleben. Von ganzem Herzen möchte ich Jan Taucher danken, der für mich in den letzten vier Jahren Mentor, Supervisor und Freund gewesen ist, und ohne dessen Vertrauen in meine Fähigkeiten ich diesen Weg nicht so selbstbewusst hätte gehen können. Mein Dank gebührt in gleichem Maße Allanah Paul, die es verstand, mich während dieses Projekts ständig neu zu motivieren und sich regelmäßig meiner Probleme annahm. Das meiste über wissenschaftliches Arbeiten habe ich wohl von Silvan Goldenberg gelernt. Vielen Dank für die Zeit, die Du Dir genommen hast, und für Deinen Spaß am Lehren. Michael Sswat hat mir derweil unter Wasser beigebracht worauf es ankommt. Die sonnigen Stunden an Bord von Wassermann und Rita während unserer Taucheinsätze zählen zu meinen mit Abstand schönsten Arbeitserlebnissen. Außerdem möchte ich gerne Andreas Oschlies danken, der sich zusammen mit Ulf und Allanah stets Zeit für meine ISOS-Meetings genommen hat und dessen Professionalität und Fairness ich bewundere.

Besonderer Dank gebührt ebenfalls meiner Mutter Dagmar und meiner Schwester Anna-Lena, die sich über die Jahre hinweg immer und immer wieder meiner Klagen annehmen mussten – ob sie wollten, oder nicht. Noch schlimmer kann es nur meiner Partnerin Clara ergangen sein, die vor allem während der Schreibphase meiner Dissertation viele der Strapazen mit mir geteilt hat. Ich bin unendlich dankbar, Dich in den letzten Monaten an meiner Seite gehabt zu haben. Mein langjähriger Freund Jakob hat mich auf so einigen Pfaden begleitet – dieser hier war davon mitnichten der einfachste. Danke für Dein stets offenes Ohr. Sehr geholfen haben mir zudem Hanna und unsere wöchentlichen Updates (nicht nur) über den Stand unserer Arbeit. Und zwar bei Kaffee und Kieler Sonnenschein. Können wir das bitte bis zur Rente so weiter machen? Euch allen danke ich für Eure anhaltende Unterstützung und Liebe.

Ulf's Arbeitsgruppe zeichnet sich sicherlich durch hochkarätige Wissenschaft und aufregende KOSMOS Experimente aus. Das Beste an ihr sind jedoch die Menschen. Ich kann mir schwerlich vorstellen, jemals wieder ein Team zu finden, mit dem ich mich so wohl fühle, wie mit meinen Kolleg'innen am GEOMAR. Viele, neben denen ich die letzten fünf Jahren gearbeitet habe, sind zu guten Freunden geworden. Carsten als Büro-Partner mit Joaquin und Leila im Nachbarbüro sind eine unschlagbare Kombination. Als fellow PhDs wusstet Ihr stets genau, „wie das halt so ist". Zu beobachten, wie Antonia sich von einer Schüler-Praktikantin zur waschechten Wissenschaftlerin entwickelt hat, war wundervoll. Ich hatte riesiges Glück, Euch um mich herum zu haben.

Meinen Kolleg'innen, auch den bis hierher unerwähnten, danke ich für die spannende und amüsante Zeit. Ich wünsche Euch von ganzem Herzen alles Gute für den weiteren Weg.

7 Curriculum Vitae

Moritz Baumann

M.Sc. Biological Oceanography

GEOMAR Helmholtz Centre for Ocean Research Kiel

Holtenauer Strasse 209, 24106 Kiel, Germany

+49-176-31164741

mbaumann@geomar.de

Personal information:

Nationality:	German
Date of birth:	02/22/1993
Place of birth:	Konstanz, Germany

Academic
background

02/2019 – now	**PhD Candidate** at GEOMAR Helmholtz Centre for Ocean Research Kiel and Christian-Albrechts-Universität zu Kiel, Germany
	Thesis title: The influence of artificial upwelling on the efficiency of the biological carbon pump
10/2018 – 02/2019	**Research Assistant** at GEOMAR Helmholtz Centre for Ocean Research Kiel, research division Marine Biogeochemistry, working group Biological Oceanography
10/2016 – 09/2018	**Master of Science** in Biological Oceanography at GEOMAR Helmholtz Centre for Ocean Research Kiel and Christian-Albrechts-Universität zu Kiel, Germany
	Thesis title: Temporal development in N-P-Si elemental pools during simulated artificial upwelling
2016	**Scientific Diving Education** at Christian-Albrechts-Universität zu Kiel, Germany, Institute for Geosciences (Scientific Diving Center)
10/2012 – 09/2016	**Bachelor of Science** in Biology at Christian-Albrechts-Universität zu Kiel, Germany
	Thesis title: Vergleichende Untersuchung der Gemeinschafts-zusammensetzung der Größenklassen benthischer Fauna in den Tiefenschichten mariner Sedimente nahe der Antarktischen Halbinsel

Field experience

2020 (2 months)	KOSMOS mesocosm campaign in Callao Bay, Lima, Peru
2019 (1.5 months)	Land-based mesocosm campaign in Taliarte, Gran Canaria, Spain
2018 (2.5 months)	KOSMOS mesocosm campaign in Taliarte, Gran Canaria, Spain
2018 (1 month)	*RV Polarstern* cruise PS 114
2017 (1.5 months)	Land-based mesocosm campaign in Taliarte, Gran Canaria, Spain
2017 (2 weeks)	*RV Alkor* cruise AL 499

Publication record

<u>Published manuscripts (peer reviewed):</u>

Baumann, **M.**, Taucher, J., Paul, A. J., Heinemann, M., Vanharanta, M., Bach, L. T., Spilling, K., Ortiz, J., Arístegui, J., Hernández-Hernández, N., Baños, I., and Riebesell, U.: Effect of Intensity and Mode of Artificial Upwelling on Particle Flux and Carbon Export, *Frontiers in Marine Science*, 8, 742142, 2021.

<u>Manuscripts under review:</u>

Baumann, **M.**, Paul, A. J., Taucher, J., Bach, L. T., Goldenberg, S., Stange, P., Minutolo, F., Riebesell, U.: Drivers of Particle Sinking Velocities in the Peruvian Upwelling System, *Biogeosciences*, under review.

Goldenberg, S., Taucher, J., Fernández-Méndez, M., Ludwig, A., Arístegui, J., **Baumann**, **M.**, Ortiz, J., Riebesell, U.: Nutrient composition (Si:N) as driver of plankton communities during artificial upwelling, *Frontiers in Marine Science*, under review.

Gómez-Letona, M., Sebastian, M., Baños, I., Montero, M. F., Barrancos, C. P., **Baumann**, **M.**, Riebesell, U. , Arístegui, J.: Artificial upwelling leads to a large increase in surface dissolved organic matter concentrations, *Frontiers in Marine Science*, under review.

<u>Manuscripts in preparation:</u>

Baumann, **M.**, Goldenberg, S., Taucher, J., Fernández-Méndez, M., Ortiz, J., Haussmann, J., Riebesell, U.: Counteracting effects of nutrient composition (Si:N) on export flux under artificial upwelling. In preparation.

Spilling, K., Heinemann, M., Vanharanta, M., **Baumann**, **M.**, Noche-Ferreira, A., Suessle, P., Riebesell, U.: Respiration rate scales inversely with sinking speed of settling marine aggregates. In preparation.

8 Eidesstattliche Erklärung

Hiermit bestätige ich, dass die vorliegende Arbeit mit dem Titel:

The influence of artificial upwelling on the efficiency
of the biological carbon pump

von mir selbstständig verfasst worden ist und keine weiteren Quellen und Hilfsmittel als die angegebenen verwendet wurden. Die vorliegende Arbeit ist unter Einhaltung der Regeln guter wissenschaftlicher Praxis der Deutschen Forschungsgemeinschaft entstanden und wurde weder im Rahmen eines Prüfungsverfahrens an anderer Stelle vorgelegt noch veröffentlicht. Veröffentlichte oder zur Veröffentlichung eingereichte Manuskripte wurden kenntlich gemacht. Mir wurde kein akademischer Grad entzogen.

Ich erkläre mich einverstanden, dass diese Arbeit an die Bibliotheken des GEOMAR Helmholtz-Zentrum für Ozeanforschung Kiel und der Christian-Albrechts-Universität zu Kiel weitergeleitet wird.

Kiel, den 24. August 2022   Moritz Baumann